Ultrashort Laser Pulse Phenomena

Fundamentals, Techniques and Applications on a Femtosecond Time Scale

Jean-Claude Diels and Wolfgang Rudolph

February 22, 2021

Contents

Chapter 2

Femtosecond Optics

2.1 Introduction

Whether short pulses or continuous radiation, light should follow the rules of "classical optics". There are, however, some properties related to the bending, propagation, and focalization of light that are specific to fs pulses. Ultrashort pulses are more "unforgiving" of some "defects" of optical systems, as compared to ordinary light of large spectral bandwidth, i.e., white light.[1] Studying optical systems with fs pulses helps in turn to improve the understanding and performances of these systems in white light. We will study properties of basic elements (coatings, lenses, prisms, gratings) and some simple combinations thereof. The dispersion of the index of refraction is the essential parameter for most of the effects to be discussed in this chapter. Some values are listed for selected optical materials in Table 2.1. As already noted in Chapter 1, the second derivative of the index of refraction is positive over the visible spectrum for most transparent materials, corresponding to a positive group velocity dispersion (GVD). There is a sign reversal of the GVD in fused silica around 1.3 μm, which has led to zero dispersion or negative dispersion fibers.

Often a transparent material will be characterized by a fit of the index of refraction as a function of wavelength. Values for most nonlinear materials can be found in ref. [1]. A common form is the Sellmeier equation:

$$n^2(\lambda_\ell) = 1 + \frac{B_1\lambda_\ell^2}{\lambda_\ell^2 - C_1} + \frac{B_2\lambda_\ell^2}{\lambda_\ell^2 - C_2} + \frac{B_3\lambda_\ell^2}{\lambda_\ell^2 - C_3} \tag{2.1}$$

[1] Such light can be regarded as superposition of random fluctuations (short light pulses), the mean duration of which determines the spectral width. A measurement of the light intensity, however, averages over these fluctuations.

In the case of fused silica, the parameters are[1]:

$$\begin{array}{ll} B_1 & 6.96166300 \cdot 10^{-1}\ \mu\mathrm{m}^{-2} \\ B_2 & 4.07942600 \cdot 10^{-1}\ \mu\mathrm{m}^{-2} \\ B_3 & 8.97479400 \cdot 10^{-1}\ \mu\mathrm{m}^{-2} \\ C_1 & 4.67914826 \cdot 10^{-3}\ \mu\mathrm{m}^{2} \\ C_2 & 1.35120631 \cdot 10^{-2}\ \mu\mathrm{m}^{2} \\ C_3 & 9.79340025 \cdot 10^{+1}\ \mu\mathrm{m}^{2} \end{array}$$

with the wavelength λ_ℓ expressed in microns. Another example of a possible fit function is the Laurent series formula:

$$n^2(\lambda_\ell) = A + B\lambda_\ell^2 + \frac{C}{\lambda_\ell^2} + \frac{D}{\lambda_\ell^4} + \frac{E}{\lambda_\ell^6} + \frac{F}{\lambda_\ell^8} \tag{2.2}$$

For crystalline quartz with extraordinary and ordinary index n_e and n_o, respectively, the parameters are[2]:

Parameter	for n_e	for n_o	Unit
A	$2.38490000 \cdot 10^{+0}$	$2.35728000 \cdot 10^{+0}$	
B	$-1.25900000 \cdot 10^{-2}$	$-1.17000000 \cdot 10^{-2}$	$\mu\mathrm{m}^{-2}$
C	$1.07900000 \cdot 10^{-2}$	$1.05400000 \cdot 10^{-2}$	$\mu\mathrm{m}^{2}$
D	$1.65180000 \cdot 10^{-4}$	$1.34143000 \cdot 10^{-4}$	$\mu\mathrm{m}^{4}$
E	$-1.94741000 \cdot 10^{-6}$	$-4.45368000 \cdot 10^{-7}$	$\mu\mathrm{m}^{6}$
F	$9.36476000 \cdot 10^{-8}$	$5.92362000 \cdot 10^{-8}$	$\mu\mathrm{m}^{8}$

The wavelength λ_ℓ being expressed in microns.

An interesting material for its very high index in the visible–near infrared is ZnS. The first and second order dispersion are plotted in Fig. 2.1.

We shall start this chapter with an analysis of a simple Michelson interferometer.

2.2 White light and short pulse interferometry

Incoherent radiation has received increasing attention as the poor man's fs source (even the wealthiest experimentalist will now treat bright incoherent sources with a certain amount of deference). The similarities between white light and femtosecond light pulses are most obvious when studying coherence properties, but definitely transcend the field of coherent interactions.

[2]The values for fused silica and quartz are courtesy of CVI, Albuquerque, New Mexico (www.cvi.com).

material	λ_ℓ	$n(\omega_\ell)$	$n'(\omega_\ell)$ 10^{-2}	$n'(\lambda_\ell)$ 10^{-2}	$n''(\omega_\ell)$ 10^{-3}	$n''(\lambda_\ell)$	$n'''(\omega_\ell)$ 10^{-4}	$n'''(\lambda_\ell)$
	[nm]		[fs]	[μm^{-1}]	[fs^2]	[μm^{-2}]	[fs^3]	[μm^{-3}]
BK7	400	1.5307	1.13	-13.	3.0	1.10	6.9	-12.
	500	1.5213	0.88	-6.6	2.3	.396	7.7	-3.5
	620	1.5154	0.75	-3.6	1.6	.150	13	-1.1
	800	1.5106	0.67	-2.0	0.06	0.05	39	-.29
	1000	1.5074	0.73	-1.4	-3.2	0.016	114	-.09
SF6	400	1.8674	5.8	-67.	30	7.40	214	-120
	500	1.8236	3.7	-28.	16	2.00	86	-21.
	620	1.8005	2.7	-13.	12	.70	50	-5.3
	800	1.7844	2.0	-5.9	8	.22	56	-1.2
	1000	1.7757	1.71	-3.2	4	0.08	115	-.36
SF10	400	1.7784	4.6	-54.	24	5.9	183	-98.
	500	1.7432	3.0	-22.	13	1.6	69	-17.
	620	1.7244	2.2	-11.	9	.56	42	-4.2
	800	1.7112	1.7	-5.0	6	.17	58	-1.0
	1000	1.7038	1.5	-2.8	2	0.06	132	-0.3
SF14	400	1.8185	5.3	-62.	27	6.8	187	-10.9
	500	1.7786	2.8	-25.	15	1.9	85	-2.0
	620	1.7576	2.5	-12.	10	.63	50	-4.8
	800	1.7430	1.8	-5.5	7	.20	54	-1.1
	1000	1.7349	1.6	-3.0	3.4	0.072	110	-.33
SQ1	248	1.5121	2.36	-72.	11	15.	76	-520.
	308	1.4858	1.35	-27.	4.1	3.3	23	-66.0
	400	1.4701	0.93	-11.	2.3	.86	6	-9.80
	500	1.4623	0.73	-5.5	1.8	.32	6	-2.80
	620	1.4574	0.62	-3.0	1.2	.13	13	-0.89
	800	1.4533	0.58	-1.7	-0.4	0.04	41	-0.24
	1000	1.4504	0.67	-1.3	-3.8	0.012	121	-0.08
	1300	1.4469	1.0	-1.1	-14	-.0003	446	-0.02
	1500	1.4446	1.4	-1.2	-27	-.0031	915	-0.01
LaSF9	620	1.8463	2.28	-11.2	9.04	.50		
	800	1.8326	1.76	-5.20	5.79	.17		
ZnSe	620	2.586	14.24	-30.	117.3	2.0		-15.
	800	2.511	8.35	-15.	63.3	0.69		-3.

Table 2.1: Dispersion parameters for some optical materials. BK7 is the most commonly used optical glass. The SF... are dispersive heavy flint glasses. SQ1 is fused silica. The dispersion parameters for the glasses were calculated with Sellmeir's equations and data from various optical catalogs. The data for the UV wavelengths must be considered as order of magnitude approximations. The ZnSe data are taken from Ref. [2]. Using Eqs. (1.124)–(1.128), the dispersion values given in terms of $n(\Omega)$ can easily be transformed into the corresponding values for $k(\Omega)$.

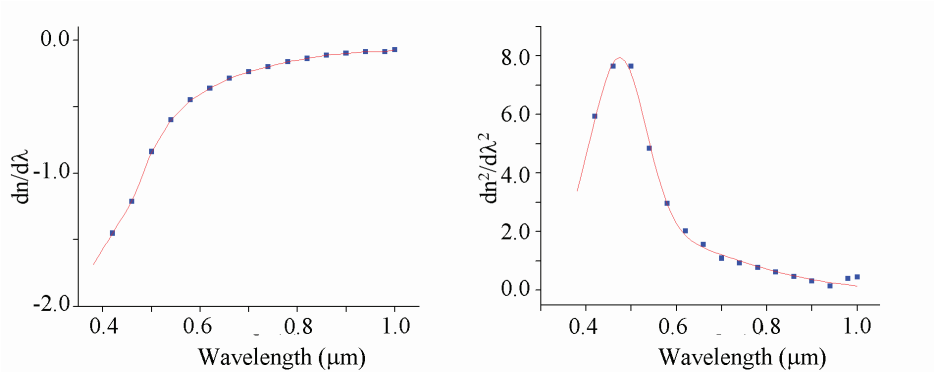

Figure 2.1: First order dispersion in μm^{-1} (left) and second order dispersion in μm^{-2} (right) of ZnS.

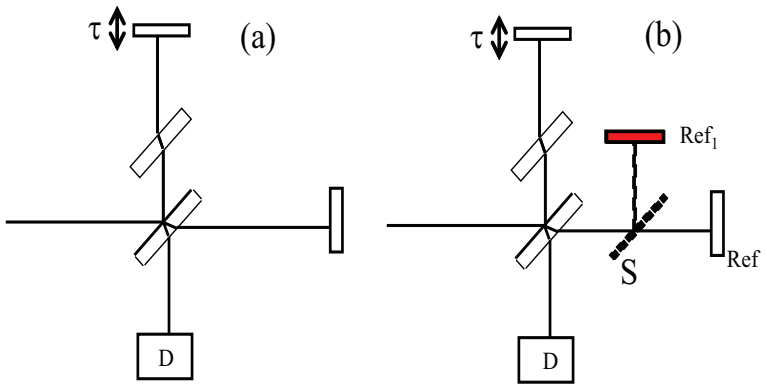

Figure 2.2: Left: balanced Michelson interferometer. Right: for the measurement of mirror dispersion, a reflecting sample is inserted between the beam splitter and the reference mirror Ref. (dotted line). The deflected beam is shown as a dashed line orthogonal to the displaced reference mirror Ref$_1$.

Let us consider the basic Michelson interferometer sketched in Fig. 2.2. The *real* field on the detector, resulting from the interferences of E_1 and E_2, is $E = E_1(t-\tau)+E_2(t)$ with τ being the delay parameter. The intensity at the output of the interferometer is given by the electric field squared averaged over one light period

T [Eq. (1.29)]:

$$\begin{aligned} I(t,\tau) &= \epsilon_0 cn \frac{1}{T}\int_{t-T/2}^{t+T/2} [E_1(t'-\tau)+E_2(t')]^2 dt' \\ &= 2\epsilon_0 cn[\tilde{E}_1^+(t-\tau)+\tilde{E}_2^+(t)][\tilde{E}_1^-(t-\tau)+\tilde{E}_2^-(t)] \\ &= \frac{1}{2}\epsilon_0 cn\Big\{\mathcal{E}_1^2(t-\tau)+\mathcal{E}_2^2(t) \\ &\quad + \tilde{\mathcal{E}}_1^*(t-\tau)\tilde{\mathcal{E}}_2(t)e^{i\omega_\ell\tau}+\tilde{\mathcal{E}}_1(t-\tau)\tilde{\mathcal{E}}_2^*(t)e^{-i\omega_\ell\tau}\Big\}. \end{aligned} \tag{2.3}$$

Here again, we have chosen to decompose the field in an amplitude function $\tilde{\mathcal{E}}$ and a phase function centered around a somewhat arbitrary average frequency of the radiation, ω_ℓ, as in Eqs. (1.18) and (1.19).

The actual signal recorded at the output of the interferometer is the intensity, $\bar{I}$, averaged over the response time τ_R of the detector. In the case of ultrashort pulses $\tau_R \gg \tau_p$ holds and what is being measured is the time integral $\int_{-\infty}^{+\infty} I(t',\tau)dt'$. We will use the notation $\langle\ \rangle$ for either integration or averaging, which results in a quantity that is time independent. Assuming thus that all fluctuations of the signal are averaged out by the detector's slow response, the measured signal reduces to the following expression:

$$\boxed{\begin{aligned} \bar{I}(\tau) &= \frac{\epsilon_0 cn}{4}\Big\{\langle\tilde{\mathcal{E}}_1^2\rangle+\langle\tilde{\mathcal{E}}_2^2\rangle+\Big\langle\tilde{\mathcal{E}}_1^*(t-\tau)\tilde{\mathcal{E}}_2(t)e^{i\omega_\ell\tau}+\tilde{\mathcal{E}}_1(t-\tau)\tilde{\mathcal{E}}_2^*(t)e^{-i\omega_\ell\tau}\Big\rangle\Big\} \\ &= \epsilon_0 cn\Big\{A_{11}(0)+A_{22}(0)+\tilde{A}_{12}^+(\tau)+\tilde{A}_{12}^-(\tau)\Big\}. \end{aligned}} \tag{2.4}$$

On the right hand side of the first line in Eq. (2.4) we recognize correlation functions similar to that in Eq. (1.39), except that they involve the electric fields rather than the intensities. In complete analogy with the definitions of the complex electric fields, the two complex functions correspond to positive and negative spectral components[3] of a correlation function $A_{12}(\tau) = \tilde{A}_{12}^+(\tau)+\tilde{A}_{12}^-(\tau)$, where, e.g., the positive frequency component is defined as:

$$\begin{aligned} \tilde{A}_{12}^+(\tau) &= \frac{1}{4}\langle\tilde{\mathcal{E}}_1^*(t-\tau)\tilde{\mathcal{E}}_2(t)e^{i\omega_\ell\tau}\rangle \\ &= \frac{1}{2}\tilde{\mathcal{A}}_{12}(\tau)e^{i\omega_\ell\tau} \end{aligned} \tag{2.5}$$

The Fourier transform of the correlation of two functions is the product of the Fourier transforms [3]:

[3] Spectrum is defined here with respect to the conjugate variable of the delay parameter τ.

$$\begin{aligned}\tilde{A}^{+}_{12}(\Omega) &= \int_{-\infty}^{\infty}\tilde{A}^{+}_{12}(\tau)e^{-i\Omega\tau}d\tau = \int_{-\infty}^{\infty}\tilde{\mathcal{A}}_{12}(\tau)e^{-i(\Omega\tau-\omega_\ell)}d\tau \\ &= \frac{1}{4}\tilde{\mathcal{E}}^{*}_{1}(\Omega-\omega_\ell)\tilde{\mathcal{E}}_{2}(\Omega-\omega_\ell) \\ &= \tilde{E}^{*}_{1}(\Omega)\tilde{E}_{2}(\Omega) \qquad (2.6)\end{aligned}$$

In the ideal case of infinitely thin beam splitter, nondispersive broadband reflectors and beam splitters, $\tilde{E}_1 = \tilde{E}_2$, and the Fourier transform (2.6) is real. Correspondingly, the correlation defined by Eq. (2.5) is an electric field autocorrelation which is a symmetric function with respect to the delay origin $\tau = 0$. This fundamental property is of little practical importance when manipulating data from a real instrument, because, in the optical time domain, it is difficult to determine exactly the "zero delay" point, which requires measurement of the relative delays of the two arms with an accuracy better than 100 Å. It is therefore more convenient to use an arbitrary origin for the delay τ, and use the generally complex Fourier transformation of Eq. (2.6).

For an ideally balanced interferometer, the output from the two arms is identical, and the right–hand side of Eq. (2.6) is simply the spectral intensity of the light. This instrument is therefore referred to as a Fourier spectrometer.

Let us turn our attention to the slightly "unbalanced" Michelson interferometer. For instance, with a single beam splitter of finite thickness d', the beam 2 will have traversed $L = d'/\cos(\theta_r) = d$ (θ_r being the angle of refraction) more glass than beam 1 (Fig. 2.2). It is well known that the "white light" interference fringes are particularly elusive, because of the short coherence length of the radiation, which translates into a very restricted range of delays over which a fringe pattern can be observed. How will that fringe pattern be modified and shifted by having one beam traverse a path of length $2d$ in glass rather than in air (assumed here to be dispersionless)? Let $\tilde{E}_1(t)$ refer to the field amplitude at the detector, corresponding to the beam that has passed through the unmodified arm with the least amount of glass. Using Eq. (1.177) with $R = 1$, $\Psi(\Omega) = k(\Omega)L$ and considering only terms with $n \leq 2$ in the expansion of Ψ, cf. Eq. (1.179), we find the second beam through the simple transformation:

$$\begin{aligned}\tilde{E}_2(\Omega) &= \tilde{E}_1(\Omega)\exp\{-iL[k(\Omega)-\Omega/c]\} \\ &\approx \tilde{E}_1(\Omega)\exp\left\{-i\left[\left(k_\ell-\frac{\Omega}{c}\right)L + k'_\ell L(\Omega-\omega_\ell) + \frac{k''_\ell L}{2}(\Omega-\omega_\ell)^2\right]\right\} \qquad (2.7)\end{aligned}$$

where, as outlined earlier, $(k'_\ell)^{-1} = \left(\left[\frac{dk}{d\Omega}\right]_{\omega_\ell}\right)^{-1}$ determines the group velocity of a

wave packet centered around ω_ℓ and $k''_\ell = \left[\frac{d^2k}{d\Omega^2}\right]_{\omega_\ell}$ is responsible for group velocity dispersion (GVD). The time dependent electric field is given by the Fourier transform of Eq. (2.7). Neglecting GVD we find for the complex field envelope:

$$\tilde{\mathcal{E}}_2(t) = e^{-i(k_\ell + k'_\ell \omega_\ell)L} \tilde{\mathcal{E}}_1 \left[t - (k'_\ell - 1/c)L\right]. \tag{2.8}$$

Apart from an unimportant phase factor the obvious change introduced by the glass path in one arm of the interferometer is a shift of time origin, i.e., a shift of the maximum of the correlation. This is a mere consequence of the longer time needed for light to traverse glass instead of air. The shift in "time origin" measured with the "unbalanced" versus "balanced" Michelson is

$$\begin{aligned} \Delta\tau &= \left(k'_\ell - \frac{1}{c}\right)L \\ &= \frac{L}{c}\left\{(n-1) + \omega_\ell \left[\frac{dn}{d\Omega}\right]_{\omega_\ell}\right\} \\ &= \frac{L}{c}\left\{(n-1) - \lambda_\ell \left[\frac{dn}{d\lambda}\right]_{\lambda_\ell}\right\}, \end{aligned} \tag{2.9}$$

where we replaced k'_ℓ by Eq. (1.127). The first term in the right-hand side of the second and third equation represents the temporal delay resulting from the difference of the optical pathlength in air ($n \approx 1$) and glass. The second term contains the contribution from the group velocity in glass. In the above derivation, we have not specifically assumed that the radiation consists of short pulses. It is also the case for white light continuous wave (cw) radiation that the group velocity contributes to the shift of zero delay introduced by an unbalance of dispersive media between the two arms of the interferometer.

The third (and following) terms of the expansion of $k(\Omega)$ account for the deformation of the fringe pattern observed in the recording of Fig. 2.3. The propagation can be more easily visualized in the time domain for fs pulses. The group velocity delay is due to the pulse envelope "slipping" with respect to the waves. The group velocity *dispersion* causes different parts of the pulse spectrum to travel at different velocity, resulting in pulse deformation. The result of the Michelson interferogram is a cross-correlation between the field amplitude of the "original" pulse and the signal propagated through glass.

The same considerations can be applied to white light, which can be viewed as a temporal random distribution of ultrashort pulses. The concept of incoherent radiation being constructed out of a statistical time sequence of ultrashort pulses is also useful for studying coherence in light–matter interactions, as will be studied in detail in Chapter **??** on coherent interactions.

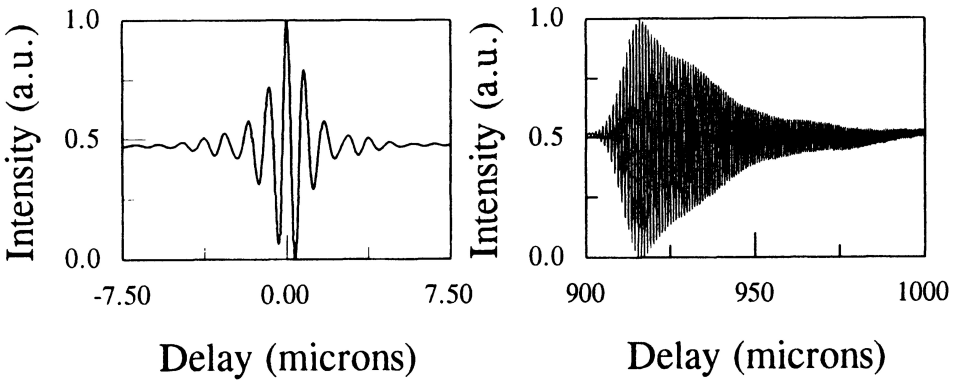

Figure 2.3: "White light" Michelson interferogram. The fringes of the balanced interferometer are shown on the left. The fringe pattern shifts to the right and is broadened by the insertion of a thin quartz plate in one arm of the interferometer.

The correlation [Eqs. (2.4) and (2.5)] is maximum for exactly overlapping statistical phase and intensity fluctuations from both arms of the interferometer. These fluctuations have a duration of the order of the inverse bandwidth of the radiation, hence can be in the fs range for broad bandwidth light. Each of these individual fs spikes will travel at the group velocity. Dispersion in group velocity causes individual frequency components of these spikes to travel at different speeds, resulting most often in pulse stretching. If the source for the interferogram of Fig. 2.3 had been a fs pulse, the recording on the right of the figure would represent the cross–correlation between the field of the stretched–out pulse $\tilde{\mathcal{E}}_2(t)$ with the original (shorter) pulse $\tilde{\mathcal{E}}_1(t)$ (of which the autocorrelation is shown on the left of the figure). Such a measurement can be used to determine the shape of the field $\tilde{\mathcal{E}}_2(t)$. The limiting case of a cross–correlation between a δ function and an unknown function yields the function directly. Indeed, the unbalanced Michelson is a powerful tool leading to a complete determination of the shape of fs signals, in amplitude and phase, as will be seen in Chapter **??**.

In the case of the incoherent radiation used for the recording of Fig. 2.3, the broadened signal on the right merely reflects the "stretching" of the statistical fluctuations of the white light. This measurement however provides important information on material properties essential in fs optics. To illustrate this point we will show how the displacement of the "zero delay" point in the interferogram of Fig. 2.3 can be used to determine the first terms of an expansion of the transfer function of linear optical elements.

According to Eq. (2.6), the Fourier transform of the correlation function $\tilde{A}^+_{11}(\tau)$ measured with the balanced interferometer[4] is simply the spectral field intensity of the source. It is difficult, and not essential, to determine exactly the zero point, and therefore the measurement generally provides $\tilde{A}^+_{11}(\tau+\tau_e)\exp(i\varphi_e)$, which is the function $\tilde{A}^+_{11}(\tau)$ with an unknown phase (φ_e) and delay (τ_e) error. Similarly, the cross-correlation measured after addition of a dielectric sample of thickness $L/2$ in one arm of the interferometer (right hand side of Fig. 2.3) is $\tilde{A}^+_{12}(\tau+\tau_f)\exp\left(i\varphi_f\right)$, which is the function $\tilde{A}^+_{12}(\tau)$ with an unknown phase (φ_f) and delay (τ_f) error. The ratio of the Fourier transforms of both measurements is:

$$\begin{aligned}\frac{\tilde{A}^+_{12}(\Omega)}{\tilde{A}^+_{11}(\Omega)}\frac{e^{-i(\Omega\tau_f-\varphi_f)}}{e^{-i(\Omega\tau_e-\varphi_e)}} &= \frac{\tilde{E}_2(\Omega)}{\tilde{E}_1(\Omega)}e^{-i[\Omega(\tau_f-\tau_e)-(\varphi_f-\varphi_e)]} \\ &= e^{-i[k(\Omega)L+\Omega(\tau_f-\tau_e)-(\varphi_f-\varphi_e)]}, \end{aligned} \tag{2.10}$$

where we have made use of Eqs. (2.6) and (2.7). Unless special instrumental provisions have been made to make ($\varphi_f = \varphi_e$), and ($\tau_f = \tau_e$), this measurement will not provide the first two terms of a Taylor expansion of the dispersion function $k(\Omega)$. This is generally not a serious limitation, since, physically, the undetermined terms are only associated with a phase shift and delay of the fs pulses. The white light interferometer is an ideal instrument to determine the second and higher order dispersions of a sample. Writing the complex Fourier transforms of the interferograms in amplitude and phase:

$$\begin{aligned}\tilde{A}_{12}(\Omega) &= A_{12}(\Omega)e^{\psi_{12}(\Omega)} \\ \tilde{A}_{11}(\Omega) &= A_{11}(\Omega)e^{\psi_{11}(\Omega)}\end{aligned} \tag{2.11}$$

we find that, for an order (n) larger than 1, the dispersion is simply given by:

$$\frac{d^{(n)}k}{d\Omega^{(n)}} = -\left[\frac{d^{(n)}\psi_{12}}{d\Omega^{(n)}} - \frac{d^{(n)}\psi_{11}}{d\Omega^{(n)}}\right] \tag{2.12}$$

Equation (2.12) is not limited to dielectric samples. Instead, any optical transfer function $\tilde{H}$ which can be described by an equation similar to Eq. (1.176), can be determined from such a procedure. For instance, the preceding discussion remains valid for absorbing materials, in which case the wave vector is complex, and Eq. (2.12) leads to a complete determination of the real and imaginary part of the index of refraction of the sample versus frequency. Another example is the response of an optical mirror, as we will see in the following subsection.

[4] $\tilde{A}^+_{11}(\tau)$ corresponds to the third term $\tilde{A}^+_{12}(\tau)$ in Eq. (2.4) taken for identical beams (subscript 1 = subscript 2), not to be confused with the first term $A_{11}(0)$ in that same equation.

2.3 Dispersion of interferometric structures

2.3.1 Mirror dispersion

In optical experiments mirrors are used for different purposes and are usually characterized only in terms of their reflectivity at a certain wavelength. The latter gives a measure about the percentage of incident light intensity which is reflected. In dealing with femtosecond light pulses, one has however to consider the dispersive properties of the mirror [4, 5]. This can be done by analyzing the optical transfer function which, for a mirror, is given by

$$\tilde{H}(\Omega) = R(\Omega)e^{-i\Psi(\Omega)}. \tag{2.13}$$

It relates the spectral amplitude of the reflected field $\tilde{E}_r(\Omega)$ to the incident field $\tilde{E}_0(\Omega)$

$$\tilde{E}_r(\Omega) = R(\Omega)e^{-i\Psi(\Omega)}\tilde{E}_0(\Omega). \tag{2.14}$$

Here $R(\Omega)^2$ is the reflection coefficient and $\Psi(\Omega)$ is the phase response of the mirror. As mentioned earlier a nonzero $\Psi(\Omega)$ in a certain spectral range is unavoidable if $R(\Omega)$ is frequency dependent. Depending on the functional behavior of $\Psi(\Omega)$ (cf. Section 1.3 in Chapter 1), reflection at a mirror not only introduces a certain intensity loss but may also lead to a change in the pulse shape and to chirp generation or compensation. These effects are usually more critical if the corresponding mirror is to be used in a laser. This is because its action is multiplied by the number of effective cavity round trips of the pulse. Such mirrors are mostly fabricated as dielectric multilayers on a substrate. By changing the number of layers and layer thickness a desired transfer function, i.e., reflectivity and phase response, in a certain spectral range can be realized. As an example, Fig. 2.4 shows the amplitude and phase response of a broadband high–reflection mirror and a weak output coupler. Note that, although both mirrors have very similar reflection coefficients around a center wavelength λ_0, the phase response differs greatly. The physical explanation of this difference is that $R(\Omega)$ [or $R(\lambda)$] far from $\omega_0 = 2\pi c/\lambda_0$ (not shown) influences the behavior of $\Psi(\Omega)$ [or $\Psi(\lambda)$] near ω_0.

Before dealing with the influence of other optical components on fs pulses, let us discuss some methods to determine experimentally the mirror characteristics. In this respect the Michelson interferometer is not only a powerful instrument to analyze a sample in transmission, but it can also be used to determine the dispersion and reflection spectrum of a mirror. The interferogram from which the reference spectrum can be obtained is shown on the left of Fig. 2.3. Such a symmetric interference pattern can only be achieved in a well compensated Michelson interferometer (left part of Fig. 2.2) with identical (for symmetry) mirrors in both arms,

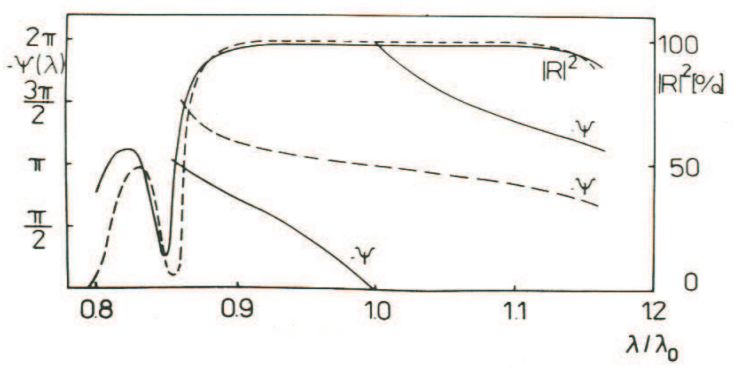

Figure 2.4: Amplitude and phase response for a high reflection multilayer mirror (dashed line) and a weak output coupler (solid line) as a function of the wavelength (from [5]).

which are also broadband (to obtain a narrow correlation pattern). For a most accurate measurement, the mirror to be measured should be *inserted* in one arm of the interferometer rather than substituted to one of the reference mirrors. Otherwise, the dispersive properties of that reference mirror cannot be cancelled. In Fig. 2.2 (left), a sample mirror is indicated as the dotted line, deflecting the beam (dashed lines) towards a displaced end mirror. As in the example of the transmissive sample, insertion of the reflective sample can in general not be done without losing the relative phase and delay references. The cross-correlation measured after substitution of the sample mirror in one arm of the interferometer (right hand side of Fig. 2.3) is $\tilde{A}^+_{12}(\tau+\tau_f)\exp\left(i\varphi_f\right)$, which is the function $\tilde{A}^+_{12}(\tau)$ with an unknown phase (φ_f) and delay (τ_f) error. The ratio of the Fourier transforms of both measurements is in analogy with Eq (2.10):

$$\begin{aligned}\frac{\tilde{A}^+_{12}(\Omega)}{\tilde{A}^+_{11}(\Omega)}\frac{e^{-i(\Omega\tau_f-\varphi_f)}}{e^{-i(\Omega\tau_e-\varphi_e)}} &= \frac{\tilde{E}_2(\Omega)}{\tilde{E}_1(\Omega)}e^{-i[\Omega(\tau_f-\tau_e)-(\varphi_f-\varphi_e)]} \\ &= R(\Omega)^2 e^{-i[2\Psi(\Omega)+\Omega(\tau_f-\tau_e)-(\varphi_f-\varphi_e)]}. \qquad (2.15)\end{aligned}$$

This function is independent of the dispersive and absorptive properties of the reference mirrors. The squared field reflection coefficient and the factor 2 in the phase account for the fact that the beam is reflected twice on the sample mirror. Both the amplitude R and phase Ψ of the transfer function $\tilde{H}(\Omega)$ can be extracted from the measurement, with the limitation that, in general, this measurement will not provide the first two terms of a Taylor expansion of the phase function $\Psi(\Omega)$. Again, this is not a serious limitation, since, physically, the undetermined terms are only associated with a phase shift and delay of the fs pulses. Using the notations of

Eqs. (2.11), the phase shift $-\Psi(\Omega)$ upon reflection of the mirror is simply given by:

$$\Psi(\Omega) = -\frac{1}{2}\left[\psi_{12}(\Omega) - \psi_{11}(\Omega) + a + b\Omega\right] \tag{2.16}$$

where a and b are constants that can generally not be determined,

The Michelson interferometer using white light is one of the simplest and most powerful tools to measure the dispersion of transmissive and reflective optics. Knox *et al.* [6] used it to measure directly the group velocity by measuring the delay induced by a sample, at selected wavelengths (the wavelength selection was accomplished by filtering white light). Naganuma *et al.* [7] used essentially the same method to measure group delays, and applied the technique to the measurement of "alpha parameters" (current dependence of the index of refraction in semiconductors) [8]. In fs lasers, the frequency dependence of the complex reflection coefficient of the mirrors contributes to an overall cavity dispersion. Such a dispersion can be exploited for optimal pulse compression, provided there is a mechanism for matched frequency modulation in the cavity. Dispersion will simply contribute to pulse broadening of initially unmodulated pulses, if no intensity or time dependent index is affecting the pulse phase, as will be discussed later. It is therefore important to diagnose the fs response of dielectric mirrors used in a laser cavity.

A direct method is to measure the change in shape of a fs pulse, after reflection on a dielectric mirror, as proposed and demonstrated by Weiner *et al.* [9]. It is clear in the *frequency domain* that the phases of the various frequency components of the pulse are being scrambled, and therefore the pulse shape should be affected. What is physically happening in the time domain is that the various dielectric layers of the coating accumulate more or less energy at different frequencies, resulting in a delay of some parts of the pulse. Therefore, significant pulse reshaping with broadband coatings occurs only when the coherence length of the pulse length is comparable to the coating thickness. Pulses of less than 30 fs duration were used in Refs. [10, 9]. As shown above, determination of the dispersion in the frequency domain can be made with a simple Michelson interferometer. The latter being a *linear measurement*, yields the same result with incoherent white light illumination or femtosecond pulses of the same bandwidth.

An alternate method, advantageous for its sensitivity, but limited to the determination of the group velocity dispersion, is to compare glass and coating dispersion inside a fs laser cavity. As will be seen in Chapter **??**, an adjustable thickness of glass is generally incorporated in the cavity of mode-locked dye and solid state lasers, to tune the amount of group velocity dispersion for minimum pulse duration. The dispersion of mirrors can be measured by substituting mirrors with different coatings in one cavity position, and noting the change in the amount of glass re-

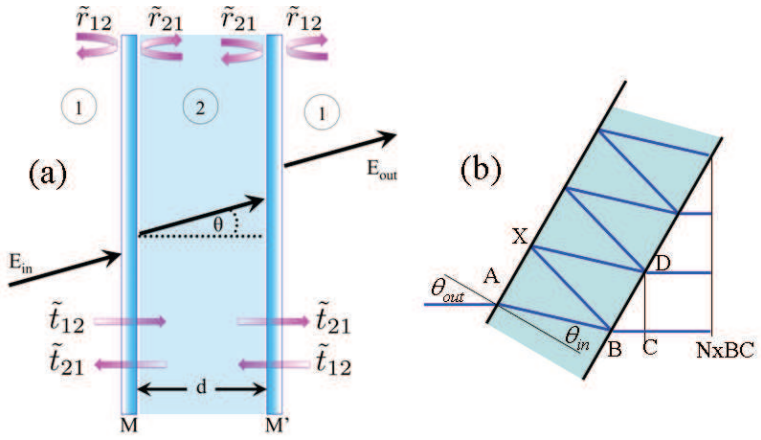

Figure 2.5: Schematic diagram of a Fabry-Perot interferometer. (a)Normal incidence. $\tilde{t}_{12}$ is the transmission from outside (1) to inside (2); $\tilde{t}_{21}$ the transmission from inside (2) to outside (1); $\tilde{r}_{12}$ the reflection from outside (1) to inside (2) and $\tilde{r}_{21}$ the reflection from inside (2) to outside (1). (b) Tilted Fabry-Perot at an angle θ_{out}. The internal angle of incidence is $\theta_i n$. The fields add up in phase along a wavefront at $N \times BC$ ($N \to \infty$) from B.

quired to compensate for the additional dispersion [11, 5]. The method is very sensitive, because the effect of the sample mirror is multiplied by the mean number of cycles of the pulse in the laser cavity. It is most useful for selecting mirrors for a particular fs laser cavity.

2.3.2 Fabry-Perot and Gires-Tournois interferometer

So far we have introduced (Michelson) interferometers only as a tool to split a pulse and to generate a certain delay between the two partial pulses. In general, however, the action of an interferometer is more complex. This is particularly true for multiple-beam devices such as a Fabry–Perot interferometer. Let us consider for instance a symmetric Fabry-Perot, with two identical parallel dielectric reflectors spaced by a distance d. We will use the notations $\tilde{t}_{ij}$ for the field transmission, and $\tilde{r}_{ij}$ for the field reflection, as defined in Fig. 2.5. When the Fabry-Perot is tilted, the fields add in phase along a wavefront normal to the rays (outside the Fabry-Perot) as sketched in Fig. 2.5 (b). If k_0 is the wave vector in air and k the optical path inside the Fabry-Perot, the complex field transmission function is found by summing

the successive optical path:

$$\begin{aligned}\tilde{H}(\Omega) &= \tilde{t}_{12}\tilde{t}_{21}e^{-i(kAB+k_0N.BC)} + \\ &\quad \tilde{t}_{12}\tilde{t}_{21}e^{-ikBXD}\cdot\tilde{r}_{21}\tilde{r}_{21}e^{-i[kAB+k_0(N-1)BC]} \\ &\quad +\tilde{t}_{12}\tilde{t}_{21}\left(e^{-ikBXD}\cdot\tilde{r}_{21}\tilde{r}_{21}\right)^2 e^{-i[kAB+k_0(N-2)BC]}+\ldots \end{aligned} \tag{2.17}$$

The exponential $\exp[-ik_0NBC]$ can be put in factor of the whole expression. Being just a phase factor, it can be ignored. The optical path AB is $nd/\cos\theta_{in}$, where n is the index of refraction inside the Fabry-Perot, while the difference in optical path $BXD-BC$ appearing in the power series is:

$$\frac{2nd}{\cos\theta_{in}} - 2nd\tan\theta_{in}\sin\theta_{out} = \frac{2nd}{\cos\theta_{in}} - \frac{2nd\sin^2\theta_{in}}{\cos\theta out} = \frac{2nd\cos\theta_{in}}{c}. \tag{2.18}$$

Substituting in Eq. (2.17):

$$\tilde{H}(\Omega) = \tilde{t}_{12}\tilde{t}_{21}e^{-i(kd/\cos\theta_{in})}\frac{1}{1-\tilde{r}_{21}^2e^{-2ikd\cos\theta}}. \tag{2.19}$$

Taking into account the interface properties derived in Appendix E, $\tilde{t}_{12}\tilde{t}_{21}-\tilde{r}_{12}\tilde{r}_{21}=1$ and $\tilde{r}_{12}=-\tilde{r}_{21}^*$, the field transmission reduces to:

$$\boxed{\tilde{H}(\Omega) = \frac{(1-R)e^{-ikd/\cos\theta_{in}}}{1-Re^{i\delta}}} \tag{2.20}$$

where

$$\delta(\Omega) = 2\varphi_r - 2k(\Omega)d\cos\theta_{in} \tag{2.21}$$

is the total phase shift of a round-trip inside the Fabry-Perot, including the phase shift φ_r upon reflection on each mirror, θ_{in} is the angle of incidence on the mirrors (inside the Fabry-Perot), and $R=|\tilde{r}_{12}|^2$ is the intensity reflection coefficient of each mirror [12].

Similarly, one finds the complex reflection coefficient of the Fabry-Perot:

$$\boxed{\tilde{\mathcal{R}}(\Omega) = \frac{\sqrt{R}\left(e^{i\delta}-1\right)}{1-Re^{i\delta}}.} \tag{2.22}$$

One can easily verify that, if — and only if — kd is real:

$$|\mathcal{R}|^2+|\mathcal{T}|^2=1 \tag{2.23}$$

Equations (2.20) and (2.22) are the transfer functions for the field spectrum. The dependence on the frequency argument Ω occurs through $k=n(\Omega)\Omega/c$ and possibly $\varphi_r(\Omega)$. With $n(\Omega)$ complex, the medium inside the Fabry-Perot is either an

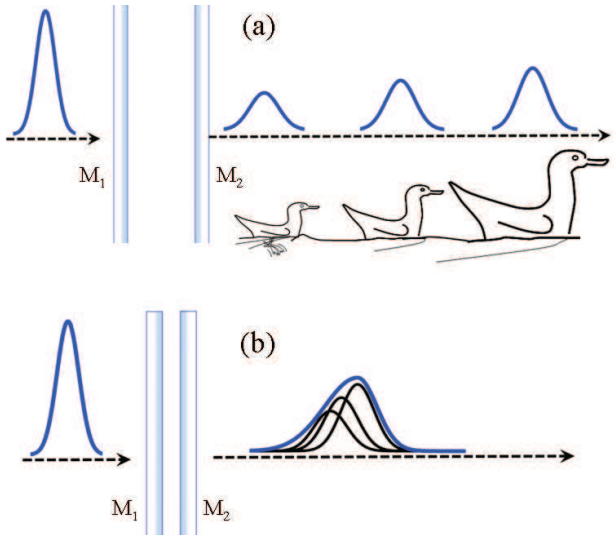

Figure 2.6: Effect of a Fabry-Perot interferometer on a light pulse. (a) If the mirror spacing is larger than the geometrical length of the incident pulse, an exponentially decaying sequence of pulses follows the Fabry-Perot, like ducklings follow mother duck. (b) If the mirror spacing is smaller than the geometric length of the incident pulse, the pulse spectrum is spectrally filtered, resulting a longer transmitted pulse.

absorbing or an amplifying medium, depending on the sign of the imaginary part of the index. We refer to a problem at the end of this chapter for a study of the Fabry-Perot with gain.

The functions $\tilde{H}(\Omega)$ and $\tilde{\mathcal{R}}(\Omega)$ are complex transfer functions, which implies that, for instance, the transmitted field is:

$$\tilde{E}_{out}(\Omega) = \mathcal{T}(\Omega)\tilde{E}_{in}(\Omega) \tag{2.24}$$

where $\tilde{E}_{in}$ is the incident field. Equation (2.24) takes into account all the dynamics of the field and of the Fabry-Perot. In the case of a Fabry-Perot of thickness $d \ll c\tau_p$, close to resonance ($\delta(\Omega) \ll 1$), the transmission function $\tilde{H}(\Omega)$ is a Lorentzian, with a real and imaginary part connected by the Kramers Kronig relation. We refer to a problem at the end of this chapter to show how dispersive properties of a Fabry-Perot can be used to shape a chirped pulse.

In the case of a Fabry-Perot of thickness $d \gg c\tau_p$, the pulse spectrum covers a large number of Fabry-Perot modes. Hence the product (2.24) will represent a frequency comb, of which the Fourier transform is a train of pulses. Intuitively indeed, we expect the transmission and/or reflection of a Fabry-Perot interferometer to consist of a train of pulses of decreasing intensity if the spacing d between the two mirrors is larger than the geometrical pulse length, [Fig. 2.6(a)]. The latter condition prevents interference between field components of successive pulses. The free spectral range of the Fabry–Perot interferometer is much smaller than the spectral width of the pulse. On the other hand if d is smaller than the pulse length the output field is determined by interference, as illustrated in Fig. 2.6(b). An example of a corresponding device was the dielectric multilayer mirror discussed before, which can be considered as a sequence of many Fabry–Perot interferometers. Here the free spectral range of one interferometer is much broader than the pulse spectrum and it is the behavior around a resonance which determines the shape of pulse envelope and phase. The actual pulse characteristics can easily be determined by multiplying the field spectrum of the incident pulse with the corresponding transfer function (2.20). For a multilayer mirror this function can be obtained from a straightforward multiplication of matrices for the individual layers [13].

Among the various types of interferometers that can be used for pulse shaping, we choose to detail here the Gires–Tournois interferometer [14]. Its striking feature is a very high and almost constant amplitude transmission while the spectral phase can be tuned continuously. This device can be used to control the GVD in a fs laser in a similar manner as gratings and prisms. The Gires–Tournois is topologically identical to a ring interferometer, with all mirrors but one being perfect reflectors. The lone transmitting mirror is used as input and output. As with the Gires–Tournois, the output amplitude is unity, whether or not the wave inside the

Figure 2.7: Schematic diagram of a Gires–Tournois interferometer.

ring is at resonance or not. It is left as an exercise at the end of this chapter to transpose the formulae of the Gires–Tournois to the situation of a ring interferometer.

A sketch of the Gires–Tournois interferometer is shown in Fig. 2.7. It is a special type of a Fabry-Perot interferometer with one mirror (mirror M_2) having a reflection coefficient of (almost) 1. Consequently the device is used in reflection. In this case the transfer function is given by

$$R(\Omega)e^{-i\Psi(\Omega)} = \frac{-r + e^{i\delta}}{1 - re^{i\delta}} \tag{2.25}$$

where δ is the phase delay[5] between two successive partial waves that leave the interferometer and r is the (real) amplitude reflection of M_1 (assumed to be non-dispersive). It can easily be shown that the reflectivity of the device is $|R| = 1$, i.e., there is practically no change in the pulse energy. The phase response determined by Eq. (2.25) can be written as

$$\Psi(\Omega) = -\arctan\left[\frac{(r^2-1)\sin\delta}{2r-(r^2+1)\cos\delta}\right] \tag{2.26}$$

Taking the derivative of both sides of this expression, and dividing by $[\tan^2\Psi + 1]$ yields:

$$\frac{d\Psi}{d\Omega} = \frac{(r^4-1) - 2r(r^2-1)\cos\delta}{(1+r^2)^2 + 4r\cos\delta[r\cos\delta - (1+r^2)]}\frac{d\delta}{d\Omega}. \tag{2.27}$$

[5] In the definition of the phase delay (2.21) applied to the Gires-Tournois interferometer, θ is the *internal* angle.

It is interesting to find the expression for the group delay at the exact resonances, i.e. the values of Ω that make $\delta = 2N\pi$:

$$\left.\frac{d\Psi}{d\Omega}\right|_{res} = \left(\frac{r+1}{r-1}\right)\left.\frac{d\delta}{d\Omega}\right|_{res} \tag{2.28}$$

The group velocity dispersion of the device is calculated from the second derivative of the expression (2.27):

$$\begin{aligned}\frac{d^2\Psi}{d\Omega^2} &= \frac{(r^4-1)-2r(r^2-1)\cos\delta}{(1+r^2)^2+4r\cos\delta[r\cos\delta-(1+r^2)]}\frac{d^2\delta}{d\Omega^2} \\ &+\frac{2r(r^2-1)\sin\delta\left[4r(r^2+1)\cos\delta-4r^2\cos^2\delta-r^2-3\right]}{\{(1+r^2)^2+4r\cos\delta[r\cos\delta-(1+r^2)]\}^2}\left(\frac{d\delta}{d\Omega}\right)^2.\end{aligned} \tag{2.29}$$

Note that, as pointed out in the problem at the end of this chapter, the same expressions can be derived for the transmission of a ring resonator. At the resonances of the device, $\delta = 2N\pi$, and the GVD is:

$$\left.\frac{d^2\Psi}{d\Omega^2}\right|_{res} = \left(\frac{r+1}{r-1}\right)\left.\frac{d^2\delta}{d\Omega^2}\right|_{res}. \tag{2.30}$$

As shown in the definition Eq. (2.21), the second derivative of δ contains the group velocity dispersion ($-k$") of the material inside the interferometer. This material dispersion is enhanced by the factor $(r+1)/(r-1)$ in condition of resonance. This factor can be very large in the case a of high finesse resonator ($1-r \ll 1$).

The GVD given by Eq. (2.29) can be tuned continuously by adjusting δ which can be either through a change of the mirror separation d or through a change of the external angle of incidence Θ. Gires and Tournois [14] conceived this interferometer to adapt to optical frequencies the pulse compression technique used in radar (sending a frequency modulated pulse through a dispersive delay line). Duguay and Hansen were the first to apply this device for the compression of pulses from a He-Ne laser [16]. Since typical pulse durations were on the order of several hundred ps the mirror spacing needed to be in the order of few mm. To use the interferometer for the shaping of fs pulses the corresponding mirror spacing has to be in the order of few microns. Heppner and Kuhl [17] overcame this obvious practical difficulty by designing a Gires–Tournois interferometer on the basis of dielectric multilayer systems, as illustrated in Fig. 2.8(a). The 100% mirror M_2 is a sequence of dielectric coatings with alternating refractive index deposited on a substrate. A certain spacer of optical thickness d consisting of a series of $\lambda/2$ layers of one and the same material is placed on top of M_2. The partially reflective

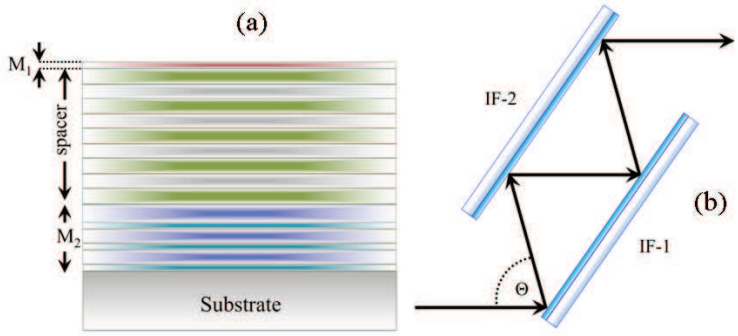

Figure 2.8: Gires-Tournois interferometer for fs light pulses using dielectric multilayers. By rotating two parallel interferometers the overall dispersion can be adjusted through a change of the external angle of incidence Θ and the number of reflections. Note, the beam direction is not changed. The lateral displacement can be compensated by a second pair of interferometers (from [15]).

surface M_1 is realized by one $\lambda/4$ layer of high refractive index. The dispersion of this compact device can be tuned by changing the angle of incidence and/or the number of passes through the interferometer. A possible arrangement which was successfully applied for GVD adjustments in fs lasers [15] is shown in Fig. 2.8(b).

Let us inspect in more detail the actual transfer function of the multilayer Gires-Tournois interferometer taking into account the mirror dispersion. In most generality, the first reflecting face of the Gires Tournois is a multi-layer dielectric coating, which we will model as an infinitely thin layer with complex reflection coefficient $\tilde{r}_{ij} = r\exp\left(i\varphi_{r,ij}\right)$ and transmission coefficient $\tilde{t}_{ij} = t\exp\left(i\varphi_{t,ij}\right)$. The subscripts $i, j = 1,2$ refer to air (1) and spacer dielectric (2). As indicated in Fig. 2.7, $\tilde{t}_{12}$ is the transmission coefficient from air to the spacer, through the multilayer dielectric mirror M_1; $\tilde{r}_{12}$ the reflection coefficient of M_1 to a beam incident from the air, *etc* .... Let us designate by δ the phase shift accumulated by the wave having propagated from the first reflecting layer to the total reflector and back to the first layer:

$$\delta(\Omega) = -2k(\Omega)d\cos\theta + \varphi_{r2} = -\frac{2\Omega n(\Omega)d\cos\theta}{c} + \varphi_{r2}, \tag{2.31}$$

where φ_{r2} is the phase shift upon reflection at the totally reflecting layer(s) (mirror M_2), and θ is the internal angle of incidence on the reflecting interfaces. The

complex (field) reflection coefficient of the structure is:

$$\begin{aligned} R(\Omega)e^{-i\Psi(\Omega)} &= \frac{\tilde{r}_{12}+(\tilde{t}_{12}\tilde{t}_{21}-\tilde{r}_{12}\tilde{r}_{21})e^{i\delta}}{1-\tilde{r}_{21}e^{i\delta}} \\ &= \frac{\tilde{r}_{12}+e^{i\delta}}{1-\tilde{r}_{21}e^{i\delta}}, \end{aligned} \tag{2.32}$$

where the last equality results from the relation between the complex amplitude reflection and transmission derived in Appendix E ($\tilde{t}_{12}\tilde{t}_{21}-\tilde{r}_{12}\tilde{r}_{21}=1$). The reflectivity of the device is:

$$|R(\Omega)|^2 = \frac{|\tilde{r}_{12}|^2+1+\tilde{r}_{12}e^{-i\delta}+\tilde{r}_{12}^*e^{i\delta}}{|\tilde{r}_{21}|^2+1-\tilde{r}_{21}^*e^{-i\delta}-\tilde{r}_{21}e^{i\delta}}, \tag{2.33}$$

which is only equal to unity if $\tilde{r}_{21}=-\tilde{r}_{12}^*$ and the media are lossless. This relation is consistent with the phase shift upon reflection on a dielectric interface. The expression for the complex reflection of the whole interferometer can be re-written in terms of the reflection coefficient $\tilde{r}_{21}$ [6]:

$$R(\Omega)e^{-i\Psi(\Omega)} = \frac{-\tilde{r}_{21}^*+e^{i\delta}}{1-\tilde{r}_{21}e^{i\delta}}. \tag{2.34}$$

Let us express the reflectivity $\tilde{r}_{21}$ in terms of its amplitude and phase: $\tilde{r}_{21} = r_{21}\exp(i\varphi_{r,21}) = r\exp(i\varphi_r)$. The phase response of the interferometer can now be calculated:

$$\Psi(\Omega) = -\arctan\frac{(r^2-1)\sin\delta(\Omega)-r\sin\varphi_r(\Omega)}{2r\cos\varphi_r(\Omega)-(1+r^2)\cos\delta(\Omega)}, \tag{2.35}$$

which is a generalization of Eq. (2.26) to the more complex multilayer Gires-Tournois structure. Only when $\varphi_r=0$ and φ_{r2} (in δ) is frequency independent in the range of interest are the dispersions described by Eqs. (2.26) and (2.35) equal. The error may be small in some real situations, as can be seen from the comparison of the approximation (2.26) with the exact phase $\Psi(\Omega)$ shown in Fig. 2.9. The latter functional dependence can be calculated directly through matrix algebra [13] taking into account a certain sequence of dielectric multilayer mirrors.

2.3.3 Chirped mirrors

As mentioned in the previous section, the Gires-Tournois interferometer exhibits a reflectivity close to one over a broad spectrum. This was accomplished by an end

[6] We recall that $\tilde{r}_{21}$ is the complex field reflection coefficient from inside the Gires Tournois, on the multilayer dielectric coating, assumed to be infinitely thin

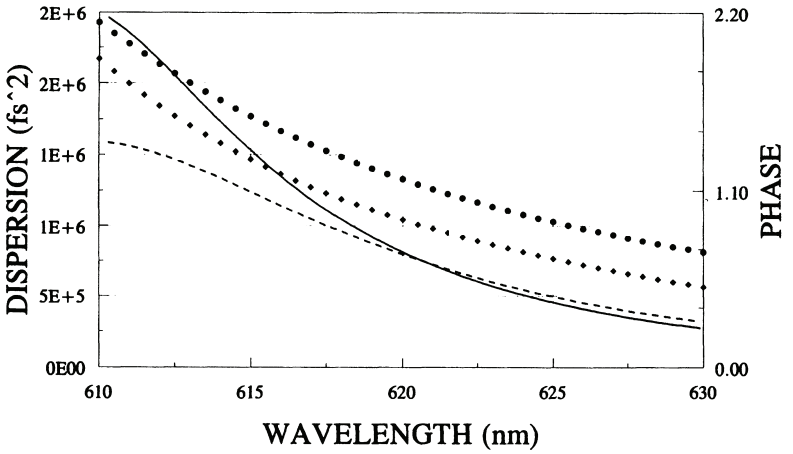

Figure 2.9: Comparison of the exact phase function $\psi(\lambda)$ (diamonds) and its second derivative $d^2\psi/d\Omega^2$ (solid line) of a Gires-Tournois interferometer with the approximation of assuming constant φ_r and φ_{r2} Eq. (2.35) (circles for ψ, dashed line for the second derivative). The Gires-Tournois interferometer has been designed for a central wavelength λ_0 = 620 nm. The curves are calculated for an external angle of incidence of 20°. For this particular example, the high reflector is made of 11 layers of TiO_2 (thickness $\lambda_0/4n$ = 67.4 nm) alternating with layers of SiO_2 (thickness $\lambda_0/4n$ = 106.9 nm) on a glass substrate (n = 1.5). The spacer consists of 5 half wave spacing of SiO_2, for a total thickness of 1068.9 nm. The top reflector (r = 0.324) consists of a quarter wave layer of TiO_2 (thickness $\lambda_0/4n$ = 67.4 nm). In applying Eq. (2.35), the values of phase shifts upon reflection were $\varphi_r = -0.0192$ (top layer) and $\varphi_{r2} = -0.0952$ (high reflector).

mirror of high reflectivity (M_2 in Fig. 2.8). The dispersion on the other hand can be controlled by the spacer and the front mirror. This is expressed in the phase $\delta(\Omega)$ and $\varphi_r(\Omega)$ in Eq. (2.35). The problem is that both mirrors at the same time form a Fabry-Perot structure that has relatively narrow resonances and subsequently a rather complicated dispersion behavior. The most desired alternative would be a process to generate a pre-defined reflection and phase behavior, $R(\Omega)$ and $\Psi(\Omega)$. Optimization programs applied to dielectric multi-layer systems offer such an intriguing and interesting possibility. A dielectric multi-layer system consists of a sequence of films characterized by a certain refractive index n_i and thickness d_i. In principle, computer algorithms can be used to find a sequence of (d_i, n_i) combinations representing individual films that come closest to a pre-defined reflection and phase behavior in a certain spectral range. Of course, there are certain technical constraints that need to be considered, for example the total thickness and number of layers, the manufacturing tolerances in n_i and d_i, and the limited choice of available refractive indices n_i (suitable materials). This approach will gain importance

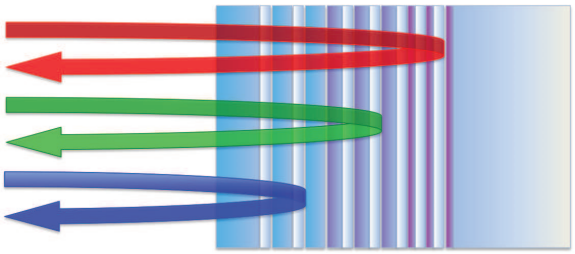

Figure 2.10: Wave packets of different center frequencies are reflected at different depths of a chirped mirror. The mirror consists of stacks of alternating high and low refractive index layers at different resonance frequencies.

in the future as the amplitude and phase responses needed become more and more complicated.

In many cases mirrors are desired that have a constant reflectivity and certain dispersion behavior, for example a constant amount of GVD within a pre-defined spectral range. This idea was pursued by Szipöks et al. [18], leading to what is now called chirped mirrors. The basic idea is sketched in Fig. 2.10. High-reflection mirrors typically consist of stacks of alternating high and low refractive index quarter-wave layers. A chirped mirror is a sequence of those stacks with changing resonance frequency. Wave-packets of different center frequency are thus reflected at different depths, making the group delay upon reflection a function of frequency.

Unfortunately this is an oversimplified picture that neglects subresonances in particular between the layers and the first air-film interface. This leads to a modulation of the GVD. For this reason computer optimization is necessary to tune the film parameters for a smooth dispersion curve.

Improvements in the initial layer sequence used as a starting point for the final computer optimization have been accomplished, for example, by modulating the ratio of the thickness of the high- and low-index layer of the chirped mirror (double chirped mirror) [19], by superimposing a quasi-periodic modulation on the linear modulation of the layer thickness [20], and by coating the backside of the substrate [21, 22]. As we will see in following chapters such mirrors have made an impressive impact on femtosecond laser source development.

2.4 Focusing elements

2.4.1 Singlet lenses

One main function of fs pulses is to concentrate energy in time and space. The ability to achieve extremely high peak power densities depends partly on the ability

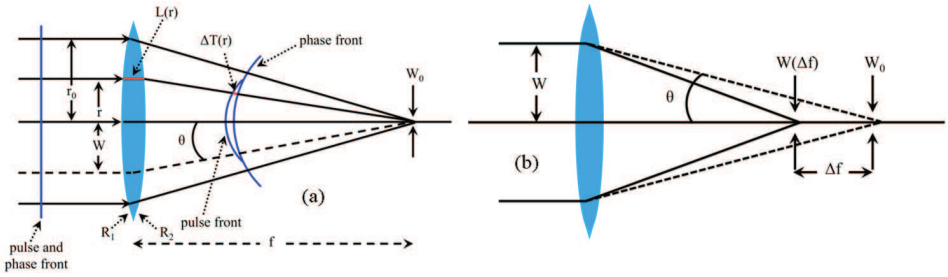

Figure 2.11: (a) delay of the pulse front with respect to the phase front, in the case of a singlet lens. (b) spread of the focal region due to chromatic aberration.

to keep pulses short in time, and concentrate them in a small volume by focusing. The difference between group and phase velocity in the lens material can reduce the peak intensity in the focal plane by delaying the time of arrival of the pulse front propagating through the lens center relative to the pulse front propagating along peripheral rays. The group velocity dispersion leads to reduction of peak intensity by stretching the pulse in time. As pointed out by Bor [23, 24], when simple focusing singlet lenses are used, the former effect can lead to several picosecond lengthening of the time required to deposit the energy of a fs pulse on focus.

Let us assume a plane pulse and phase front at the input of a spherical lens as sketched in Fig. 2.11. According to Fermat's principle the optical path along rays from the input phase front to the focus is independent of the radius coordinate r. The lens transforms the plane phase front into a spherical one which converges in the (paraxial) focus. Assimilating air as vacuum, it is only while propagating through the lens that the pulses experience a group velocity v_g different from the phase velocity $v_p = c/n$. The result is a pulse front that is delayed with respect to the (spherical) phase front, depending on the amount of glass traversed. As we have seen in Chapter 1, the group velocity is:

$$v_g = \left(\frac{dk}{d\Omega}\right)^{-1} = \frac{c}{n - \lambda_\ell \frac{dn}{d\lambda}}, \tag{2.36}$$

where λ_ℓ is the wavelength in vacuum. The difference in propagation time between the phase front and pulse front after the lens at radius coordinate r is:

$$\Delta T(r) = \left(\frac{1}{v_p} - \frac{1}{v_g}\right) L(r), \tag{2.37}$$

where $L(r)$ is the lens thickness. The group delay $\Delta T(r)$ is also the difference of the time of arrival at the focus of pulses traversing the lens at distance r from the

axis and peripheral rays touching the lens rim. Pulse parts travelling on the axis ($r = 0$) will arrive delayed in the focal plane of a positive lens compared with pulse parts traversing the lens at $r > 0$. For a spherical thin lens, the thickness L is given by

$$L(r) = \frac{r_0^2 - r^2}{2}\left(\frac{1}{R_1} - \frac{1}{R_2}\right) \tag{2.38}$$

where $R_{1,2}$ are the radii of curvature of the lens and r_0 is the radius of the lens aperture.[7] Substituting the expressions for the group velocity (2.36) and for the lens thickness (2.38) into Eq. (2.37) yields for the difference in time of arrival between a pulse passing through the lens at the rim and at r:

$$\begin{aligned} \Delta T(r) &= \frac{r_0^2 - r^2}{2c}\left(\frac{1}{R_1} - \frac{1}{R_2}\right)\left(\lambda\frac{dn}{d\lambda}\right) \\ &= \frac{r_0^2 - r^2}{2c}\lambda\frac{d}{d\lambda}\left(\frac{1}{f}\right) \end{aligned} \tag{2.39}$$

where the focal length f has been introduced by $1/f = (n-1)(R_1^{-1} - R_2^{-1})$. Equation (2.40) illustrates the connection between the radius dependent pulse delay and the chromaticity $d/d\lambda(1/f)$ of the lens. For an input beam of radius r_b the pulse broadening in the focus can be estimated with the difference in arrival time $\Delta T'$ of a pulse on an axial ray and a pulse passing through the lens at r_b:

$$\boxed{\Delta T'(r_b) = \frac{r_b^2}{2c}\lambda\frac{d}{d\lambda}\left(\frac{1}{f}\right).} \tag{2.40}$$

To illustrate the effects of group velocity delay and dispersion, let us assume that we would like to focus a 50 fs pulse at the excimer laser wavelength of 248 nm (KrF) down to a spot size of 0.6 μm, using a fused silica lens (singlet) of focal distance f = 30 mm. Let us further assume that the input beam profile is Gaussian. Since the half divergence angle in the focused beam is $\theta = \lambda/(\pi w_0)$, the radius w of the Gaussian beam [radial dependence of the electric field: $\tilde{\mathcal{E}}(r) = \tilde{\mathcal{E}}(0)\exp\{-r^2/w^2\}$] incident on the lens should be approximately $\theta f = (\lambda/\pi w_0)f \approx 4$

[7] Regarding sign considerations we will use positive (negative) $R_{1,2}$ for refracting surfaces which are concave (convex) towards the incident side.

mm. To estimate the pulse delay we evaluate $\Delta T'$ at $r_b = w$:

$$\begin{aligned}\Delta T'(r_b = w) &= \frac{w^2}{2c}\lambda\frac{d}{d\lambda}\left(\frac{1}{f}\right) \\ &= -\frac{w^2}{2cf(n-1)}\left(\lambda\frac{dn}{d\lambda}\right) \\ &= -\frac{\theta^2 f}{2c(n-1)}\left(\lambda\frac{dn}{d\lambda}\right). \end{aligned} \tag{2.41}$$

For the particular example chosen, $n \approx 1.51$, $\lambda dn/d\lambda \approx -0.17$, and the difference in time of arrival (at the focus) of the rays at $r = 0$ and $r_b = w$ is ≈ 300 fs, which can be used as a rough measure of the pulse broadening.

The effect of the chromaticity of the lens on the spatial distribution of the light intensity near the focal plane is a spread of the optical energy near the focus, because different spectral components of the pulse are focused at different points on axis. For a bandwidth limited Gaussian pulse of duration $\tau_p = \sqrt{2\ln 2}\,\tau_{G0}$ with spectral width $\Delta\lambda = 0.441\lambda^2/c\tau_p$, the focus spreads by the amount:

$$\Delta f = -f^2\,\frac{d(1/f)}{d\lambda}\Delta\lambda = -\frac{f\lambda^2}{c(n-1)}\frac{0.441}{\tau_p}\frac{dn}{d\lambda}. \tag{2.42}$$

Applying Eq. (2.42) to our example of a 30 mm fused silica lens to focus a 50 fs pulse, we find a spread of $\Delta f = 60\ \mu$m, which is large compared to the Rayleigh range of a diffraction limited focused monochromatic beam $\rho_0 = w_0/\theta \approx 5\ \mu$m. We can therefore write the following approximation for the broadening of the beam: $w(\Delta f)/w_0 = \sqrt{1+(\Delta f/2\rho_0)^2} \approx (\Delta f/2\rho_0)$. Substituting the value for Δf from Eq. (2.42):

$$\frac{w(\Delta f)}{w_0} = -\frac{0.44\pi}{\tau_p}\frac{\theta^2 f}{2c(n-1)}\left(\lambda\frac{dn}{d\lambda}\right) \approx -0.44\pi\frac{\Delta T'}{\tau_p}. \tag{2.43}$$

We note that the spatial broadening of the beam due to the spectral extension of the pulse, as given by Eq. (2.43), is (within a numerical factor) the same expression as the group velocity delay [Eq. (2.41)] relative to the pulse duration. In fact, neither expression is correct, in the sense that they do not give a complete description of the spatial and temporal evolution of the pulse near the focus. An exact calculation of the focalization of a fs pulse by a singlet is presented in the subsection that follows.

In addition to the group delay effect, there is a direct temporal broadening of the pulse *in the lens itself* due to GVD in the lens material, as discussed in Section 1.5. Let us take again as an example the fused silica singlet of 30 mm focal length and

of 16 mm diameter used to focus a 248 nm laser beam to a 0.6 μm spot size. The broadening will be largest for the beam on axis, for which the propagation distance through glass is $L(r = 0) = d_0 = r_0^2/\{2f(n-1)\} = 2.1$ mm. Using for the second-order dispersion at 250 nm $\lambda d^2n/d\lambda^2 \approx 2.1\ \mu\text{m}^{-1}$ [23], we find from Eq. (1.136) that a 50 fs (FWHM) unchirped Gaussian pulse on axis will broaden to about 60 fs. If the pulse has an initial upchirp such that the parameter a defined in Eq. (1.41) is $a = -5$, it will broaden on axis to 160 fs. At a wavelength of 800 nm, where the dispersion is much smaller than in the UV (see Table 2.1), a bandwidth limited 50 fs pulse would only broaden to 50.4 fs.

The example above illustrates the differences between peak intensity reduction at the focal point of a lens resulting from the difference between group and phase velocity, and effects of group velocity dispersion in the lens material. The latter is strongly chirp dependent, while the former is not. The spread of pulse front arrival time in the focal plane is independent of the pulse duration and is directly related to the spot size that will be achieved (the effect is larger for optical arrangements with a large F-number). The *relative* broadening of the focus, $\propto \Delta T'/\tau_p$, is however larger for shorter pulses. The group velocity dispersion effect is pulse width dependent, and, in typical materials, becomes significant only for pulse durations well below 100 fs in the VIS and NIR spectral range.

2.4.2 Space-time distribution of the pulse intensity at the focus of a lens

The geometrical optical discussion of the focusing of ultrashort light pulses presented above gives a satisfactory order of magnitude estimate for the temporal broadening effects in the focal plane of a lens. We showed this type of broadening to be associated with chromatic aberration. Frequently the experimental situation requires an optimization not only with respect to the temporal characteristics of the focused pulse, but also with respect to the achievable spot size. To this aim we need to analyze the space-time distribution of the pulse intensity in the focal region of a lens in more detail. The general procedure is to solve either the wave equation (1.78), or better the corresponding diffraction integral[8], which in Fresnel approximation was given in Eq. (1.192). However, we cannot simply separate space and time dependence of the field with a product ansatz (1.188) since we expect the chromaticity of the lens to induce an interplay of both. Instead we will solve the diffraction integral for each "monochromatic" Fourier component of the input field $\tilde{E}_0(\Omega)$ which will result in the field distribution in a plane (x, y, z) behind the lens, $\tilde{E}(x, y, z, \Omega)$. The time-dependent field $\tilde{E}(x, y, z, t)$ then is obtained through

[8] For large F numbers the Fresnel approximation may no longer be valid, and the exact diffraction integral including the vector properties of the field should be applied.

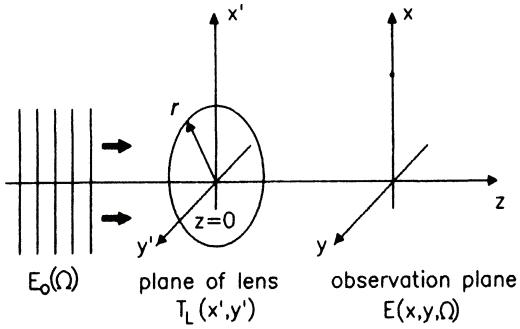

Figure 2.12: Diffraction geometry for focusing.

the inverse Fourier transform of $\tilde{E}(x,y,z,\Omega)$ so that we have for the intensity distribution:

$$I(x,y,z,t) \propto |\mathcal{F}^{-1}\{\tilde{E}(x,y,z,\Omega)\}|^2. \tag{2.44}$$

The geometry of this diffraction problem is sketched in Fig. 2.12. Assuming plane waves of amplitude $E_0(\Omega) = E_0(x',y',z'=0,\Omega)$ at the lens input, the diffraction integral to be solved reads, apart from normalization constants:

$$E(x,y,z,\Omega) \propto \frac{\Omega}{c}\int\int E_0(\Omega)T_L(x',y')T_A(x',y')e^{-i\frac{k}{2z}[(x'-x)^2+(y'-y)^2]}dx'dy' \tag{2.45}$$

where T_L and T_A are the transmission function of the lens and the aperture stop, respectively. The latter can be understood as the lens rim in the absence of other beam limiting elements. The lens transmission function describes a radially dependent phase delay which in case of a thin, spherical lens can be written:

$$T_L(x',y') = \exp\left\{-i\frac{\Omega}{c}\left[nL(r') + d_0 - L(r')\right]\right\} \tag{2.46}$$

with $r'^2 = x'^2 + y'^2$ and

$$L(r') = d_0 - \frac{r'^2}{2}\left(\frac{1}{R_1} - \frac{1}{R_2}\right) = d_0 - \frac{r'^2}{2(n-1)f}, \tag{2.47}$$

where d_0 is the thickness in the lens center. Note that because of the dispersion of the refractive index n, the focal length f becomes frequency dependent. For a spherical opening of radius r'_0 the aperture function T_A is simply:

$$T_A(r') = \begin{cases} 1 & \text{for} \quad x'^2 + y'^2 = r'^2 \le r'^2_0 \\ 0 & \text{otherwise} \end{cases} \tag{2.48}$$

If we insert Eq. (2.47) into Eq. (2.46) we can rewrite the lens transmission function as:

$$T_L(x',y') = \exp\left\{-i\left[k_g(\Omega)d_0 - \left(k_g(\Omega) - \frac{\Omega}{c}\right)\frac{r'^2}{2}\left(\frac{1}{R_1} - \frac{1}{R_2}\right)\right]\right\}, \tag{2.49}$$

where

$$k_g(\Omega) = \frac{\Omega}{c}n(\Omega) \tag{2.50}$$

is the wave vector in the glass material. Substituting this transmission function in the diffraction integral Eq.(2.45) we find for the field distribution in the focal plane:

$$\begin{aligned} E(\Omega) \;\propto\; & \frac{\Omega}{c}e^{-ik_g(\Omega)d_0}\iint T_A E_0(\Omega)\exp\left[i\left(k_g(\Omega) - \frac{\Omega}{c}\right)\frac{r'^2}{2}\left(\frac{1}{R_1} - \frac{1}{R_2}\right)\right] \\ & \times e^{-i\frac{k}{2z}\left[(x'-x)^2+(y'-y)^2\right]}dx'dy' \end{aligned} \tag{2.51}$$

The exponent of the second exponential function is radially dependent and is responsible for the focusing, while the first one describes propagation through a dispersive material of length d_0. For a closer inspection let us assume that the glass material is only weakly dispersive so that we may expand $k_g(\Omega)$ and $[k_g(\Omega) - \Omega/c]$ up to second order. In both exponential functions this will result in a sum of terms proportional to $(\Omega - \omega_\ell)^m$ $(m = 0, 1, 2)$. According to our discussion in the section about linear elements, optical transfer functions which have the structure $\exp[-ib_1(\Omega - \omega_\ell)]$ give rise to a certain pulse delay. Because b_1 is a function of r' this delay becomes radius dependent, a result which has already been expected from our previous ray-optical discussion. The next term of the expansion $(m = 2)$ is responsible for pulse broadening in the lens material.

A numerical evaluation of Eq. (2.51) and subsequent inverse Fourier transform [Eq. (2.44)] allows one to study the complex space-time distribution of the pulse intensity behind a lens. An example is shown in Fig. 2.13. In the aberration-free case we recognize a spatial distribution corresponding to the Airy disc and no temporal distortion. The situation becomes more complex if chromaticity plays a part. We see spatial as well as temporal changes in the intensity distribution. At earlier times the spatial distribution is narrower. This can easily be understood if we remember that pulses from the lens rim (or aperture edge) arrive first in the focal plane and are responsible for the field distribution. At later times pulses from inner parts of the lens arrive. The produced spot becomes larger since the effective aperture size is smaller. If we use achromatic doublets (cf. next Section 2.4.3) the exponential proportional to $(\Omega - \omega_\ell)$ in the corresponding diffraction integral does not appear. The only broadening then is due to GVD in the glass material.

Interesting effects occur if spherical aberration is additionally taken into account [26] which is essential to correctly model strong focusing with singlet lenses. As known from classical optics, spherical aberration results in different focal

Figure 2.13: Space-time distribution of the pulse intensity in the focal plane of a lens: (a) Focusing without chromatic or spherical aberration, (b) Focusing with chromatic aberration $\tau/T = 20$. The input pulse was chosen to vary as $e^{-(t/T)^2}$. v is the optical coordinate defined as $v = r_0' k_\ell \sqrt{x^2 + y^2}/f_\ell$ and $\tau = T'(r_0) = \left| \frac{r_0'^2 \lambda}{2fc(n-1)} n'(\lambda) \right|$ is a measure for the dispersion (from [25]). (c) Focusing with chromatic and spherical aberration. The intensity distribution in the plane of the marginal focus is shown (from [26]).

planes for beams passing through the lens at different r. Since ultrashort pulses passing through different lens annuli experience the same delay, almost no temporal broadening occurs for the light which is in focus, as illustrated in Fig. 2.13(c). The space-time distribution in the focal area can differ substantially from that obtained with a purely chromatic lens.

To measure the interplay of chromatic and spherical aberration in focusing ultrashort light pulses, one can use an experimental setup as shown in Fig. 2.14(a). The beam is expanded and sent into a Michelson interferometer. One arm contains the lens to be characterized, which can be translated so as to focus light passing through certain lens annuli onto mirror M_1. Provided the second arm has the proper length, an annular interference pattern can be observed at the output of the interferometer. The radius of this annulus is determined by the setting of Δf. If no spherical aberration is present, an interference pattern is observable only for $\Delta f \approx 0$ and a change of the time delay by translating M_2 would change the radius of the interference pattern. With spherical aberration present, at a certain Δf, an interference pattern occurs only over a delay corresponding to the pulse duration while the radius of the annulus remains constant. This can be proved by measuring the cross-correlation, i.e., by measuring the second harmonic signal as function of the time delay. The width of the cross-correlation does not differ from the width of the autocorrelation which is measured without the lens in the interferometer arm. Figure 2.14(b) shows the position of the peak of the cross-correlation as function of Δf and the corresponding r, respectively. For comparison, the delay associated with chromatic aberration alone is also shown (dashed curve).

2.4.3 Achromatic doublets

The chromaticity of a lens was found to be the cause for a radial dependence of the time of arrival of the pulse at the focal plane, as was shown by Eq.(2.40). Therefore one should expect achromatic optics to be free of this undesired pulse lengthening. To verify that this is indeed the case, let us consider the doublet shown in Fig. 2.15. The thicknesses of glass traversed by the rays in the media of index n_1 and n_2 are L_1 and L_2 and are given by:

$$L_1 = d_1 - \frac{r^2}{2}\left(\frac{1}{R_1} - \frac{1}{R_2}\right) \tag{2.52}$$

and

$$L_2 = d_2 - \frac{r^2}{2}\left(\frac{1}{R_2} - \frac{1}{R_3}\right) \tag{2.53}$$

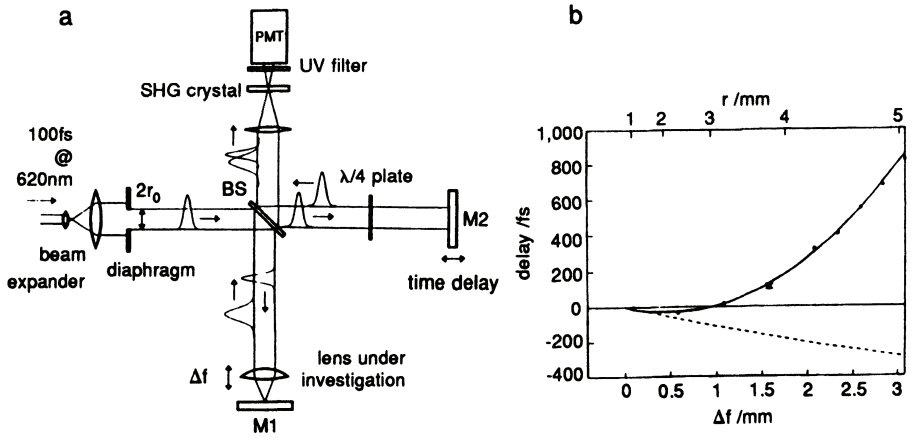

Figure 2.14: (a) Correlator for measuring the effect of chromatic and spherical aberration on the focusing of fs pulses. (b) Measured pulse delay (data points) as a function of the lens position (Δf — deviation from the paraxial focus) and the corresponding radial coordinate r of light in focus. The solid line is obtained with ray–pulse tracing; the dashed curve shows the effect of chromatic aberration only. Lens parameters: $f_0 = 12.7$ mm, BK7 glass (from [27]).

where $d_{1,2}$ is the center thickness of lens 1,2. The inverse of the focal length of the doublet lens is:

$$\frac{1}{f} = (n_1 - 1)\left(\frac{1}{R_1} - \frac{1}{R_2}\right) + (n_2 - 1)\left(\frac{1}{R_2} - \frac{1}{R_3}\right). \tag{2.54}$$

The condition of achromaticity $\frac{d}{d\lambda}(1/f) = 0$ gives an additional relation between the radii of curvature R_i and the indices n_i. The expression for the transit time in glass [23] in which we have inserted the chromaticity of the doublet is:

$$\boxed{T(r) = \frac{d_1}{c}\left\{n_1 - \lambda\frac{dn_1}{d\lambda}\right\} + \frac{d_2}{c}\left\{n_2 - \lambda\frac{dn_2}{d\lambda}\right\} + \frac{\lambda r^2}{2c}\frac{d}{d\lambda}\left(\frac{1}{f}\right).} \tag{2.55}$$

Equation (2.55) indicates that, for an achromatic doublet for which the third term on the right hand side vanishes, the transit time has no more radial dependence. The phase front and wave front are thus parallel, as sketched in Fig. 2.15. In this case, the only mechanism broadening the pulse at the focus is group velocity dispersion. The latter can be larger than with singlet lenses since achromatic doublets usually contain more glass.

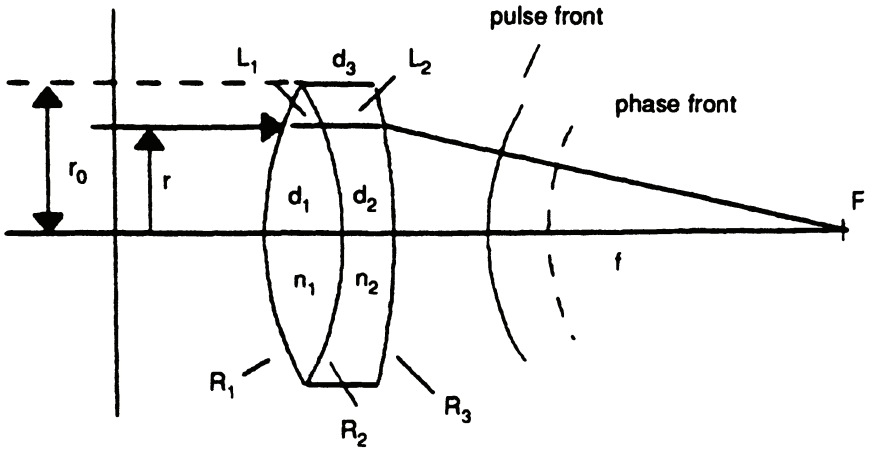

Figure 2.15: Ray tracing in an achromat (from [23]).

2.4.4 Focusing mirrors

Another way to avoid the chromatic aberration and thus pulse broadening is to use mirrors for focusing. With spherical mirrors and on-axis focusing the first aberration to be considered is the spherical one. The analysis of spherical aberration of mirrors serves also as a basis to the study of spherical aberration applied to lenses.

Let us consider the situation of Fig. 2.16, where a plane pulse- and wavefront impinge upon a spherical mirror of radius of curvature R. The reflected rays are the tangents of a caustic — the curve commonly seen as light reflects off a coffee cup. Rays that are a distance r off-axis intersect the optical axis at point T which differs from the paraxial focus F in the paraxial focal plane Σ'. The difference in arrival time between pulses travelling along off-axis rays and on-axis pulses in the paraxial focal plane is:

$$\Delta T = \frac{1}{c}\left[\overline{VQ} - \left(\overline{PS} + \frac{R}{2}\right)\right]. \tag{2.56}$$

Through simple geometrical considerations on can find an expression for ΔT in the form of an expansion in powers of (r/R). The first non-zero term of that expansion is:

$$\Delta T = \frac{3}{4}\frac{R}{c}\left(\frac{r}{R}\right)^4. \tag{2.57}$$

Likewise, one obtains for the geometrical deviation from the paraxial focus in Σ':

$$x = \frac{R}{2}\left(\frac{r}{R}\right)^3. \tag{2.58}$$

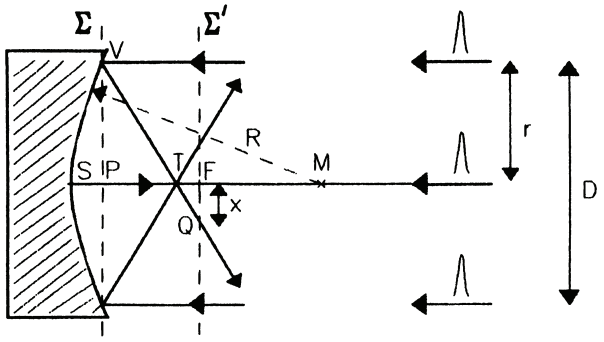

Figure 2.16: Focusing of light pulses by a spherical mirror.

For a beam diameter $D = 3$ mm and a focal length $f = 25$ mm the arrival time difference amounts to only 0.1 fs and the deviation from the paraxial focus $x \approx 1$ μm. The numbers increase rapidly with beam size; $\Delta T \approx 13$ fs, $x \approx 25$ μm for $D = 10$ mm, for example.

In experimental situations where even a small aberration should be avoided, parabolic mirrors can advantageously be used to focus collimated input beams. An example requiring such optics is upconversion experiments where fluorescence with fs rise time from a large solid angle has to be focused tightly, without modifying its temporal behavior. Elliptical mirrors should be used to focus light emerging from a point source. However, since parabolic mirrors are more readily available, a combination of parabolic mirrors may be used in lieu of an ellipsoid.

2.5 Elements with angular dispersion

2.5.1 Introduction

Besides focusing elements there are various other optical components which modify the temporal characteristics of ultrashort light pulses through a change of their spatial propagation characteristics.

Even a simple prism can provide food for thought in fs experiments. Let us consider an expanded parallel beam of short light pulses incident on a prism, and diffracted by the angle $\beta = \beta(\Omega)$, as sketched in Fig. 2.17. As discussed in Chapter 1, a Gaussian beam with beam waist w_0 self diffracts by an angle of approximately $\theta = \lambda/\pi w_0$. In the case of a short pulse (or white light), this diffraction has to be combined with a spectral diffraction, since the light is no longer monochromatic, and different spectral components will be deflected by the prism with a different angle $\beta = \beta(\Omega)$. If the pulse is sufficiently short, both effects are of the

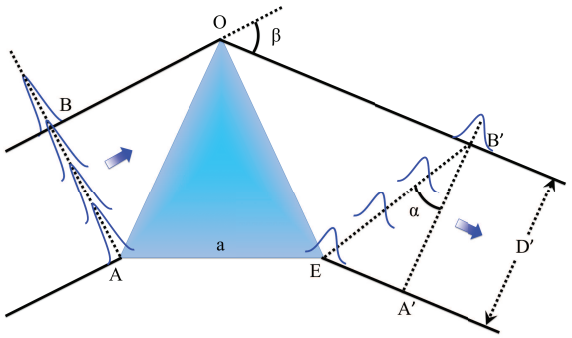

Figure 2.17: Pulse front tilt introduced by a prism. The position of the (plane) wavefronts is indicated by the dashed lines $\overline{AB}$ and $\overline{A'B'}$.

same order of magnitude, resulting in a complex space-time problem that can no longer be separated. Throughout this section, whether considering group delays or group velocity dispersion, we will consider sufficiently broad beams, and sufficiently short propagation distances L_p behind the prism. This will allow us to neglect the change in beam diameter due to propagation and spectral diffraction after the prism. In most cases we will also approximate the beam with a flat profile. At the end of this chapter the interplay of of propagation and spectral diffraction effects will be discussed for Gaussian beams.

As discussed by Bor *et al.* [24], the prism introduces a tilt of the pulse front with respect to the phase front. As in lenses, the physical origin of this tilt is the difference between group and phase velocity. According to Fermat's principle the prism transforms a phase front $\overline{AB}$ into a phase front $\overline{A'B'}$. The transit times for the phase and pulse fronts along the marginal ray $\overline{BOB'}$ are equal ($v_p \sim v_g$ in air). In contrast the pulse is delayed with respect to the phase in any part of the ray that travels through a certain amount of glass. This leads to an increasing delay across the beam characterized by a certain tilt angle α. The maximum arrival time difference in a plane perpendicular to the propagation direction is $(D'/c)\tan\alpha$.

Before discussing pulse front tilt more thoroughly, let us briefly mention another possible prism arrangement where the above condition for L_p is not necessary. Let us consider for example the symmetrical arrangement of four prisms sketched in Fig. 2.18. During their path through the prism sequence, different spectral components travel through different optical distances. At the output of the fourth prism all these components are again equally distributed in one beam. The net effect of the four prisms is to introduce a certain amount of GVD leading to broadening of an unchirped input pulse. We will see later in this chapter that this particular GVD can be interpreted as a result of angular dispersion and can have a sign opposite to

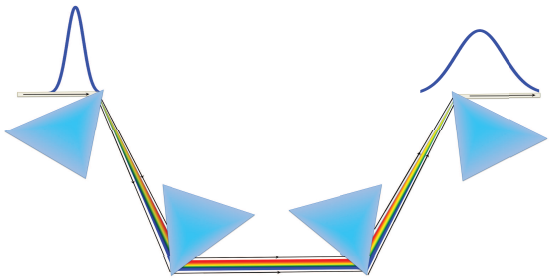

Figure 2.18: Pulse broadening in a four prism sequence.

that of the GVD introduced by the glass material constituting the prisms.

2.5.2 Tilting tilt of pulse fronts of pulse fronts

In an isotropic material the direction of energy flow — usually identified as ray direction — is always orthogonal to the surfaces of constant phase (*wave fronts*) of the corresponding propagating wave. In the case of a beam consisting of ultrashort light pulses, one has to consider in addition planes of constant intensity (*pulse fronts*). For most applications it is desirable that these pulse fronts be parallel to the phase fronts and thus orthogonal to the propagation direction. In the section on focusing elements we have already seen how lenses cause a radially dependent difference between pulse and phase fronts. This leads to a temporal broadening of the intensity distribution in the focal plane. There are a number of other optical components which introduce a tilt of the pulse front with respect to the phase front and to the normal of the propagation direction, respectively. One example was the prism discussed in the introduction of this section. As a general rule, the pulse front tilting should be avoided whenever an optimum focalization of the pulse energy is sought. There are situations where the pulse front tilt is desirable to transfer a temporal delay to a transverse coordinate. Applications exploiting this property of the pulsefront tilt are pulse diagnostics (Chapter **??**) and travelling wave amplification (Chapter **??**).

The general approach for tilting pulse fronts is to introduce an optical element in the beam path which retards the pulse fronts as a function of a coordinate transverse to the beam direction. This is schematically shown in Fig. 2.19 for an element that changes only the propagat ion direction of a (plane) wave. Let us assume that a wavefront $\overline{AB}$ is transformed into a wavefront $\overline{A'B'}$. From Fermat's principle it follows that the optical pathlength P_{OL} between corresponding points at the wavefronts $\overline{AB}$ and $\overline{A'B'}$ must be equal:

$$P_{OL}(BB') = P_{OL}(PP') = P_{OL}(AA'). \tag{2.59}$$

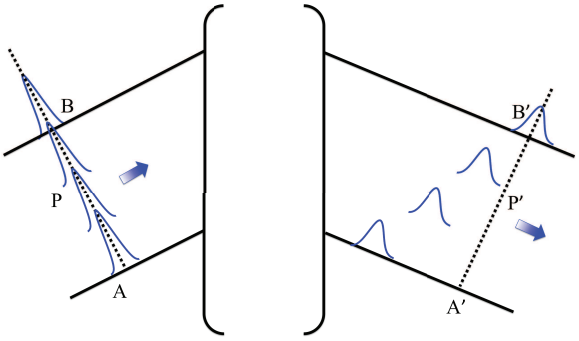

Figure 2.19: Delay of the pulse front with respect to the phase front.

Since the optical pathlength corresponds to a phase change $\Delta\Phi = 2\pi P_{OL}/\lambda$, the propagation time of the wavefronts can be written as

$$T_{phase} = \frac{\Delta\Phi}{\omega_\ell} \tag{2.60}$$

where we referred to the center frequency of the pulse. This phase change is given by

$$\Delta\Phi = \int_P^{P'} k(s)ds = \frac{\omega_\ell}{c}\int_P^{P'} n(s)ds = \omega_\ell \int_P^{P'} \frac{ds}{v_p(s)} \tag{2.61}$$

where s is the coordinate along the beam direction. In terms of the phase velocity the propagation time is

$$T_{phase} = \int_P^{P'} \frac{ds}{v_p(s)}. \tag{2.62}$$

The propagation time of the pulse fronts however, T_{pulse}, is determined by the group velocity

$$T_{pulse} = \int_P^{P'} \frac{ds}{v_g(s)} = \int_P^{P'} \left|\frac{dk}{d\Omega}\right|_{\omega_\ell} ds. \tag{2.63}$$

From Eqs. (2.62) and (2.63) the difference in propagation time between phase front and pulse front becomes

$$\Delta T(P,P') = T_{phase} - T_{pulse} = \int_P^{P'} \left(\frac{1}{v_p} - \frac{1}{v_g}\right) ds = \int_P^{P'} \left[\frac{k_\ell}{\omega_\ell} - \left.\frac{dk}{d\Omega}\right|_{\omega_\ell}\right] ds, \tag{2.64}$$

which can be regarded as a generalization of Eq. (2.37).

A simple optical arrangement to produce pulse front tilting is an interface separating two different optical materials – for instance air (vacuum) and glass

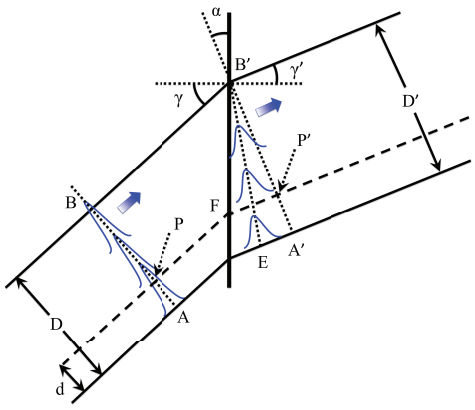

Figure 2.20: Pulse front tilt through refraction at an interface.

(Fig. 2.20). At the interface F the initial beam direction is changed by an angle $\beta = \gamma - \gamma'$ where γ and γ' obey Snell's law $\sin\gamma = n(\omega_\ell)\sin\gamma'$. The point A of an incident wavefront $\overline{AB}$ is refracted at time $t = t_0$. It takes the time interval T_{phase} to recreate the wavefront $\overline{A'B'}$ in medium 2, which propagates without distortion with a phase velocity $v_p = c/n(\omega_\ell)$. The time interval T_{phase} is given by

$$T_{phase} = \frac{n\overline{AA'}}{c} = \frac{\overline{BB'}}{c} = \frac{\overline{PF} + n\overline{FP'}}{c} = \frac{D\,\tan\gamma}{c}. \tag{2.65}$$

The beam path from B to B' is through a nondispersive material and thus pulse front and wavefront coincide at B'. In contrast the phase front and pulse front propagate different distances during the time interval T_{phase} in medium 2 and thus become separated. Since in (most) optical materials the group velocity is smaller than the phase velocity the pulse front is delayed with respect to the phase front. In our case this delay increases linearly over the beam cross section. The characteristic tilt angle α between pulse and phase fronts is given by

$$\tan\alpha = \frac{\overline{EA'}}{D'}. \tag{2.66}$$

From simple geometrical considerations we find for the two distances

$$\overline{EA'} = \left(\frac{c}{n} - v_g\right) T_{phase} = \left(\frac{c}{n} - v_g\right) \frac{D}{c} \tan\gamma \tag{2.67}$$

and

$$D' = D\frac{\cos\gamma'}{\cos\gamma} = D\frac{\sqrt{n^2 - \sin^2\gamma}}{n\cos\gamma}. \tag{2.68}$$

Inserting Eqs. (2.67) and (2.68) in Eq. (2.66) and using the expression for the group velocity, we obtain for α

$$\tan\alpha = \frac{\omega_\ell n'(\omega_\ell)}{\omega_\ell n'(\omega_\ell) + n(\omega_\ell)} \frac{\sin\gamma}{\sqrt{n^2 - \sin^2\gamma}}. \tag{2.69}$$

Following this procedure we can also analyze the pulse front at the output of a prism, cf. Fig. 2.17. The distance $\overline{EA'}$ is the additional pathlength over which the phase has travelled as compared to the pulse path. Thus, we have

$$\overline{EA'} = v_p \left[\frac{a}{v_g} - \frac{a}{v_p}\right] = a\omega_\ell n'(\omega_\ell) \tag{2.70}$$

which results in a tilt angle

$$\tan\alpha = \frac{a}{b}\omega_\ell n'(\omega_\ell) = -\frac{a}{b}\lambda_\ell \left.\frac{dn}{d\lambda}\right|_{\lambda_\ell} \tag{2.71}$$

where $b = D'$ is the beam width.

As pointed out by Bor [24], there is a general relation between pulse front tilt and the angular dispersion $d\beta/d\lambda$ of a dispersive device which reads

$$\boxed{\tan\alpha = \lambda\left|\frac{d\beta}{d\lambda}\right|.} \tag{2.72}$$

The latter equation can be proven easily for a prism, by using the equation for the beam deviation, $d\beta/d\lambda = (a/b)(dn/d\lambda)$, in Eq. (2.71). Similarly to prisms, gratings produce a pulse front tilt, as can be verified easily from the sketch of Fig. 2.21. To determine the tilt angle we just need to specify the angular dispersion in Eq. (2.72) using the grating equation.

2.5.3 GVD through angular dispersion!angular dispersion — General

Angular dispersion has been advantageously used for a long time to resolve spectra or for spectral filtering, utilizing the spatial distribution of the frequency components behind the dispersive element (e.g., prism, grating). In connection with fs optics, angular dispersion has the interesting property of introducing GVD. At first glance this seems to be an undesired effect. However, optical devices based on angular dispersion, which allow for a continuous tuning of the GVD can be designed. This idea was first implemented in [28] for the compression of chirped pulses with diffraction gratings. The concept was later generalized to prisms and

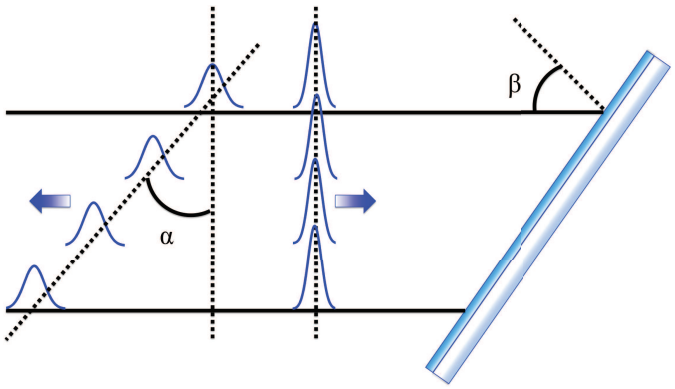

Figure 2.21: Pulse front tilt produced by diffraction at a grating in Littrow configuration.

prism sequences [29]. Simple expressions for two and four prism sequences are given in [30, 31]. From a general point of view, the diffraction problem can be treated by solving the corresponding Fresnel integrals [28, 32, 33]. We will sketch this procedure at the end of this chapter. Another successful approach is to analyze the sequence of optical elements by ray-optical techniques and calculate the optical beam path P as a function of Ω. From our earlier discussion we expect the response of any linear element to be of the form:

$$R(\Omega)e^{-i\Psi(\Omega)} \tag{2.73}$$

where the phase delay Ψ is related to the optical pathlength P_{OL} through

$$\Psi(\Omega) = \frac{\Omega}{c} P_{OL}(\Omega). \tag{2.74}$$

$R(\Omega)$ is assumed to be constant over the spectral range of interest and thus will be neglected.

We know that non-zero terms $[(d^n/d\Omega^n)\Psi \neq 0]$ of order $n \geq 2$ are responsible for changes in the complex pulse envelope. In particular

$$\frac{d^2}{d\Omega^2}\Psi(\Omega) = \frac{1}{c}\left(2\frac{dP_{OL}}{d\Omega} + \Omega\frac{d^2P_{OL}}{d\Omega^2}\right) = \frac{\lambda^3}{2\pi c^2}\frac{d^2P_{OL}}{d\lambda^2} \tag{2.75}$$

is related to the GVD parameter. We recall that, with the sign convention chosen in Eq. (2.73), the phase factor Ψ has the same sign as the phase factor $k_\ell L$. Consistent with the definition given in Eq. (1.128) a positive GVD corresponds to $\frac{d^2\Psi}{d\Omega^2} > 0$. In this chapter, we will generally express $\frac{d^2\Psi}{d\Omega^2}$ in fs^2.

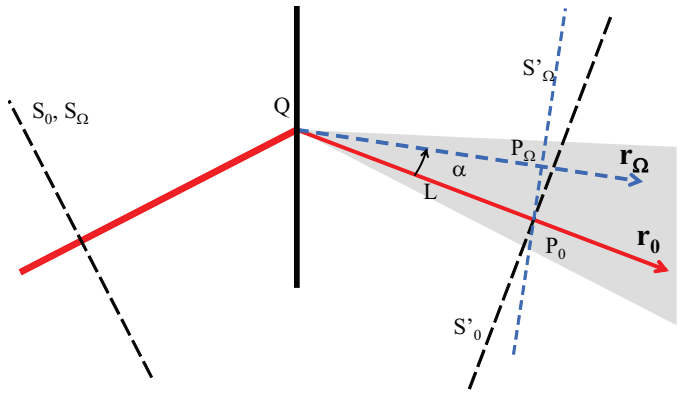

Figure 2.22: Angular dispersion causes GVD. The solid line in the middle of the figure represents the angular dispersive element, providing a frequency dependent deflection of the beam at the point of incidence Q. The different frequency components of the pulse spread out in the patterned area.

The relation between angular dispersion and GVD can be derived through the following intuitive approach. Let us consider a light ray which is incident onto an optical element at point Q, as in Fig. 2.22. At this point we do not specify the element, but just assume that it causes angular dispersion. Thus, different spectral components originate at Q under different angles, within a cone represented by the patterned area in the figure. Two rays corresponding to the center frequency ω_ℓ of the spectrum, $\vec{r}_0$, and to an arbitrary frequency Ω, $\vec{r}_\Omega$, are shown in Fig. 2.22. The respective wavefronts S are labelled with subscript "0" (for the central frequency ω_ℓ) and "Ω" (for the arbitrary frequency Ω). The planes S_Ω, S_0 and S'_Ω, S'_0 are perpendicular to the ray direction and represent (plane) wave fronts of the incident light and diffracted light, respectively. Let P_0 be our point of reference and be located on $\vec{r}_0$ where $\overline{QP_0} = L$. A wavefront S'_Ω of $\vec{r}_\Omega$ at P_Ω is assumed to intersect $\vec{r}_0$ at P_0. The optical pathlength $\overline{QP_\Omega}$ is thus

$$\overline{QP_\Omega} = P_{OL}(\Omega) = P_{OL}(\omega_\ell)\cos\alpha = L\cos\alpha \tag{2.76}$$

which gives for the phase delay

$$\Psi(\Omega) = \frac{\Omega}{c}P_{OL}(\Omega) = \frac{\Omega}{c}L\cos\alpha \tag{2.77}$$

The dispersion constant responsible for GVD is obtained by twofold derivation with respect to Ω:

$$\begin{aligned}\left.\frac{d^2\Psi}{d\Omega^2}\right|_{\omega_\ell} &= -\frac{L}{c}\left\{\sin\alpha\left[2\frac{d\alpha}{d\Omega}+\Omega\frac{d^2\alpha}{d\Omega^2}\right]+\Omega\cos\alpha\left(\frac{d\alpha}{d\Omega}\right)^2\right\}\Bigg|_{\omega_\ell} \\ &\approx -\frac{L\omega_\ell}{c}\left(\left.\frac{d\alpha}{d\Omega}\right|_{\omega_\ell}\right)^2 \end{aligned} \tag{2.78}$$

where $\sin\alpha = 0$ and $\cos\alpha = 1$ if we take the derivatives at the center frequency of the pulse, $\Omega = \omega_\ell$. The quantity $(d\alpha/d\Omega)|_{\omega_\ell}$, responsible for angular dispersion, is a characteristic of the actual optical device to be considered. It is interesting to note that the dispersion parameter is always negative independently of the sign of $d\alpha/d\Omega$ and that the dispersion increases with increasing distance L from the diffraction point. Therefore angular dispersion always results in negative GVD. Differentiation of Eq. (2.78) results in the next higher dispersion order

$$\begin{aligned}\left.\frac{d^3\Psi}{d\Omega^3}\right|_{\omega_\ell} &= -\frac{L}{c}\left\{\cos\alpha\left[3\left(\frac{d\alpha}{d\Omega}\right)^2+3\Omega\frac{d\alpha}{d\Omega}\frac{d^2\alpha}{d\Omega^2}\right]\right. \\ &+ \left.\sin\alpha\left[3\frac{d^2\alpha}{d\Omega^2}+\Omega\frac{d^3\alpha}{d\Omega^3}-\Omega\left(\frac{d\alpha}{d\Omega}\right)^3\right]\right\}\Bigg|_{\omega_\ell} \\ &\approx -\frac{3L}{c}\left[\left(\frac{d\alpha}{d\Omega}\right)^2+\Omega\frac{d\alpha}{d\Omega}\frac{d^2\alpha}{d\Omega^2}\right]\Bigg|_{\omega_\ell}, \end{aligned} \tag{2.79}$$

where the last expression is a result of $\alpha(\omega_\ell) = 0$.

The most widely used optical device for angular dispersion are prisms and gratings. To determine the dispersion introduced by them we need to specify not only the quantity $\alpha(\Omega)$ in the expressions derived above, but also the optical surfaces between which the path is being calculated. Indeed, we have assumed in the previous calculation that the beam started as a plane wave (plane reference surface normal to the initial beam) and terminates in a plane normal to the ray at a reference optical frequency ω_ℓ. The choice of that terminal plane is as arbitrary as that of the reference frequency ω_ℓ (cf. Chapter 1, Section 1.1.1). After some propagation distance, the various spectral component of the pulse will have separated, and a finite size detector will only record a portion of the pulse spectrum.

Therefore, the "dispersion" of an element has only meaning in the context of a particular application, that will associate reference surfaces to that element. This is the case when an element is associated with a cavity, as will be considered in the next section. In the following sections, we will consider combinations of elements of which the angular dispersion is compensated. In that case, a natural reference surface is the normal to the beam.

2.5.4 GVD of a cavity containing a single prism dispersion!prism

Dispersion control is an important aspect in the development of fs sources. The most elementary laser cavity as sketched in Fig. 2.23 has an element with angular dispersion. The dispersive element could be the Brewster angle laser rod itself. The cavity will be typically terminated by a curved mirror. The two reference surfaces to consider are the two end-mirror of the cavity. We have seen that negative GVD is typically associated with angular dispersion, and positive GVD with the propagation through a glass prism or laser rod [9]. One might therefore expect to be able to tune the GVD in the arrangement of Fig. 2.23 from a negative to a positive value. An exact calculation of the frequency dependence presented below shows that this is not the case, and that the GVD of this cavity is always positive.

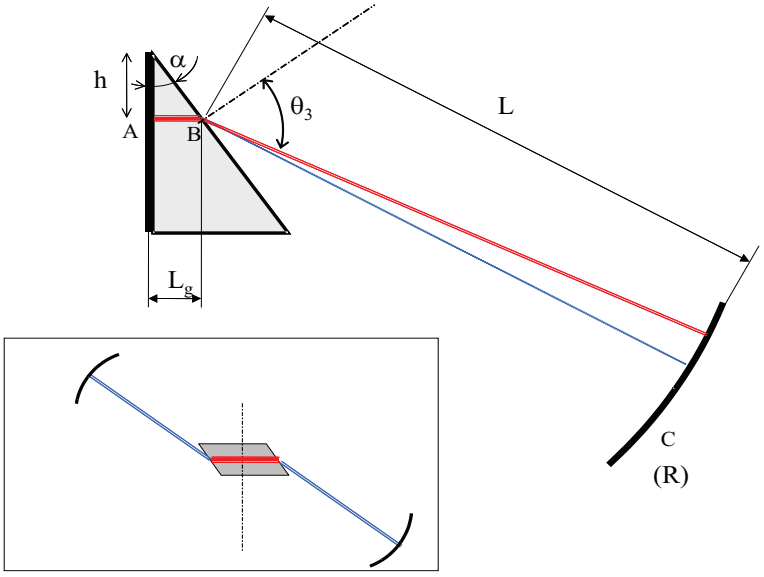

Figure 2.23: Example of a cavity with a single right angle prism. The side of the right angle is an end mirror of the cavity. The cavity is terminated by a curved mirror of radius of curvature R, at a distance L from the Brewster angle exit face of the prism. Stability of the cavity requires that $L + \overline{AB}/n < R$. Translation of the prism allows for an adjustment of the pathlength in glass L_g. The inset shows that this calculation applies to a symmetric cavity with a Brewster-angle laser rod and two spherical mirrors.

A combination of elements with a tunable positive dispersion can also be desirable in a fs laser cavity. We will consider the case of the linear cavity sketched in

[9] It is generally the case — but not always — that optical elements in the visible have positive GVD.

Fig. 2.23, whose GVD can be solved analytically.

The cavity is terminated on one end by the plane face of the prism, on the other end by a spherical mirror of curvature R. The prism–mirror distance measured at the central frequency ω_ℓ is L. The beam originates from a distance h from the apex of the prism (angle α), such that the pathlength in glass can be written as $L_g = h\tan\alpha$. For the sake of notation simplification, we define:

$$\begin{aligned} a &= \frac{h\tan\alpha}{c} \\ b &= \frac{L}{2}\left(1-\frac{L}{R}\right). \end{aligned} \tag{2.80}$$

The total phase shift for one half cavity round-trip is $\Psi(\Omega) = \Psi_{AB}(\Omega) + \Psi_{BC}(\Omega)$. The phase shift through the glass here is simply $-k(\Omega)L_g = -\Psi_{AB}(\Omega)$, with $\Psi_{AB}(\Omega)$ given by:

$$\begin{aligned} \Psi_{AB}(\Omega) &= \Psi_0 + \left.\frac{d\Psi}{d\Omega}\right|_{\omega_\ell}\Delta\Omega + \frac{1}{2}\left.\frac{d^2\Psi}{d\Omega^2}\right|_{\omega_\ell}(\Delta\Omega)^2 + \ldots \\ &\approx \Psi_0 + a\left[\Omega\frac{dn}{d\Omega} + n(\Omega)\right]_{\omega_\ell}\Delta\Omega + \frac{1}{2}a\left[2\frac{dn}{d\Omega} + \Omega\frac{d^2n}{d\Omega^2}\right]_{\omega_\ell}(\Delta\Omega)^2, \end{aligned} \tag{2.81}$$

where $\Delta\Omega = \Omega - \omega_\ell$. For the path in air, we have a phase shift $-k\overline{BC} = -\Psi_{BC}(\Omega)$, with

$$\Psi_{BC}(\Omega) = \frac{\Omega}{c}\left[L + \frac{L}{2}\left(1-\frac{L}{R}\right)\Delta\theta^2\right] = \frac{\Omega}{c}\left[L + b\Delta\theta^2\right], \tag{2.82}$$

where $\Delta\theta$ is the departure of dispersion angle from the diffraction angle at ω_ℓ. Within the small angle approximation, we have for $\Delta\theta$:

$$\Delta\theta \approx \Delta\Omega\frac{\sin\alpha}{\cos\theta_3}\frac{dn(\Omega)}{d\Omega} = \Delta\Omega\frac{dn(\Omega)}{d\Omega}. \tag{2.83}$$

The last equality ($\sin\alpha = \cos\theta_3$) applies to the case where θ_3 equals the Brewster angle. The GVD dispersion of this cavity is thus:

$$\left.\frac{d^2\Psi}{d\Omega^2}\right|_{\omega_\ell} = \left.\frac{d^2\Psi_{AB}}{d\Omega^2}\right|_{\omega_\ell} + \left.\frac{d^2\Psi_{BC}}{d\Omega^2}\right|_{\omega_\ell} = a\left(2\frac{dn}{d\Omega} + \Omega\frac{d^2}{d\Omega^2}\right)_{\omega_\ell} + \frac{2b\omega_\ell}{c}\left(\left.\frac{dn}{d\Omega}\right|_{\omega_\ell}\right)^2, \tag{2.84}$$

or, using the wavelength dependence of the index of refraction, and taking into account that, for the Brewster prism, $\tan\alpha = 1/n(\omega_\ell)$:

$$\left.\frac{d^2\Psi}{d\Omega^2}\right|_{\omega_\ell} = \frac{h}{nc}\left(\frac{\lambda}{2\pi c}\right)\left(\lambda^2\frac{d^2n}{d\lambda^2}\right)\Bigg|_{\lambda_\ell} + b\frac{\lambda^3}{\pi c^2}\left(\frac{dn}{d\lambda}\right)^2\Bigg|_{\lambda_\ell} \tag{2.85}$$

The stability of the cavity requires that $R > L$, and that the coefficients a and b be positive. In the visible range, most glasses have a positive GVD dispersion ($k" > 0$ or $d^2n/d\lambda^2 > 0$). Therefore, in a cavity with a single prism as sketched in Fig. 2.23, the group velocity dispersion is adjustable through the parameter h, but always positive.

The calculation above applies to a simple solid state laser cavity as sketched in the inset of Fig.2.23, with a Brewster angle laser rod. The contribution to the dispersion from each side of the dash-dotted line are additive. Even in this simple example, we see that the total dispersion is not only due to the propagation through the glass, but there is also another contribution due to angular dispersion. It is interesting to compare Eqs. (2.78), which gives a general formula associated with angular dispersion, with Eq. (2.85). Both expression involve the square of the angular dispersion, but with opposite sign.

Femtosecond pulses have been obtained through adjustable GVD compensation with a single prism in a dye ring laser cavity [34]. As in the case of Fig. 2.23, the spectral narrowing that would normally take place because of the angular dispersion of the prism was neutralized by having the apex of the prism at a waist of the resonator. In that particular case, the adjustable positive dispersion of the prism provided pulse compression because of the negative chirp introduced by saturable absorption below resonance, as detailed in Chapter **??**.

2.5.5 Group velocity control with pairs of prisms ixdispersion !prism

Pairs of elements

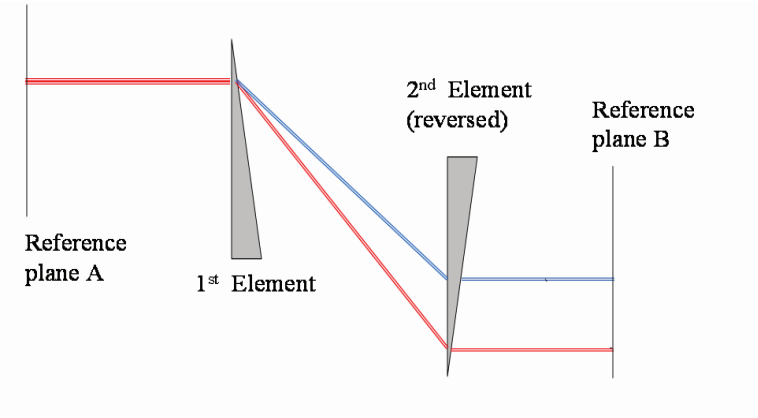

Figure 2.24: Pair of elements with angular dispersion arranged for zero net angular dispersion. The elements are most often prisms or gratings.

In most applications, a second element will be associated to the first one, such that the angular dispersion introduced by the first element is compensated, and all frequency components of the beam are parallel again, as sketched in Fig. 2.24. The elements will generally be prisms or gratings.

As before, we start from a first reference surface A normal to the beam. It seems then meaningful to chose the second reference surface B at the exit of the system that is normal to the beam. There is no longer an ambiguity in the choice of a reference surface, as in the previous section with a single dispersive element. At any particular frequency, Fermat's principle states that the optical pathes are equal from a point of the wavefront A to the corresponding point on the wavefront B. This is not to say that these distances are not frequency dependent. The spectral components of the beam are still separated in the transverse direction. For that reason, a pair of prisms or gratings provides a way to "manipulate" the pulse spectrum by spatially filtering (amplitude or phase filter) the various Fourier components.

Calculation for matched isosceles prisms.

One of the most commonly encountered case of Fig. 2.24, is that where the two angular dispersive elements are isosceles prisms. Prisms have the advantage of smaller insertion losses, which is particularly important with the low gain solid state lasers used for fs applications.

There are numerous contributions to the group velocity dispersion that makes this problem rather complex:

a) Group velocity dispersion due to propagation in glass for a distance L.

b) Group velocity dispersion introduced by the changes in optical path L in each prism, due to angular dispersion.

c) Group velocity dispersion due to the angular dispersion after one prism, propagation of the beam over a distance ℓ, and as a result propagation through different thicknesses of glass at the next prism.

These considerations by themselves are sufficient to write an expression for the second order dispersion of a pair of prism, using the properties established earlier in this chapter for the relation between angular dispersion and second order dispersion. This expression differs from the most commonly used expression for calculation the dispersion of a pair of prisms [30]. The shortcomings of the latter expressions are:

- The expression of Fork and Gordon [30] implies that the separation between the prisms has both a positive and negative effect, which is not correct.

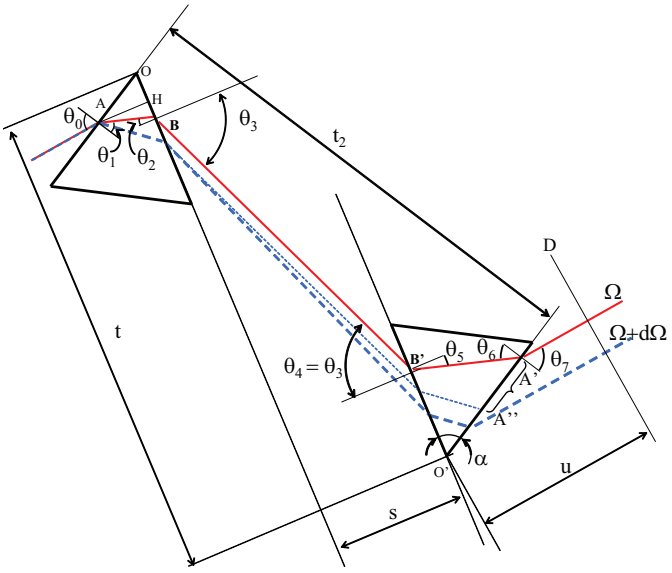

Figure 2.25: Typical two prisms sequence as used in fs laser cavities. The relative position of the prisms is defined by the distance t and the spacing s between the parallel faces OB and $O'B'$. The initial beam enters the prism at a distance $\overline{OA} = a$ from the apex. The distance t_2 between the parallel faces OA and $O'A'$ is $t_2 = t\sin\alpha + s\cos\alpha$. The solid line $ABB'A'D$ traces the beam path at an arbitrary frequency Ω. The beam at the frequency upshifted by $d\Omega$ is represented by the dashed line. The dotted line indicates what the optical path would be in the second prism, if the distance $\overline{BB'}$ were reduced to zero (this situation is detailed in Fig. B.1). "D" is a point on the phase front a distance u from the apex O' of the second prism. In most cases we will associate the beam path for a ray at Ω with the path of a ray at the center frequency ω_ℓ.

- The only optical path considered is that between the two prisms; the beam displacement after the second prism is not calculated.
- The expression applies only for the case of tip to tip propagation in the prisms

In addition to the simple derivation based on the properties of angular dispersion, a rigorous derivation has been made by calculating exactly the optical pathways between parallel wavefronts before and after the pair of prisms [35]. The details of this calculation are reproduced in Appendix B. The result is in agreement with the easily derivable equation based on the properties (a), (b) and (c) cited above:

$$\begin{aligned}\left.\frac{d^2\Psi}{d\Omega^2}\right|_{\omega_\ell} &= \frac{L_g}{c}\left[2\left.\frac{dn}{d\Omega}\right|_{\omega_\ell}+\omega_\ell\left.\frac{d^2n}{d\Omega^2}\right|_{\omega_\ell}\right] \\ &\quad -\frac{\omega_\ell}{c}(L)\left(\left.\frac{d\theta_3}{d\Omega}\right|_{\omega_\ell}\right)^2-\frac{n\omega_\ell}{c}L_g\left(\left.\frac{d\theta_1}{d\Omega}\right|_{\omega_\ell}\right)^2 \end{aligned} \quad (2.86)$$

This equation applies to any pair of identical isosceles prisms in the parallel face configuration represented in Fig. 2.25, for an arbitrary angle of incidence. L is the distance between prisms along the beam at ω_ℓ, and L_g is the total distance of glass traversed. The group velocity dispersion is simply the sum of three contributions:

1. The (positive) GVD due to the propagation of the pulse through a thickness of glass L_g.
2. The negative GVD contribution due to the angular dispersion $d\theta_3/d\Omega$ applied to Eq. (2.78) over a distance $\overline{BB'} = s/\cos\theta_3$.
3. The negative GVD contribution due to the angular dispersion $d\theta_1/d\Omega$ (deflection of the beam at the first interface) applied to Eq. (2.78) over a distance L_g in the glass of index n.

In most practical situations it is desirable to write Eq. (B.18) in terms of the input angle of incidence θ_0 and the prism apex angle α. The necessary equations can be derived from Snell's law and Eq. (B.16):

$$\begin{aligned}\frac{d}{d\Omega}\theta_1 &= \frac{1}{n}\left[n^2-\sin^2(\theta_0)\right]^{-\frac{1}{2}}\left[n\cos\theta_0\frac{d\theta_0}{d\Omega}-\sin\theta_0\frac{dn}{d\Omega}\right] \\ \frac{d}{d\Omega}\theta_3 &= \left[1-n^2\sin^2(\alpha-\theta_1)\right]^{-\frac{1}{2}}\left[n\cos(\alpha-\theta_1)\frac{d\theta_1}{d\Omega}+\sin(\alpha-\theta_1)\frac{dn}{d\Omega}\right],\end{aligned} \quad (2.87)$$

where $\theta_1 = \arcsin\left(n^{-1}\sin\theta_0\right)$ and $d\theta_0/d\Omega = 0$.

For the particular case of Brewster angle prisms and minimum deviation (symmetric beam path through the prism for $\Omega = \omega_\ell$), we can make the substitutions $d\theta_1/dn = -1/n^2$, and $d\theta_3/dn = 2$. Using $\theta_0 = \theta_3 = \theta_4 = \theta_7$, the various angles are related by:

$$\begin{aligned} \tan\theta_0 &= n \\ \sin\theta_0 = \cos\theta_1 &= \frac{n}{\sqrt{1+n^2}} \\ \cos\theta_0 = \sin\theta_1 &= \frac{1}{\sqrt{1+n^2}} \\ \sin\alpha &= \frac{2n}{n^2+1} \end{aligned} \tag{2.88}$$

The total second order dispersion in this case becomes:

$$\boxed{\left.\frac{d^2\Psi}{d\Omega^2}\right|_{\omega_\ell} = \frac{L_g}{c}\left[2\left.\frac{dn}{d\Omega}\right|_{\omega_\ell} + \omega_\ell \left.\frac{d^2n}{d\Omega^2}\right|_{\omega_\ell}\right] - \frac{\omega_\ell}{c}\left(4L + \frac{L_g}{n^3}\right)\left(\left.\frac{dn}{d\Omega}\right|_{\omega_\ell}\right)^2,} \tag{2.89}$$

In terms of wavelength:

$$\boxed{\left.\frac{d^2\Psi}{d\Omega^2}\right|_{\omega_\ell} = \frac{\lambda_\ell^3}{2\pi c^2}\left[L_g \left.\frac{d^2n}{d\lambda^2}\right|_{\lambda_\ell} - \left(4L + \frac{L_g}{n^3}\right)\left(\left.\frac{dn}{d\lambda}\right|_{\lambda_\ell}\right)^2\right].} \tag{2.90}$$

In many practical devices, $L >> L_g$ and the second term of Eq. (2.90) reduces to $L(dn/d\lambda)^2$.

It is left as a problem at the end of this chapter to calculate the exact third order dispersion for a pair of prisms. If the angular dispersion in the glass can be neglected ($L >> L_g$), the third order dispersion for a Brewster angle prism is:

$$\begin{aligned} &\Psi'''_{\text{tot}}(\omega_\ell) \approx \\ &\quad \frac{\lambda_\ell^4}{(2\pi c)^2 c}\left[12L\left(n'^2\left[1 - \lambda_\ell n'(n^{-3} - 2n)\right] + \lambda_\ell n' n''\right) - L_g(3n'' + \lambda_\ell n''')\right]. \end{aligned} \tag{2.91}$$

To simplify the notation, we have introduced n', n'' and n''' for the derivatives of n with respect to λ taken at λ_ℓ.

The presence of a negative contribution to the group velocity dispersion due to angular dispersion offers the possibility of tuning the GVD by changing $L_g = g/\sin\theta_0$ (g is the thickness of the glass slab formed by bringing the two prisms

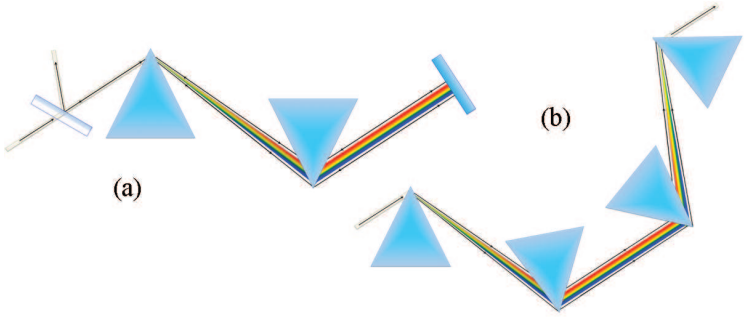

Figure 2.26: Set-ups for adjustable GVD without transverse displacement of spectral components. (a) two prisms followed by end mirror (configuration used mostly in linear cavities). (b) 4 prisms (used in ring cavities). The GVD is tuned by translating one or more prisms into the beam.

together, as shown in Fig. B.1) in Appendix B. A convenient method is to simply translate one of the prisms perpendicularly to its base, which alters the glass path while keeping the beam deflection constant. It will generally be desirable to avoid a transverse displacement of spectral components at the output of the dispersive device. Two popular prism arrangements which do not separate the spectral components of the pulse are sketched in Fig. 2.26. The beam is either sent through two prism, and retro-reflected by a plane mirror, or sent directly through a sequence of four prisms. In these cases the dispersion as described by Eq. (B.18) doubles. The values of Ψ'', Ψ''', etc. that are best suited to a particular experimental situation can be predetermined through a selection of the optimum prism separation $s/\cos\theta_3$, the glass pathlength L_g, and the material (cf. Table 2.1). Such optimization methods are particularly important for the generation of sub-20 fs pulses in lasers [36, 37] that use prisms for GVD control.

In this section we have derived analytical expressions for dispersion terms of increasing order, in the case of identical isoceles prism pairs, in exactly antiparallel configuration. It is also possible by methods of pulse tracing through the prisms to determine the phase factor at any frequency and angle of incidence [30, 38, 39, 31, 40]. The more complex studies revealed that the GVD and the transmission factor R [as defined in Eq. (2.73)] depend on the angle of incidence and apex angle of the prism. In addition, any deviation from the Brewster condition increases the reflection losses. An example is shown in Fig. 2.27.

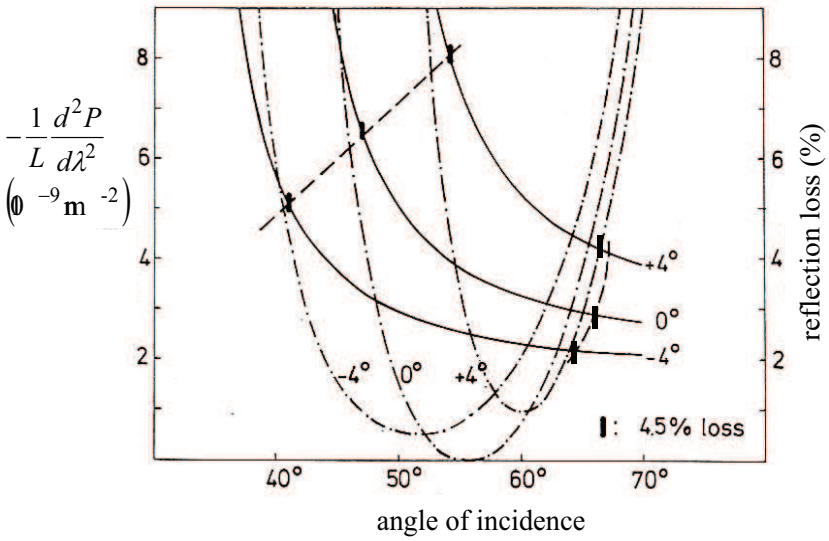

Figure 2.27: Dispersion (solid lines) and reflection losses (dash-dotted lines) of a two-prism sequence (SQ1 - fused silica) as a function of the angle of incidence on the first prism surface. Symmetric beam path through the prism at the central wavelength is assumed. Curves for three different apex angles (-4^o, 0^o, 4^o) relative to $\alpha = 68.9^o$ (apex angle for a Brewster prism at 620 nm) are shown. The tic marks on the dashed lines indicate the angle of incidence and the dispersion where the reflection loss is 4.5%. (from [31]).

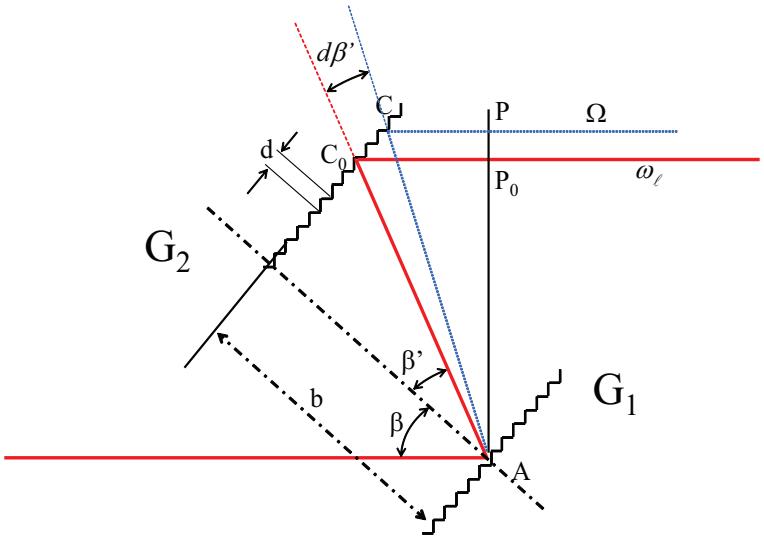

Figure 2.28: Two parallel gratings produce GVD without net angular dispersion. For convenience a reference wavefront is assumed so that the extension of $\overline{PP_0}$ intersects G_1 at A.

2.5.6 GVD introduced by gratings gratings

Gratings can produce larger angular dispersion than prisms. The resulting negative GVD was first utilized by Treacy to compress pulses of a Nd:glass laser [28]. In complete analogy with prisms, the simplest practical device consists of two identical elements arranged as in Fig. 2.28 for zero net angular dispersion. The dispersion introduced by a pair of parallel gratings can be determined by tracing the frequency dependent ray path. The optical path length $\overline{ACP}$ between A and an output wavefront $\overline{PP_o}$ is frequency dependent and can be determined with help of Fig. (2.28) to be:

$$\overline{ACP} = \frac{b}{\cos(\beta')}\left[1+\cos(\beta'+\beta)\right] \tag{2.92}$$

where β is the angle of incidence, β' is the diffraction angle for the frequency component Ω and b is the normal separation between G_1 and G_2. If m is the order of diffraction, the angle of incidence and the diffraction angle are related through the grating equation

$$\sin\beta' - \sin\beta = \frac{2m\pi c}{\Omega d} \tag{2.93}$$

where d is the grating constant. The situation with gratings is however different than with prisms, in the sense that the optical path of two parallel rays out of grating G_1 impinging on adjacent grooves of grating G_2 will see an optical path

difference $\overline{CP} - \overline{C_0P_0}$ of $m\lambda$, m being the diffraction order. Thus, as the angle β' changes with wavelength, the phase factor $\Omega\overline{ACP}/c$ increments by $2m\pi$ each time the ray $\overline{AC}$ passes a period of the ruling of G_2 [28]. Because only the relative phase shift across $\overline{PP_0}$ matters, we may simply count the rulings from the (virtual) intersection of the normal in A with G_2. Thus, for the mth order diffraction we find for $\Psi(\Omega)$:

$$\Psi(\Omega) = \frac{\Omega}{c}\overline{ACP}(\Omega) - 2m\pi\frac{b}{d}\tan(\beta'). \tag{2.94}$$

The group delay is given by:

$$\begin{aligned}\frac{d\Psi}{d\Omega} &= \left(\frac{b}{c}\right)\frac{1+\cos(\beta+\beta')}{\cos\beta'} + \frac{\Omega b}{c\cos^2\beta'}\{\sin\beta'\,[1+\cos(\beta+\beta')] \\ &\quad -\cos\beta'\sin(\beta+\beta')\}\frac{d\beta'}{d\Omega} + \frac{2m\pi}{d}\frac{b}{\cos^2\beta'}\frac{d\beta'}{d\Omega} \\ &= \left(\frac{b}{c}\right)\frac{1+\cos(\beta+\beta')}{\cos\beta'} = \frac{\overline{ACP}(\Omega)}{c}.\end{aligned} \tag{2.95}$$

In deriving the last equation, we have made use of the grating equation $\sin\beta' - \sin\beta = 2\pi c/(\Omega d)$. Equation (2.95) shows remarkable properties of gratings. The group delay is simply equal to the phase delay, and not explicitly dependent on the grating order. The carrier to envelope delay is zero. The second order derivative, obtained by differentiation of Eq. (2.95), is:

$$\begin{aligned}\frac{d^2\Psi}{d\Omega^2} &= \frac{b}{c}\frac{1}{\cos^2\beta'}\{\sin\beta'\,[1+\cos(\beta+\beta')] - \cos\beta'[\sin(\beta+\beta')]\}\frac{d\beta'}{d\Omega} \\ &= \left(\frac{b}{d}\right)\frac{2m\pi}{\omega_\ell\cos\beta'}\left.\frac{d\beta'}{d\Omega}\right|_{\omega_\ell} = \frac{-4\pi^2m^2c}{\omega_\ell^3\cos^2\beta'}\frac{L}{d^2},\end{aligned} \tag{2.96}$$

where we have again made use of the grating equation, and used the distance $L = b/\cos\beta'$ between the gratings along the ray at $\Omega = \omega_\ell$. Using wavelengths instead of frequencies:

$$\boxed{\left.\frac{d^2\Psi}{d\Omega^2}\right|_{\omega_\ell} = -\frac{\lambda_\ell}{2\pi c^2}\left(\frac{m\lambda_\ell}{d}\right)^2\frac{L}{\cos^2\beta'(\lambda_\ell)}.} \tag{2.97}$$

where $\cos^2\beta'(\omega_\ell) = 1 - [2\pi c/(\omega_\ell d) + \sin\beta]^2$. The third derivative can be written as

$$\left.\frac{d^3\Psi}{d\Omega^3}\right|_{\omega_\ell} = -\frac{3}{\omega_\ell}\left.\frac{d^2\Psi}{d\Omega^2}\right|_{\omega_\ell}\left[1 + \frac{2}{3}\frac{m\lambda_\ell}{d}\frac{sin\beta'}{\cos^2\beta'}\right]. \tag{2.98}$$

To decide when the third term in the expansion [as defined in Eq. (1.179)] of the phase response of the grating needs to be considered we evaluate the ratio

$$R_G = \left|\frac{b_3(\Omega-\omega_\ell)^3}{b_2(\Omega-\omega_\ell)^2}\right| = \left|\frac{\Psi'''(\omega_\ell)}{3\Psi''(\omega_\ell)}\right||\Omega-\omega_\ell| \approx \frac{\Delta\omega_p}{\omega_\ell}\left[1 + \frac{2}{3}\frac{m\lambda_\ell}{d}\frac{sin\beta'}{\cos^2\beta'}\right] \tag{2.99}$$

where the spectral width of the pulse $\Delta\omega_p$ was used as an average value for $|\Omega-\omega_\ell|$. Obviously it is possible to minimize (or tune) the ratio of second- and third- order dispersion by changing the grating constant and the angle of incidence. The second order dispersion increases with the square of the ratio $m\lambda_\ell/d\cos\beta'$, thus faster than the ratio R_G that is proportional to that quantity. Grazing incidence, multiple order may be considered when very large dispersion needs to be achieved on a relatively narrow bandwidth.

The derivation of Eq. (2.97) could have been shortened considerably by using the general relation between angular dispersion and GVD, Eq. (2.78). Indeed, deriving from Eq. (2.93) the angular dispersion of a grating

$$\left.\frac{d\beta'}{d\Omega}\right|_{\omega_\ell} = -\frac{2\pi c}{\omega_\ell^2 d\cos\beta'}, \tag{2.100}$$

and inserting in Eq. (2.78), we also obtain Eq. (2.97).

2.5.7 Grating pairs for pulse compressors

For all practical purpose, a pulse propagating from grating G_1 to G_2 can be considered as having traversed a linear medium of length L characterized by a negative dispersion. We can write Eq. (2.97) in the form of:

$$\left.\frac{d^2\Psi}{d\Omega^2}\right|_{\omega_\ell} = k_\ell'' L = -\left\{\frac{\lambda_\ell}{2\pi c^2}\left(m\frac{\lambda_\ell}{d}\right)^2 \frac{1}{\cos^2\beta'(\omega_\ell)}\right\} L. \tag{2.101}$$

Referring to Table 1.4 of Chapter 1, a bandwidth limited Gaussian pulse of duration τ_{G0}, propagating through a dispersive medium characterized by the parameter k_ℓ'', broadens to a Gaussian pulse of duration τ_G

$$\tau_G = \tau_{G0}\sqrt{1+\left(\frac{L}{L_d}\right)^2}, \tag{2.102}$$

with a linear chirp of slope:

$$\ddot{\varphi} = \frac{2L/L_d}{1+(L/L_d)^2}\,\frac{1}{\tau_{G0}^2} \tag{2.103}$$

where the parameter L_d relates both to the parameters of the grating and to the minimum (bandwidth limited) pulse duration:

$$L_d = \frac{\tau_{G0}^2}{2|k_\ell''|} = \pi\left(\frac{c\tau_{G0}}{m\lambda_\ell}\right)^2 \frac{d}{\lambda_\ell}\cos^2\beta'(\omega_\ell). \tag{2.104}$$

Conversely, a pulse with a positive chirp of magnitude given by Eq. (2.103) and duration corresponding to Eq. (2.102) will be compressed by the pair of gratings to a duration τ_{G0}. A pulse compressor following a pulse stretcher is used in numerous amplifications systems and will be dealt with in Chapter **??**. The "compressor" is a pair of gratings with optical path L, designed for a compression ratio $\tau_G/\tau_{G0} = L/L_d$ [10]. The ideal compressor of length L will restore the initial (before the stretcher) unchirped pulse of duration τ_0. To a departure x from the ideal compressor length L, corresponds a departure from the ideal unchirped pulse of duration τ_0:

$$\tau_G = \tau_{G0}\sqrt{1+\frac{x^2}{L_d^2}}. \tag{2.105}$$

This pulse is also given a chirp coefficient (cf. Table 1.4) $\bar{a} = x/L_d$.

In most compressors, the transverse displacement of the spectral components at the output of the second grating can be compensated by using two pairs of gratings in sequence or by sending the beam once more through the first grating pair. As with prisms, the overall dispersion then doubles. Tunability is achieved by changing the grating separation b. Unlike with prisms, however, the GVD is always negative. The order of magnitude of the dispersion parameters of some typical devices is compiled in Table 2.2.

The choice between gratings and prism for controllable dispersion is not always a simple one. Prisms pairs have lower losses than gratings (the total transmission through a grating pair usually does not exceed 80%), and are therefore the preferred intracavity dispersive element. Gratings are often used in amplifier chain where extremely high compression and stretching ratio are desired, which implies a small L_d. It should be noted however that L_d is not only determined by the properties of the prism or grating, but is also proportional to τ_{G0}^2 as shown by Eq. (2.104). Therefore, prisms stretcher-compressors are also used in medium power amplifiers for sub-20 fs pulses. The disadvantage of prisms is that the beam has to be transmitted through glass, which, for high power pulses, is a nonlinear medium.

2.5.8 Combination of focusing and angular dispersive elements

A disadvantage of prism and grating sequences is that for achieving large GVD the length L between two diffraction elements becomes rather large, cf. Eq.(2.78). As proposed by Martinez *et al.* [41] the GVD of such devices can be considerably increased (or decreased) by using them in connection with focusing elements such as telescopes. Let us consider the optical arrangement of Fig. 2.29, where a telescope is placed between two gratings.

[10] In all practical cases with a pair of gratings, $(L/L_d)^2 \gg 1$.

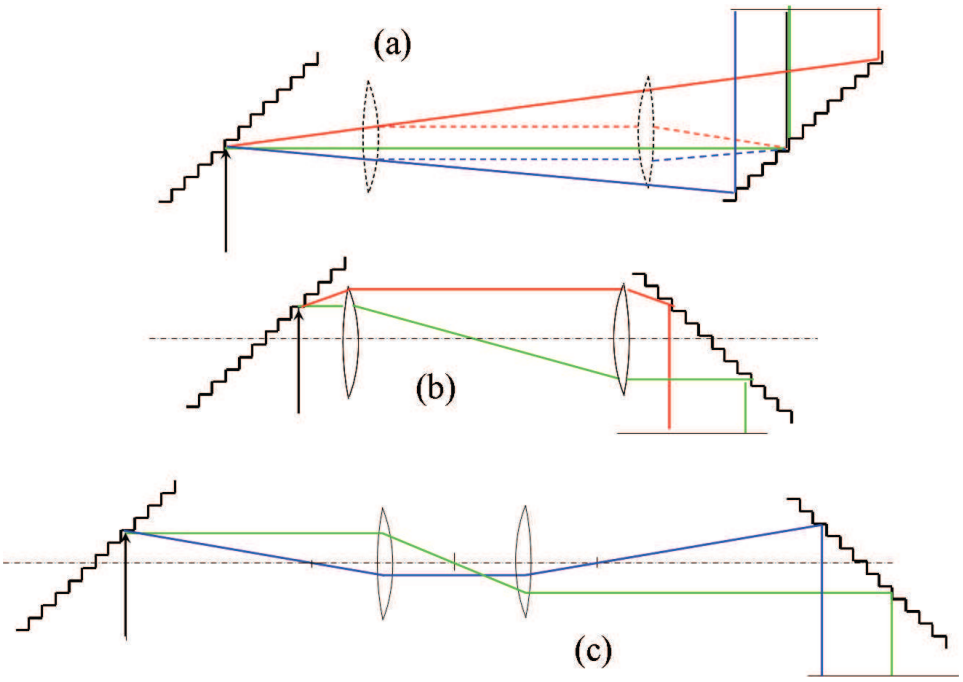

Figure 2.29: Combination of a grating pair and a telescope. (a) Comparison of a standard two grating combination of negative dispersion, and a zero-dispersion arrangement. The solid lines show the beam paths in the standard configuration, as discussed in the previous section and in Fig. 2.28. The total phase shift is largest for the red beam and smallest for the blue beam. The dashed line corresponds to the zero-dispersion configuration, where the gratings are both at a focal point of each lens, and the lens are spaced by two focal distances. It is easily seen that all the optical paths are equal length. (b) Positive dispersion configuration. The spacing between the gratings is smaller than $4f$, while the lens spacing remains $2f$. The green beam has a longer optical path than the red beam. (c) The grating spacing is larger than 4f (the lenses being still $2f$ apart). This is still a negative dispersion configuration: the blue beam has a shorter optical path than the green beam.

Device	λ_ℓ [nm]	ω_ℓ [fs^{-1}]	Ψ'' [fs^2]
fused silica (L_g = 1 cm)	620	3.04	535
	800	2.36	356
Brewster prism pair, fused silica L = 50 cm	620	3.04	-760
	800	2.36	-523
grating pair b = 20 cm; $\beta = 0^o$ d = 1.2 μm	620	3.04	-9.3 10^4
	800	2.36	-3 10^5

Table 2.2: Values of second-order dispersion for typical devices.

The solid lines in Fig. 2.29(a) show the optical path through a pair of parallel gratings, for beam of decreasing wavelength from red (top) to blue (bottom). With two lenses inserted between the gratings, such that the distance between gratings $L = 4f$, all optical paths are rigourously equal (zero dispersion configuration). Therefore, Eq. (2.97) is still valid, provided the distance L between gratings is replaced by $L - 4f$. Since the telescope implies an image inversion, the orientation of the second grating should be reversed, as in Fig. 2.29(b), in which the distance L is smaller than $4f$. The sign of $L - 4f$ is negative, making the second order dispersion Eq. (2.97) *positive*. The green optical path experiences several additional 2π phase shifts on the grating as compared to the red one. Such an arrangement is used in amplifier systems to stretch pulses (chirped pulse amplification [42, 43]. When the distance between gratings is increased beyond $L = 4f$ [Fig. 2.29(c)] the blue beam experiences a larger phase shift than the green beam, indicating negative dispersion.

More generally, as shown in Fig. 2.30, the grating-lens configuration does no need to be symmetrical, neither do the lenses need to have the same focal distance. Let Δ be the distance from the left grating to the left lens of focal distance f, and Δ' the distance from the right grating to the right lens of focal distance f', the overall dispersion is given by:

$$\boxed{\left.\frac{d^2\Psi}{d\Omega^2}\right|_{\omega_\ell} = -\frac{\omega_\ell}{c}\left(\left.\frac{d\alpha}{d\Omega}\right|_{\omega_\ell}\right)^2\left(\Delta + M^2\Delta'\right)} \tag{2.106}$$

where a magnification factor $M = f'/f$ has been introduced. Indeed, the angular dispersion of G_1 is magnified by M to $M(d\alpha/d\Omega)$. For the second grating to produce a parallel output beam its dispersion must be M times larger than that of G_1.

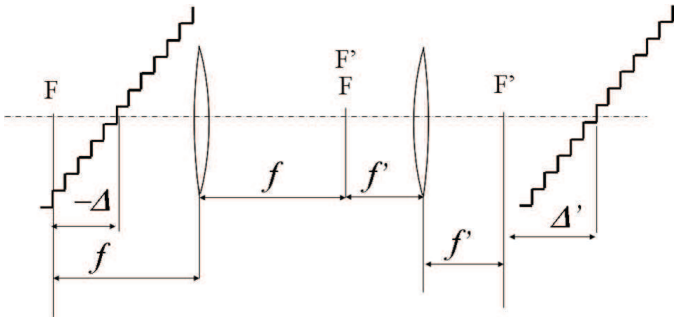

Figure 2.30: Most general configuration of grating-lens combination.

Matrix tools have been developed to compute the propagation of Gaussian beams through a system of gratings. The matrices used are 3×3, an extension of the conventional $ABCD$ matrices for Gaussian beams, with an additional column containing two additional terms to account for angular dispersion. Details can be found in references [44, 45, 46].

In summary, the use of telescopes in connection with grating or prism pairs allows us to increase or decrease the amount of GVD as well as to change the sign of the GVD. Interesting applications of such devices include the recompression of pulses after very long optical fibers [41] and extreme pulse broadening (> 1000) before amplification [42]. A more detailed discussion of this type of dispersers, including the effects of finite beam size, can be found in [33].

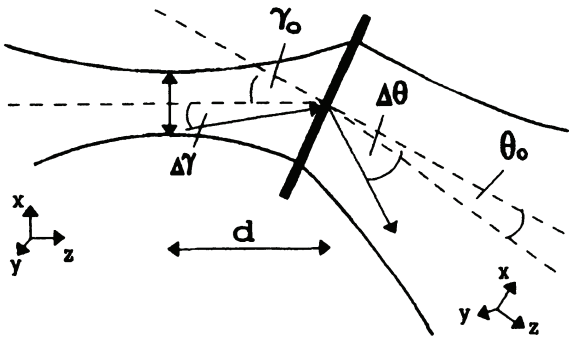

Figure 2.31: Interaction of a Gaussian beam with a disperser.

2.6 Wave-optical description of angular dispersion!angular dispersive elements

Because our previous discussion of pulse propagation through prisms, gratings, and other elements was based on ray-optical considerations, it failed to give details about the influence of a finite beam size. These effects can be included by a wave-optical description which is also expected to provide new insights into the spectral, temporal, and spatial field distribution behind the optical elements. We will follow the procedure developed by Martinez [33], and use the characteristics of Gaussian beam propagation, i.e., remain in the frame of paraxial optics.

First, let us analyze the effect of a single element with angular dispersion as sketched in Fig. 2.31. The electric field at the disperser can be described by a complex amplitude $\tilde{U}(x,y,z,t)$ varying slowly with respect to the spatial and temporal coordinate:

$$E(x,y,z,t) = \frac{1}{2}\tilde{U}(x,y,z,t)e^{i(\omega_\ell t - k_\ell z)} + c.c. \tag{2.107}$$

Using Eq. (**??**) the amplitude at the disperser can be written as

$$\tilde{U}(x,y,t) = \tilde{\mathcal{E}}_0(t)\exp\left[-\frac{ik_\ell}{2\tilde{q}(d)}(x^2+y^2)\right] = \tilde{U}(x,t)\exp\left[\frac{-ik_\ell y^2}{2\tilde{q}(d)}\right] \tag{2.108}$$

where $\tilde{q}$ is the complex beam parameter, d is the distance between beam waist and disperser, and $\tilde{\mathcal{E}}_0$ is the amplitude at the disperser. Our convention shall be that x and y refer to coordinates transverse to the respective propagation direction z. Further, we assume the disperser to act only on the field distribution in the x direction, so that the field variation with respect to y is the same as for free space

propagation of a Gaussian beam. Hence, propagation along a distance z changes the last term in Eq. (2.108) simply through a change of the complex beam parameter $\tilde{q}$. According to Eq. (**??**) this change is given by

$$\tilde{q}(d+z) = \tilde{q}(d) + z. \tag{2.109}$$

To discuss the variation of $\tilde{U}(x,t)$ it is convenient to transfer to frequencies $\bar{\Omega}$ and spatial frequencies ρ applying the corresponding Fourier transforms

$$\tilde{U}(x,\bar{\Omega}) = \int_{-\infty}^{\infty} \tilde{U}(x,t) e^{-i\bar{\Omega}t} dt \tag{2.110}$$

and

$$\tilde{U}(\rho,\bar{\Omega}) = \int_{-\infty}^{\infty} \tilde{U}(x,\bar{\Omega}) e^{-i\rho x} dx. \tag{2.111}$$

A certain spatial frequency spectrum of the incident beam means that it contains components having different angles of incidence. Note that $\bar{\Omega}$ is the variable describing the spectrum of the envelope (centered at $\bar{\Omega} = 0$), while $\Omega = \bar{\Omega} + \omega_\ell$ is the actual frequency of the field. In terms of Fig. 2.31 this is equivalent to a certain angular distribution $\Delta\gamma$. The spatial frequency ρ is related to $\Delta\gamma$ through

$$\Delta\gamma = \frac{\rho}{k_\ell}. \tag{2.112}$$

For a plane wave, $\tilde{U}(\rho,\bar{\Omega})$ exhibits only one non-zero spatial frequency component which is at $\rho = 0$. The disperser not only changes the propagation direction ($\gamma_0 \rightarrow \theta_0$) but also introduces a new angular distribution $\Delta\theta$ of beam components which is a function of the angle of incidence γ and the frequency $\bar{\Omega}$

$$\begin{aligned} \Delta\theta &= \Delta\theta(\gamma,\Omega) \\ &= \left.\frac{\partial\theta}{\partial\gamma}\right|_{\gamma_0} \Delta\gamma + \left.\frac{\partial\theta}{\partial\Omega}\right|_{\omega_\ell} \bar{\Omega} \\ &= \alpha\Delta\gamma + \beta\bar{\Omega}. \end{aligned} \tag{2.113}$$

The quantities α and β are characteristics of the disperser and can easily be determined, for example, from the prism and grating equations.[11] By means of Eq. (2.112) the change of the angular distribution $\Delta\gamma \rightarrow \Delta\theta$ can also be interpreted as a transformation of spatial frequencies ρ into spatial frequencies $\rho' = \Delta\theta k_\ell$ where

$$\rho' = \alpha k_\ell \Delta\gamma + k_\ell \beta\bar{\Omega} = \alpha\rho + k_\ell\beta\bar{\Omega}. \tag{2.114}$$

[11] For a Brewster prism adjusted for minimum deviation we find $\alpha = 1$ and $\beta = -(\lambda^2/\pi c)(dn/d\lambda)$. The corresponding relations for a grating used in diffraction order m are $\alpha = \cos\gamma_0/\cos\theta_0$ and $\beta = -m\lambda^2/(2\pi cd\cos\theta_0)$.

Just behind the disperser we have an amplitude spectrum $\tilde{U}_T(\rho', \bar{\Omega})$ given by

$$\tilde{U}_T(\rho', \bar{\Omega}) = C_1 \tilde{U}\left(\frac{1}{\alpha}\rho' - \frac{k_\ell}{\alpha}\beta\bar{\Omega}, \bar{\Omega}\right) \tag{2.115}$$

where C_1 and further constants C_i to be introduced are factors necessary for energy conservation that shall not be specified explicitly. In spatial coordinates the field distribution reads

$$\begin{aligned}
\tilde{U}_T(x, \bar{\Omega}) &= \int_{-\infty}^{\infty} \tilde{U}_T(\rho', \bar{\Omega}) e^{i\rho' x} d\rho' \\
&= C_1 \int_{-\infty}^{\infty} \tilde{U}\left(\frac{1}{\alpha}\rho' - \frac{k_\ell}{\alpha}\beta\bar{\Omega}, \bar{\Omega}\right) e^{i\rho' x} d\rho' \\
&= C_1 \int_{-\infty}^{\infty} \tilde{U}(\rho, \bar{\Omega}) e^{i\alpha\rho x} e^{ik_\ell\beta\bar{\Omega}x} d(\alpha\rho) \\
&= C_2 e^{ik_\ell\beta\bar{\Omega}x} \tilde{U}(\alpha x, \bar{\Omega}).
\end{aligned} \tag{2.116}$$

The disperser introduces a phase factor $\exp\left(ik_\ell\beta\bar{\Omega}x\right)$ and a magnification factor α. For the overall field distribution we obtain with Eqs. (2.108), (2.109), and (2.116)

$$\tilde{U}_T(x, y, \bar{\Omega}) = C_3 \tilde{\mathcal{E}}_0(\bar{\Omega}) e^{ik_\ell\beta\bar{\Omega}x} \exp\left[-\frac{ik_\ell}{2\tilde{q}(d)}\left(\alpha^2 x^2 + y^2\right)\right]. \tag{2.117}$$

The field a certain distance L away from the disperser is connected to the field distribution Eq. (2.117) through a Fresnel transformation which describes the free space propagation. Thus, it can be written as

$$\begin{aligned}
\tilde{U}_T(x, y, L, \bar{\Omega}) &= C_4 \exp\left[\frac{-ik_\ell y^2}{2\tilde{q}(d+L)}\right] \int \tilde{\mathcal{E}}_0(\bar{\Omega}) e^{ik_\ell\beta\bar{\Omega}x'} \\
&\times \exp\left[-i\frac{k_\ell}{2\tilde{q}(d)}\alpha^2 x'^2\right] \exp\left[-\frac{i\pi}{L\lambda}(x - x')^2\right] dx'.
\end{aligned} \tag{2.118}$$

Solving this integral yields an analytical expression for the spectral amplitude

$$\begin{aligned}
\tilde{U}_T(x, y, L, \bar{\Omega}) = C_5 \tilde{\mathcal{E}}_0(\bar{\Omega}) \exp\left[-ik_\ell \frac{x^2}{2L}\right] \\
\times \exp\left[-ik_\ell \frac{y^2}{2\tilde{q}(d+L)}\right] \exp\left\{\frac{ik_\ell L}{2} \frac{\tilde{q}(d)}{\tilde{q}(d+\alpha^2 L)} \left[\frac{x^2}{L^2} + 2\frac{\beta x}{L}\bar{\Omega} + \beta^2\bar{\Omega}^2\right]\right\}.
\end{aligned} \tag{2.119}$$

The phase term proportional to $\bar{\Omega}^2$ is responsible for GVD according to our discussion in the section on linear elements. As expected from our ray-optical treatment,

this term increases with increasing distance L and originates from angular dispersion β. The term linear in $\bar{\Omega}$ varies with the transverse coordinate x. It describes a frequency variation across the beam and accounts for different propagation directions of different spectral components. We know that exponentials proportional to $b_1\bar{\Omega}$ result in a pulse delay, as discussed previously following Eq. (1.181). Since $b_1 \propto x$ the pulse delay changes across the beam — a feature which we have called tilt of pulse fronts. This proves the general connection between angular dispersion and pulse front tilting introduced earlier in a more intuitive way.

For a collimated input beam and $\alpha = 1$ we can estimate

$$\frac{\tilde{q}(d)}{\tilde{q}(d+\alpha^2 L)} \approx 1 \tag{2.120}$$

and the temporal delay becomes $b_1 = k_\ell \beta x$. Looking at the beam at a certain instant the corresponding spatial delay is $k_\ell \beta x c$. Thus, we find for the tilt angle α

$$|\tan\alpha| = \left|\frac{d}{dx}(k_\ell \beta x c)\right| = \omega_\ell \left|\frac{d\theta}{d\bar{\Omega}}\Big|_{\bar{\Omega}=0}\right| = \lambda_\ell \left|\frac{d\theta}{d\lambda}\Big|_{\lambda_\ell}\right| \tag{2.121}$$

which confirms our previous results, cf. Eq. (2.72). With the same approximation we obtain for the GVD term:

$$\frac{d^2\Psi}{d\bar{\Omega}^2} = 2b_2 = -k_\ell L\beta^2 = -\frac{L\omega_\ell}{c}\left(\frac{d\theta}{d\Omega}\Big|_{\omega_\ell}\right)^2 \tag{2.122}$$

in agreement with Eq. (2.78).

For compensating the remaining angular dispersion we can use a properly aligned second disperser which has the parameters $\alpha' = 1/\alpha$ and $\beta' = \beta/\alpha$. According to our general relation for the action of a disperser (2.116) the new field distribution after this second disperser is given by

$$\begin{aligned} \tilde{U}_F &= C_2 e^{ik_\ell \frac{\beta}{\alpha}\bar{\Omega}x} \tilde{U}_T\left(\frac{x}{\alpha}, y, L, \bar{\Omega}\right) \\ &= C_6 \tilde{\mathcal{E}}_0(\bar{\Omega}) e^{\frac{i}{2}k_\ell \bar{\Omega}^2\beta^2 L} \exp\left\{\frac{-ik_\ell}{2}\left[\frac{(x+\alpha\beta\bar{\Omega}L)^2}{\tilde{q}(d+\alpha^2 L)} + \frac{y^2}{\tilde{q}(d+L)}\right]\right\}, \end{aligned} \tag{2.123}$$

which again exhibits the characteristics of a Gaussian beam. Hence, to account for an additional propagation over a distance L', we just have to add L' in the arguments of $\tilde{q}$. As discussed by Martinez [33] $\alpha \neq 1$ gives rise to astigmatism (the position of the beam waist is different for the x and y directions) and only for a well-collimated input beam does the GVD not depend on the travel distance L'

after the second disperser. For $\alpha = 1$ and $q(d + L + L') \approx q(0)$ (collimated input beam) the field distribution becomes

$$\boxed{\tilde{U}_F(x, y, L, \bar{\Omega}) = C_6 \tilde{\mathcal{E}}_0(\bar{\Omega}) e^{\frac{i}{2} k_\ell \beta^2 L \bar{\Omega}^2} \exp\left\{ -\frac{(x + \beta \bar{\Omega} L)^2 + y^2}{w_0^2} \right\}.} \tag{2.124}$$

The first phase function is the expected GVD term. The $\bar{\Omega}$ dependence of the second exponential indicates the action of a frequency filter. At constant position x, its influence increases with increasing $(\beta \bar{\Omega} L / w_0)^2$, i.e., with the ratio of the lateral displacement of a frequency component Ω and the original beam waist. The physics behind is that after the second disperser, not all frequency components can interfere over the entire beam cross-section, leading to an effective bandwidth reduction and thus to pulse broadening. If the experimental situation requires even this to be compensated, the beam can be sent through an identical second pair of dispersers (e.g., prisms). Within the approximations introduced above we just have to replace L by $2L$ in Eqs. (2.123),(2.124). For a well collimated beam ($\beta \bar{\Omega} L / w_0 \ll 1$) this results in

$$\tilde{U}_{F2}(x, y, L, \bar{\Omega}) = C_7 \tilde{\mathcal{E}}_0(\bar{\Omega}) e^{i k_\ell \beta^2 L \bar{\Omega}^2} e^{-(x^2 + y^2)/w_0^2}. \tag{2.125}$$

In this (ideal) case the only modification introduced by the dispersive element is the phase factor leaving the beam characteristics unchanged.

It is quite instructive to perform the preceding calculation with a temporally chirped input pulse as in Eq. (1.41) having a Gaussian spatial as well as temporal profile [33]:

$$\tilde{\mathcal{E}}_0(t) = \mathcal{E}_0 e^{-(1+ia)(t/\tau_G)^2} e^{-(x^2 + y^2)/w_0^2}. \tag{2.126}$$

The (temporal) Fourier transform yields

$$\tilde{\mathcal{E}}_0(\bar{\Omega}) = C_8 \exp\left(i \frac{\bar{\Omega}^2 \tilde{\tau} a}{4} \right) \exp\left(-\frac{\bar{\Omega}^2 \tilde{\tau}^2}{4} \right) \exp\left(-\frac{x^2 + y^2}{w_0^2} \right) \tag{2.127}$$

with $\tilde{\tau}^2 = \tau_G^2 / (1 + a^2)$, where according to our discussion following Eq. (1.47) $\tau_G / \tilde{\tau}$ is the maximum possible shortening factor after chirp compensation. This pulse is to travel through an ideal two-prism sequence described by Eq. (2.124) where βL has to be chosen so as to compensate exactly the quadratic phase term of the input pulse Eq. (2.127). Under this condition the insertion of Eq. (2.127) into Eq. (2.124) yields

$$\tilde{U}_F(x, y, \bar{\Omega}, L) = C_9 e^{-\bar{\Omega}^2 \tilde{\tau}^2 / 4} \exp\left[-\frac{(x + \beta \bar{\Omega} L)^2 + y^2}{w_0^2} \right]. \tag{2.128}$$

The time dependent amplitude obtained from Eq. (2.128) after inverse Fourier transform is

$$\tilde{\mathcal{E}}(t) = C_{10}\exp\left(\frac{-t^2}{\tilde{\tau}^2(1+u^2)}\right)\exp\left[\left(\frac{-x^2}{(1+u^2)w_0^2} - \frac{y^2}{w_0^2}\right)\right]\exp\left[\frac{-iu^2xt}{(1+u^2)\beta L}\right], \quad (2.129)$$

where $u = 2\beta L/(\tilde{\tau}w_0)$. The last exponential function accounts for a frequency sweep across the beam which prevents the different frequency components from interfering completely. As a result, the actual shortening factor is $\sqrt{1+u^2}$ times smaller than the theoretical one, as can be seen from the first exponential function. The influence of such a filter can be decreased by using a large beam size. A measure of this frequency filter, i.e., the magnitude of the quantity $(1+u^2)$, can be derived from the second exponent. Obviously the quantity $(1+u^2)$ is responsible for a certain ellipticity of the output beam which can be measured.

2.7 Optical matrices optical matrix for dispersive systems

In Chapter 1 we pointed out the similarities between Gaussian beam propagation and pulse propagation. Even though this fact has been known for many years [47, 28], it was only recently that optical matrices have been introduced to describe pulse propagation through dispersive systems [48, 44, 49, 50, 51] in analogy to optical ray matrices. The advantage of such an approach is that the propagation through a sequence of optical elements can be described using matrix algebra. Dijaili *et al.* [50] defined a 2×2 matrix for dispersive elements which relates the complex pulse parameters (cf. Table 1.4) of input and output pulse, $\tilde{p}$ and $\tilde{p}'$, to each other. Döpel [48] and Martinez [49] used 3×3 matrices to describe the interplay between spatial (diffraction) and temporal (dispersion) mechanisms in a variety of optical elements, such as prisms, gratings and lenses, and in combinations of them. The advantage of this method is the possibility to analyze complicated optical systems such as femtosecond laser cavities with respect to their dispersion — a task of increasing importance, as attempts are being made to propagate ultrashort pulses near the bandwidth limit through complex optical systems. The analysis is difficult since the matrix elements contain information pertaining to both the optical system and of pulse.

One of the most comprehensive approaches to describe ray and pulse characteristics in optical elements by means of matrices is that of Kostenbauder [51]. He defined 4×4 matrices which connect the input and output ray and pulse coordinates to each other. As in ray optics, all information about the optical system is carried in the matrix while the spatial and temporal characteristics of the pulse are

represented in a ray-pulse vector $(x, \Theta, \Delta t, \Delta\nu)$. Its components are defined by position x, slope Θ, time t and frequency ν. These coordinates have to be understood as *difference quantities* with respect to the coordinates of a *reference pulse*. The spatial coordinates are similar to those known from the ordinary $\begin{pmatrix} A & B \\ C & D \end{pmatrix}$ ray matrices. However, the origin of the coordinate system is defined now by the path of a diffraction limited reference beam at the average pulse frequency. This reference pulse has a well-defined arrival time at any reference plane; the coordinate Δt, for example, is the difference in arrival time of the pulse under investigation. In terms of such coordinates and using a 4×4 matrix, the action of an optical element can be written as

$$\begin{pmatrix} x \\ \Theta \\ \Delta t \\ \Delta\nu \end{pmatrix}_{out} = \begin{pmatrix} A & B & 0 & E \\ C & D & 0 & F \\ G & H & 1 & I \\ 0 & 0 & 0 & 1 \end{pmatrix} \begin{pmatrix} x \\ \Theta \\ \Delta t \\ \Delta\nu \end{pmatrix}_{in} \tag{2.130}$$

where A, B, C, D are the components of the ray matrix and the additional elements are

$$E = \frac{\partial x_{out}}{\partial \Delta\nu_{in}}\,, \quad F = \frac{\partial \Theta_{out}}{\partial \Delta\nu_{in}}\,, \quad G = \frac{\partial \Delta t_{out}}{\partial x_{in}}\,, \quad H = \frac{\partial \Delta t_{out}}{\partial \Theta_{in}}\,, \quad I = \frac{\partial \Delta t_{out}}{\partial \Delta\nu_{in}}. \tag{2.131}$$

The physical meaning of these matrix elements is illustrated by a few examples of elementary elements in Fig. 2.32. The occurrence of the zero-elements can easily be explained using simple physical arguments, namely (i) the center frequency must not change in a linear (time invariant) element and (ii) the ray properties must not depend on t_{in}. It can be shown that only six elements are independent of each other [51] and therefore three additional relations between the nine nonzero matrix elements exists. They can be written as

$$\begin{aligned} AD - BC &= 1 \\ BF - ED &= \lambda_\ell H \\ AF - EC &= \lambda_\ell G. \end{aligned} \tag{2.132}$$

Using the known ray matrices [52] and Eq. (2.131), the ray-pulse matrices for a variety of optical systems can be calculated. Let us construct as an example the matrix for an air-glass interface. The various elements can be calculated directly from Snell's law. Let Θ_{in} be the angle of incidence, and Θ_{out} the angle of refraction.

A system matrix can be constructed as the ordered product of matrices corresponding to the elementary operations (as in the example of the prism constructed from the product of two interfaces and a propagation in glass). An important feature of a system of dispersive elements is the frequency dependent optical beam

matrix element	function	example
E	position dispersion	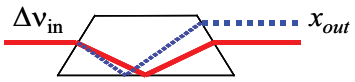
F	angular dispersion	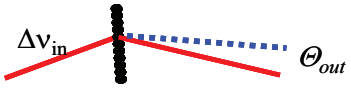
G	tilt of pulse front	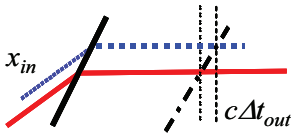
H	delay due to angular disp.	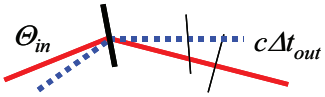
I	delay due to spectrum	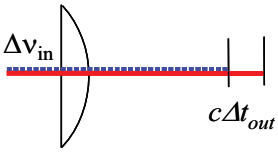

Figure 2.32: Illustration of the function performed by the matric elements E, F, G, H, and I. The path of the reference beam at the central wavelength is represented by the solid line, while the dotted line indicates the displaced path caused by Θ_{in}, x_{in} or $\Delta\nu_{in}$. A dispersive prism introduces a transverse wavelength dependent displacement of the beam, x_{out}. To a change in optical frequency $\Delta\nu_{in}$ from the central frequency ν_ℓ corresponds an angular deviation Θ_{out} at a dispersive interface. At the same dispersive interface, to a transverse displacement x_{in} left of the interface corresponds an energy front tilt $\Delta t_{out} = G x_{in}$ right of the interface. There is also a contribution to the energy front tilt associated with the angular dispersion, which is $\Delta t_{out} = H\Theta_{in}$. Finally, on axis of a lens which has chromatic aberration, the displaced wavelength suffers a delay $\Delta t_{out} = I\Delta\nu_{in}$.

path P, and the corresponding phase delay Ψ. This information is sufficient for geometries that do not introduce a change in the beam parameters. Examples which have been discussed in this respect are four-prism and four-grating sequences illuminated by a well-collimated beam.

As shown in Ref. [51], Ψ can be expressed in terms of the coordinates of the

Lens or Mirror ($\mathcal{M}_L$)	**Brewster Prism** ($\mathcal{M}_{BP}$)
$\begin{pmatrix} 1 & 0 & 0 & 0 \\ -1/f & 1 & 0 & 0 \\ 0 & 0 & 1 & 0 \\ 0 & 0 & 0 & 1 \end{pmatrix}$	$\begin{pmatrix} 1 & L_g/n^3 & 0 & -\frac{SL_g}{n^3} \\ 0 & 1 & 0 & -2S \\ -\frac{2S}{\lambda_\ell} & -\frac{L_gS}{n^3\lambda_\ell} & 1 & \frac{L_gS^2}{n^3\lambda_\ell}+2\pi L_g k''_\ell \\ 0 & 0 & 0 & 1 \end{pmatrix}$
f — focal length	$S = 2\pi \left.\frac{\partial n}{\partial\Omega}\right\|_{\omega_\ell}$, L_g — mean glass path
Dispersive Slab ($\mathcal{M}_{DS}$)	**Grating** ($\mathcal{M}_G$)
$\begin{pmatrix} 1 & L/n & 0 & 0 \\ 0 & 1 & 0 & 0 \\ 0 & 0 & 1 & 2\pi L k''_\ell \\ 0 & 0 & 0 & 1 \end{pmatrix}$	$\begin{pmatrix} -\frac{\cos\beta'}{\cos\beta} & 0 & 0 & 0 \\ 0 & -\frac{\cos\beta}{\cos\beta'} & 0 & \frac{c(\sin\beta'-\sin\beta)}{\lambda_\ell \sin\beta'} \\ \frac{\sin\beta-\sin\beta'}{c\sin\beta} & 0 & 1 & 0 \\ 0 & 0 & 0 & 1 \end{pmatrix}$
$k''_\ell = \left.\frac{d^2k}{d\Omega^2}\right\|_{\omega_\ell}$, L_g – thickness of slab	β – angle of incidence, β' – diffraction angle

Table 2.3: Examples of Ray-Pulse Matrices

system matrix as

$$\Psi = \frac{\pi\Delta\nu^2}{B}(EH - BI) - \frac{\pi}{B\lambda_\ell}Q(\Delta\nu) \tag{2.133}$$

where

$$Q(\Delta\nu) = \begin{pmatrix} x_{in} & x_{out} \end{pmatrix}\begin{pmatrix} A & -1 \\ -1 & D \end{pmatrix}\begin{pmatrix} x_{in} \\ x_{out} \end{pmatrix} + 2\begin{pmatrix} E & \lambda_0 H \end{pmatrix}\begin{pmatrix} x_{in} \\ x_{out} \end{pmatrix} \tag{2.134}$$

and x_{in}, x_{out} are the position coordinates of the input and output vectors, respectively. The argument $\Delta\nu$ of Q and Ψ is the cyclic frequency coordinate relative to the pulse central frequency $\Delta\nu = (\Omega - \omega_\ell)/2\pi$. The calculations according to Eq. (2.133) have to be repeated for a set of frequencies to obtain $\Psi(\nu)$. From $\Psi(\nu)$ we can then determine chirp and temporal behavior of the output pulses using the

relation (1.177) for linear elements without losses. For pulses incident on-axis ($x_{in} = 0$), Eq. (2.134) yields for the phase response

$$\Psi_M(\Delta\nu) = \frac{1}{4\pi B}\left[\left(EH - BI - \frac{1}{\lambda_\ell} DE^2\right)\Delta\nu^2 - 4\pi EH\Delta\nu\right], \tag{2.135}$$

where the index M is to express the derivation of the phase response from the ray-pulse matrix. Information about the temporal broadening can also be gained directly from the matrix element I since $\Delta t_{out} = \Delta t_{in} + \Delta\nu I$. Wave packets centered at different frequencies need different times to travel from the input to the exit plane which gives an approximate broadening of $I\Delta\nu$ for a bandwidth limited input pulse with a spectral width $\Delta\omega_\ell = 2\pi\Delta\nu_\ell$. For on-axis propagation ($x_{in} = x_{out} = 0$) we find $Q(\Delta\nu) = 0$ and the dispersion is given by the first term in Eq. (2.133). For a dispersive slab, for example, we find from Table 2.3:

$$\Psi_M = \frac{1}{2} L_g k''_\ell (\Omega - \omega_\ell)^2 \tag{2.136}$$

which agrees with Eq. (1.184) and the accompanying discussion.

As another example let us discuss the action of a Brewster prism at minimum deviation and analyze the ray-pulse at a distance L_a behind it. The system matrix is the product of ($\mathcal{M}_{BP}$) and ($\mathcal{M}_{DS}$) for free space, which is given by

$$\begin{pmatrix} 1 & B + L_a & 0 & E + FL_a \\ 0 & 1 & 0 & F \\ G & H & 1 & I \\ 0 & 0 & 0 & 1 \end{pmatrix}. \tag{2.137}$$

For the sake of simplicity the elements of the prism matrix have been noted $A, B, \ldots, H$. For the new position and time coordinate we obtain

$$x_{out} = x_{in} + (B + L_a)\Theta_{in} + (E + FL_a)\Delta\nu \tag{2.138}$$

and

$$\Delta t_{out} = Gx_{in} + H\Theta_{in} + \Delta t_{in} + I\Delta\nu. \tag{2.139}$$

Let us next verify the tilt of the pulse fronts derived earlier. The pulse front tilt can be understood as an arrival time difference Δt_{out} which depends on the transverse beam coordinate x_{out}. The corresponding tilt angle α' is then

$$\tan\alpha' = \frac{\partial(c\Delta t_{out})}{\partial x_{out}} = c\frac{\partial\Delta t_{out}}{\partial x_{in}}\frac{\partial x_{in}}{\partial x_{out}} = cG. \tag{2.140}$$

After we insert G for the Brewster prism, the tilt angle becomes (cf. Table 2.3):

$$\tan\alpha' = -2\omega_\ell \left.\frac{\partial n}{\partial \Omega}\right|_{\omega_\ell} = 2\lambda_\ell \left.\frac{\partial n}{\partial \lambda}\right|_{\lambda_\ell}. \tag{2.141}$$

This result is equivalent to Eq. (2.71) if we use $a/b = 2$, which is valid for Brewster prisms. The different signs result from the direction of the x-axis chosen here.

As a final example we want to apply the matrix formalism to discuss the field distribution behind a two-prism sequence used for pulse compression, such as the one sketched in Fig. 2.25. We assume that one prism is traversed at the apex while the second is responsible for a mean glass path L_g. The corresponding system matrix is obtained by multiplying matrix (2.137) from the left with the transposed[12] matrix of a Brewster prism. The result is

$$\begin{pmatrix} 1 & \frac{L_g}{n^3} + L_a & 0 & -S\left[\frac{L_g}{n^3} + 2L_a\right] \\ 0 & 1 & 0 & 0 \\ 0 & \frac{S}{\lambda_\ell}\left[\frac{L_g}{n^3} + 2L_a\right] & 1 & -\frac{S^2}{\lambda_\ell}\left[\frac{L_g}{n^3} + 4L_g\right] - 2\pi k''_\ell L_g \\ 0 & 0 & 0 & 1 \end{pmatrix}. \tag{2.142}$$

To get a simplified expression, we make the assumption that $L_g \ll L_a$, which allows us to neglect terms linear in L_g in favor of those linear in L_a, whenever they appear in a summation. For the second derivative of the phase response (2.135) we find

$$\Psi''(\omega_\ell) = L_g k''_\ell - \frac{8\pi}{\lambda_\ell} L_a \left(\left.\frac{dn}{d\Omega}\right|_{\omega_\ell}\right)^2 \tag{2.143}$$

which is consistent with the exact solution Eq. (B.18), within the approximation of $L_g \ll L_a$, implying negligible angular dispersion inside the prisms.

It is well known that ray matrices can be used to describe Gaussian beam propagation, e.g., [52]. The beam parameter of the output beam is connected to the input parameter by

$$\tilde{q}_{out} = \frac{A\tilde{q}_{in} + B}{C\tilde{q}_{in} + D}. \tag{2.144}$$

Kostenbauder [51] showed that, in a similar manner, the ray-pulse matrices contain all information which is necessary to trace a generalized Gaussian beam through the optical system. Using a 2×2 complex "beam" matrix ($\tilde{Q}_{in}$), the amplitude of a generalized Gaussian beam is of the form

$$\exp\left[-\frac{i\pi}{\lambda_\ell}\begin{pmatrix} x_{in} & x_{out} \end{pmatrix}\left(\tilde{Q}_{in}\right)^{-1}\begin{pmatrix} x_{in} \\ t_{in} \end{pmatrix}\right] \tag{2.145}$$

[12] Note that the second prism has an orientation opposite to the first one.

which explicitly varies as

$$\exp\left[-\frac{i\pi}{\lambda_\ell}\left(\tilde{Q}^r_{xx}x^2_{in}+2\tilde{Q}^r_{xt}x_{in}t_{in}-\tilde{Q}^r_{tt}t^2_{in}\right)\right]$$
$$\times\quad \exp\left[\frac{\pi}{\lambda_\ell}\left(\tilde{Q}^i_{xx}x^2_{in}+2\tilde{Q}^i_{xt}x_{in}t_{in}-\tilde{Q}^i_{tt}t^2_{in}\right)\right], \tag{2.146}$$

where $\tilde{Q}^r_{ij}$, $\tilde{Q}^i_{ij}$ are the real and imaginary coordinates of the matrix $(\tilde{Q}_{in})^{-1}$ and $\tilde{Q}_{xt}=-\tilde{Q}_{tx}$. The first factor in Eq.(2.146) expresses the phase behavior and accounts for the wave front curvature and chirp. The second term describes the spatial and temporal beam (pulse) profile. Note that unless $\tilde{Q}^{r,i}_{xt}=0$ the diagonal elements of $(\tilde{Q}_{in})$ do not give directly such quantities as pulse duration, beam width, chirp parameter, and wave front curvature. One can show that the field at the output of an optical system is again a generalized Gaussian beam where in analogy to (2.144) the generalized beam parameter $(\tilde{Q}_{out})$ can be written as

$$\left(\tilde{Q}_{out}\right)=\frac{\begin{pmatrix}A&0\\G&1\end{pmatrix}\left(\tilde{Q}_{in}\right)+\begin{pmatrix}B&E/\lambda_\ell\\H&I/\lambda_\ell\end{pmatrix}}{\begin{pmatrix}C&0\\0&0\end{pmatrix}\left(\tilde{Q}_{in}\right)+\begin{pmatrix}D&F/\lambda_\ell\\0&1\end{pmatrix}}. \tag{2.147}$$

The evaluation of such matrix equations is quite complex since it generally gives rather large expressions. However, the use of advanced algebraic formula-manipulation computer codes makes this approach practicable.

2.8 Numerical approaches

The analytical and quasi-analytical methods to trace pulses give much physical insight but fail if the optical systems become too demanding and/or many dispersion orders have to be considered.

There are commercial wave and ray tracing programs available that allow one to calculate not only the geometrical path through the system but also the associated phase. Thus complete information on the complex field distribution (amplitude and phase) in any desired plane is retrievable.

Problems

1. Dispersion affects the bandwidth of wave-plates. Calculate the maximum pulse duration for which a 10^{th} order quarter wave plate can be made of

crystalline quartz, at 266 nm, using the parameters given with Eq. (2.2). We require that the quarter-wave condition still be met with 5% accuracy at $\pm (1/\tau_p)$ of the central frequency. What is the thickness of the wave-plate?

2. We consider here a Fabry-Perot cavity containing a gain medium. To simplify, we assume the gain to be linear and uniform in the frequency range around a Fabry-Perot resonance of interest. Consider this system to be irradiated by a tunable probe laser of frequency ν_p.

   a Find an expression for the transmission and reflection of this Fabry-Perot with gain as a function of the frequency of the probe laser.

   b Find the gain for which the expression for the transmission tends to infinity. What does it mean?

   c Describe how the gain modifies the transmission function of the Fabry-Perot (linewidth, peak transmission, peak reflection). Sketch the transmission versus frequency for low and high gain.

   d With the probe optical frequency tuned to the frequency for which the empty (no gain) Fabry-Perot has a transmission of 50%, find its transmission factor for the value of the gain corresponding to lasing threshold.

3. Calculate the transmission of pulse propagating through a Fabry-Perot interferometer. The electric field of the pulse is given by $E(t) = \mathcal{E}(t)e^{i\omega_\ell t}$, where $\mathcal{E}(t) = \exp(-|t|/\tau)$ and $\tau = 10$ ns. The Fabry Perot cavity is 1 mm long, filled with a material of index $n_0 = 1.5$, and both mirrors have a reflectance of 99.9%. The wavelength is 1 μm. What is the transmission linewidth (FWHM) of this Fabry-Perot? Find analytically the shape (and duration) of the pulse transmitted by this Fabry Perot, assuming exact resonance.

4. Consider the same Fabry-Perot as in the previous problem, on which a Gaussian pulse (plane wave) is incident. The frequency of the Gaussian pulse is 0.1 ns^{-1} below resonance. Calculate (numerically) the shape of the pulse transmitted by this Fabry Perot, for various values of the pulse chirp a. The pulse envelope is:

$$\tilde{\mathcal{E}}(t) = e^{-(1+ia)(\frac{t}{\tau_G})^2}.$$

   Is there a value of a for which the pulse transmitted has a minimum duration?

5. Consider the Gires–Tournois interferometer. (a) As explained in the text, the reflectivity is R = constant = 1, while the phase shows a strong variation with frequency. Does this violate the Kramers–Kronig relation? Explain your answer. (b) Derive the transfer function (2.32).

6. Derive an expression for the space-time intensity distribution of a pulse in the focal plane of a chromatic lens of focal length $f(\lambda)$. To obtain an analytical formula make the following assumptions. The input pulse is bandwidth-limited and exhibits a Gaussian temporal and transverse spatial profile. The lens has an infinitely large aperture and the GVD can be neglected. [Hint: You can apply Gaussian beam analysis for each spectral component to obtain the corresponding field in the focal plane. Summation over spectral contributions (Fourier back-transform) gives then the space-time field distribution.]

7. Calculate the third order dispersion for a pair of isosceles prisms, not necessarily used at the minimum deviation angle, using the procedure that led to Eq. (B.18). Compare with Eq. (2.91).

8. Calculate the optimum pair of prisms to be inserted into the cavity of a femtosecond pulse laser at 620 nm. The criterium is that the prism pair should provide a 20% GVD tunability around -800 fs^2, and the next higher-order dispersion should be as small as possible. With the help of Table 2.1 choose a suitable prism material, calculate the apex angle of the prisms for the Brewster condition at symmetric beam path, and determine the prism separation. If needed, assume a beam diameter of 2 mm to estimate a minimum possible glass path through the prisms.

9. Derive the ray-pulse matrix (2.142) for a pair of Brewster prisms. Verify the second-order dispersion given in relation (B.18), without the assumption of $L_g \ll L_a$.

10. Derive the delay and aberration parameter of a spherical mirror as given in Eqs. (2.56) and (2.57). Explain physically what happens if a parallel input beam impinges on the mirror with a certain angle α.

11. A parallel beam with plane pulse fronts impinges on a circular aperture with radius R centered on the optic axis. The pulse is unchirped and Gaussian. Estimate the frequency shift that the diffracted pulse experiences if measured with a detector placed on the optic axis. Give a physical explanation of this shift. Make a numerical estimate for a 100 fs and a 10 fs pulse. Can this effect be used to obtain ultrashort pulses in new spectral regions by placing diffracting apertures in series? [Hint: you can start with Eq. (2.51) and take out the lens terms. For mathematical ease you can let $R \to \infty$).] Note that a frequency shift (of the same origin) occurs when the on-axis pulse spectrum of a Gaussian beam is monitored along its propagation path.

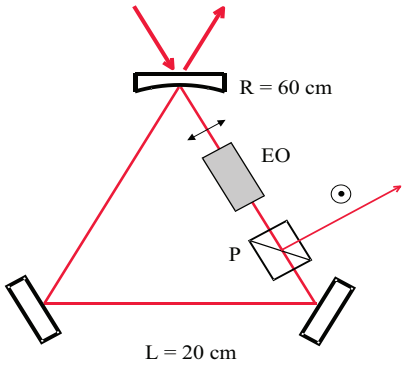

Figure 2.33: Ring resonator. Consider the electro-optic switch (EO, Pockel's cell) and the polarizing beam splitter only for part (d). The polarization of the beam circulating in the cavity gets rotated from the plane of the ring into the orthogonal direction when an electrical pulse is applied to the Pockel's cell, and extracted from the cavity by a polarizing beam splitter. The risetime of the electrical pulse is short compared to the cavity round-trip time.

12. Consider the 3-mirror ring resonator sketched in Fig. 2.33. Two of the mirrors are flat and 100% reflecting, while one mirror of field reflectivity $r = 0.9999\%$ and 60 cm curvature, serves as input and output of this resonator. We are operating at a wavelength of 800 nm. The perimeter of the ring is 60 cm. A beam with a train of pulses, of average incident power of $P_0 = 1$ mW is sent, properly aligned, into the input path of this resonator.

    a Calculate the size and location of the beam waist w_0 of the fundamental mode of this resonator, and the size of the beam (w) at the output mirror. Explain why the output power P_2 does not depend on the wavelength.

    b Derive an expression for the field inside the resonator E_i as a function of the input field E_0.

    c Consider this passive cavity being irradiated from the outside by a train of femtosecond pulses, for its use as a photon storage ring. Show that two conditions need to be fulfilled for this cavity to be exactly resonant, which may not always be simultaneously met.

    d Let us assume next that the train of pulses, with a wavelength near 800 nm, corresponds to exactly a "resonance" of this resonator, both

in frequency and repetition rate. A fast electro-optic switch is included in the ring, such that it directs the electromagnetic wave out of the resonator for a round-trip time of the cavity, every N round-trip times (cavity dumping). The switch opens in a time short compared to the round-trip time. Explain how this device can be used to create short output pulses with a larger single-pulse energy than the incident pulses. What energy could be obtained in the case of (i) $N = 100$ and (ii) $N = 5000$.

Bibliography

[1] V. G. Dmitriev, G. G. Gurzadyan, and D. N. Nikogosyan. *Handbook of Nonlinear Material*. Springer-Verlag, Berlin, 1999.

[2] F. J. Duarte. Dye lasers. In F. J. Duarte, editor, *Tunable Lasers Handbook*. Academic Press, Boston, 1994.

[3] Willian H. Press, Brian P. Flannery, Saul E. Teukolsky, and William P. Vetterling. *Numerical Recipes*. Cambridge University Press, New York, 1986.

[4] S. DeSilvestri, P. Laporta, and O. Svelto. The role of cavity dispersion in cw mode-locked lasers. *IEEE J. Quantum Electron.*, QE-20:533–539, 1984.

[5] W. Dietel, E. Dopel, K. Hehl, W. Rudolph, and E. Schmidt. Multilayer dielectric mirrors generated chirp in femtosecond dye ring lasers. *Optics Comm.*, 50:179–182, 1984.

[6] W. H. Knox, N. M. Pearson, K. D. Li, and C. A. Hirlimann. Interferometric measurements of femtosecond group delay in optical components. *Optics Lett.*, 13:574–576, 1988.

[7] K. Naganuma, K. Mogi, and H. Yamada. Group delay measurement using the fourier transform of an interferometric cross-correlation generated by white light. *Optics Lett.*, 7:393–395, 1990.

[8] K. Naganuma and H. Yasaka. Group delay and alpha-parameter measurement of 1.3 micron semiconductor traveling wave optical amplifier using the interferometric method. *IEEE J. Quantum Electron.*, 27:1280–1287, 1991.

[9] A. M. Weiner, J. G. Fujimoto, and E. P. Ippen. Femtosecond time-resolved reflectometry measurements of multiple-layer dielectric mirrors. *Opt. Lett.*, 10:71–73, 1985.

[10] A. M. Weiner, J. G. Fujimoto, and E. P. Ippen. Compression and shaping of femtosecond pulses. In D. H. Auston and K. B. Eisenthal, editors, *Ultrafast Phenomena IV*, pages 11–15, New York, 1984. Springer-Verlag.

[11] J.-C. Diels, W. Dietel, E. Dopel, J. J. Fontaine, I. C. McMichael, W. Rudolph, F. Simoni, R. Torti, H. Vanherzeele, and B. Wilhelmi. Colliding pulse femtosecond lasers and applications to the measurement of optical parameters. In D.H. Auston and K. B. Eisenthal, editors, *Ultrafast Phenomena IV*, pages 30–34, New York, 1984. Springer-Verlag.

[12] M. Born and E. Wolf. *Principles of Optics – Electromagnetic theory of propagation, interference and diffraction of light*. Pergamon Press, Oxford, New York, 1980.

[13] Miles V. Klein and Thomas E. Furtak. *Optics*. John Wiley and Sons, ISBN 0-471-87297-0, New York, 1986.

[14] J. Desbois, F. Gires, and P. Tournois. A new approach to picosecond laser pulse analysis and shaping. *IEEE J. Quantum Electron.*, QE-9:213–218, 1973.

[15] J. Kuhl and J. Heppner. Compression of fs optical pulses with dielectric multi-layer interferometers. *IEEE J. Quantum Electron.*, QE-22:182–185, 1986.

[16] M. A. Duguay and J. W. Hansen. Compression of pulses from a mode-locked He-Ne laser. *Appl.Phys.Lett.*, 14:14–15, 1969.

[17] J. Heppner and J. Kuhl. Intracavity chirp compensation in a colliding pulse mode-locked laser using thin-film interferometers. *Appl.Phys.Lett.*, 47:453–455, 1985.

[18] R. Szipöks, K. Ferenz, C. Spielman, and F. Krausz. Chirped multilayer coatings for broadband dispersion control in femtosecond lasers. *Opt. Lett.*, 19:201–203, 1994.

[19] F. X. Kärtner, N. Matuschek, T. Schibli, U. Keller, H. A. Haus, C. Heine, R. Morf, V. Scheuer, M. Tilsch, and T. Tschudi. Design and fabrication of double chirped mirrors. *Opt. Lett.*, 22:831–833, 1997.

[20] G. Tempea, F. Krausz, C. Spielman, and K. Ferenz. Dispersion control over 150 THz with chirped dielectric mirrrors. *IEEE Selected Topics in Quant. Electron.*, 4:193–196, 1998.

[21] G. Tempea, V. Yakovlev, B. Bacovic, F. Krausz, and K. Ferenz. Tilted-front interface chirped mirrors. *J. Opt. Soc. Am. B*, 18:1747–1750, 2001.

[22] N. Matuschek, L. Gallmann, D. H. Shutte, G. Steinmeyer, and U. Keller. Back-side coated chirped mirrors with smooth ultra-broadband dispersion characteristics. *Appl. Phys. B*, 71:509–522, 2000.

[23] Z. Bor. Distortion of femtosecond laser pulses in lenses and lens systems. *Journal of Modern Optics*, 35:1907–1918, 1988.

[24] Z. Bor. Distorsion of femtosecond laser pulses in lenses. *Optics Letters*, 14:119–121, 1989.

[25] M. Kempe, W. Rudolph, U. Stamm, and B. Wilhelmi. Spatial and temporal transformation of femtosecond laser pulses by lenses and lens systems. *J. Opt. Soc. Am.*, B9:1158–1165, 1992.

[26] M. Kempe and W. Rudolph. The impact of chromatic and spherical aberration on the focusing of ultrashort light pulses by lenses. *Opt. Lett.*, 18:137–139, 1993.

[27] M. Kempe and W. Rudolph. Femtosecond pulses in the focal region of lenses. *Phys. Rev.*, A48:4721–4729, 1993.

[28] E. B. Treacy. Optical pulse compression with diffraction gratings. *IEEE J. Quantum Electron.*, QE-5:454–460, 1969.

[29] F. J. Duarte and J. A. Piper. Dispersion theory of multiple prisms beam expanders for pulsed dye lasers. *Optics Comm.*, 43:303–307, 1982.

[30] R. L. Fork, O. E. Martinez, and J. P. Gordon. Negative dispersion using pairs of prism. *Opt. Lett.*, 9:150–152, 1984.

[31] V. Petrov, F. Noack, W. Rudolph, and C. Rempel. Intracavity dispersion compensation and extracavity pulse compression using pairs of prisms. *Exp. Technik der Physik*, 36:167–173, 1988.

[32] C. Froehly, B. Colombeau, and M. Vampouille. Shaping and analysis of picosecond light pulses. *Progress of Modern Optics*, XX:115–125, 1981.

[33] O. E. Martinez. Grating and prism compressor in the case of finite beam size. *J.Opt.Soc.Am.B*, 3:929–934, 1986.

[34] W. Dietel, J. J. Fontaine, and J.-C. Diels. Intracavity pulse compression with glass: a new method of generating pulses shorter than 60 femtoseconds. *Optics Letters*, 8:4–6, 1983.

[35] Ladan Arissian, Jean-Claude Diels, and Andreas Velten. Group velocity control by atomic nonlinear response in a laser cavity. In *CLEO, 2007*, page 130 (MC4), Baltimore, MA, 2007. Optical Society of America.

[36] P. F. Curley, Ch. Spielmann, T. Brabec, F. Krausz, E. Wintner, and A. J. Schmidt. Operation of a fs Ti:sapphire solitary laser in the vicinity of zero group-delay dispersion. *Opt. Lett.*, 18:54–57, 1993.

[37] M. T. Asaki, C. P. Huang, D. Garvey, J. Zhou, H. Kapteyn, and M. M. Murnane. Generation of 11 fs pulses from a self-mode-locked Ti:sapphire laser. *Opt. Lett.*, 18:977–979, 1993.

[38] O. E. Martinez, J. P. Gordon, and R. L. Fork. Negative group-velocity dispersion using diffraction. *J. Opt. Soc. Am.*, A1:1003–1006, 1984.

[39] F. J. Duarte. Generalized multiple-prism dispersion theory for pulse compression in ultrafast dye lasers. *Opt. and Quant.Electr.*, 19:223–229, 1987.

[40] C. P. J. Barty, C. L. Gordon III, and B. E. Lemoff. Multiterawatt 30-fs Ti:sapphire laser system. *Optics Lett.*, 19:1442–1444, 1994.

[41] O. E. Martinez. 3000 times grating compressor with positive group velocity dispersion: application to fiber compensation in the 1.3-1.6 μm region. *IEEE J. of Quantum Electron.*, 23:59–64, 1987.

[42] M. Pessot, P. Maine, and G. Mourou. 1000 times expansion compression of optical pulses for chirped pulse amplification. *Optics Comm.*, 62:419, 1987.

[43] M. Pessot, J. Squier, G. Mourou, and G. Vaillancourt. Chirped-pulse amplification of 100-fs pulses. *Optics Lett.*, 14:797–799, 1989.

[44] O. E. Martinez. Matrix formalism for pulse compressors. *IEEE J.Quantum Electron.*, QE-24:2530–2536, 1988.

[45] R. Guther. The *ABCD*-matrix for holographic gratings. *Optica Acta*, 11:97–104, 1981.

[46] A. E. Siegman. *ABCD*-matrix elements for a curved diffraction grating. *Journal of the Optical Society of America A*, 2:1793, 1985.

[47] S. A. Akhmanov, A. P. Sukhorov, and A. S. Chirkin. Nontationary phenomena and space-time analogy in nonlinear optics. *Sov. Phys. JETP*, 28:748–757, 1969.

[48] E. Doepel. Matrix formalism for the calculation of group delay and group-velocity dispersion in linear optical elements. *J. Mod. Opt.*, 37:237–242, 1990.

[49] O. E. Martinez. Matrix formalism for dispersive cavities. *IEEE J.Quantum Electron.*, QE-25:296–300, 1989.

[50] S. P. Dijaili, A. Dienes, and J. S. Smith. ABCD matrices for dispersive pulse propagation. *IEEE J. Quantum Electron.*, QE-26:1158–1164, 1990.

[51] A. G. Kostenbauder. Ray-pulse matrices: A rational treatment for dispersive optical systems. *IEEE J. Quantum Electron.*, QE-26:1148–1157, 1990.

[52] Anthony E. Siegman. *Lasers*. University Science Books, Mill Valley, CA, 1986.

Appendix B

Prism pair dispersion

In order to compensate the angular dispersion, the two prisms are put in opposition, in such a way that, to any face of one prism corresponds a parallel face of the other prism (Fig. 2.25).

We consider in this section a prism sequence that controls GVD, but avoids the beam divergence and energy front tilt introduced by angular dispersion.

The optical path $\overline{ABB'A'D}$ at a frequency Ω is represented by the solid line in Fig. 2.25, while the path for a ray upshifted by $d\Omega$ is represented by the dashed line. The successive angles of incidence/refraction are θ_0 and θ_1 at point A), θ_2 and θ_3 at point B, θ_4 and θ_5 at point B', and finally θ_6 and θ_7 at point A'. The two prisms are identical, with equal apex angle α and with pairs of faces oriented parallel as shown in Fig. 2.25. At any wavelength or frequency Ω:

- $\theta_3 = \theta_4$
- $\theta_2 = \theta_5$
- $\theta_1 = \theta_6$
- $\theta_0 = \theta_7$
- $\theta_1 + \theta_2 = \alpha$
- $d\theta_1/d\Omega = -d\theta_2/d\Omega$.

If the prisms are used at minimum deviation at the central wavelength, $\theta_0 = \theta_3 = \theta_4 = \theta_7$. If, in addition to being used at minimum deviation, the prisms are cut for Brewster incidence, the apex angles of both prisms are $\alpha = \pi - 2\theta_0 = \pi - 2\arctan(n)$.

The challenge is to find the frequency dependence of the optical path $\overline{ABB'A'D}$. The initial (geometrical) conditions are defined by

- The distance $a = \overline{OA}$ from the point of impact of the beam to the apex O of the first prisms. For convenience, we will use in the calculations the distance $\overline{OH} = h = \overline{OA}\cos\alpha = a\cos\alpha$,
- the separation s between the parallel faces of the prisms,
- the distance t between the apex O and O', measured along the exit face of the first prism, cf. Fig. 2.25.

The changes in path length due to dispersion can be understood from a glance at the figure, comparing the optical paths at Ω (solid line) and $\Omega + d\Omega$ (dashed line). The contributions that increase the path length are:

1. positive dispersion because of propagation through the prism material of positive dispersion ($\overline{AB}$ and $\overline{B'A'}$)
2. positive dispersion because of the increased path length $\overline{BB'}$ in air (increment $\overline{SB'''}$ in Fig. B.2)
3. positive dispersion because of the increased path length $\overline{A'D}$ in air (projection of $\overline{A'A'''}$ along the beam propagation direction).

The contributions that decrease the path length (negative dispersion) of the frequency upshifted beam can best be understood with Fig. B.1 and Fig. B.2. Fig B.1 shows the configurations of the beams if the two prisms were brought together, i.e. $\overline{BB'} = 0$. Fig. B.2 shows an expanded view of the second prism. The negative dispersion contributions emanate from:

1. The shortened path length in glass because of the angular dispersion ($\overline{AA''}$ versus $\overline{AA'}$ in Fig. B.1),
2. the shorter path length in the second prism due to the deflection of the beam by the first one (path difference $\overline{B''T}$ in Fig. B.2).

Path through glass The total path in glass is $L_g = \overline{AB} + \overline{B'A'}$ where $\overline{AB} = a\sin\alpha/\cos\theta_2$ and $\overline{B'A'} = \overline{O'B'}\sin\alpha/\cos(\alpha-\theta_2) = \overline{O'B'}\sin\alpha/\cos\theta_1$, with:

$$\overline{O'B'} = t - s\tan\theta_3 - a(\cos\alpha + \sin\alpha\tan\theta_2). \tag{B.1}$$

We thus have for the total transmitted path in glass:

$$\begin{aligned} L_g = \overline{AB} + \overline{B'A'} &= \frac{a\sin\alpha}{\cos\theta_2} + [t - s\tan\theta_3 - a(\cos\alpha + \sin\alpha\tan\theta_2)]\,\frac{\sin\alpha}{\cos\theta_1} \\ &= (t - s\tan\theta_3)\,\frac{\sin\alpha}{\cos\theta_1}. \end{aligned} \tag{B.2}$$

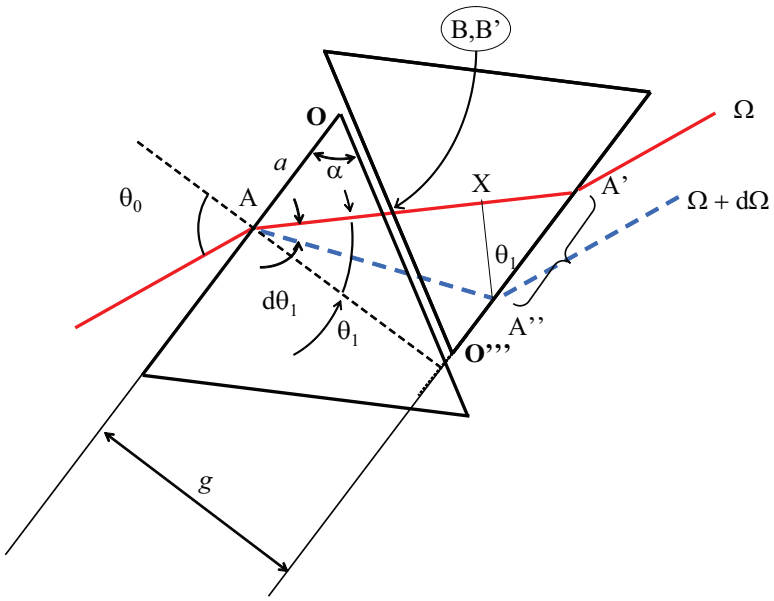

Figure B.1: Beam passage through the two prisms, when the distance $\overline{BB'}$ (in Fig. 2.25) has been reduced to zero. The distance between the apexes O and O' has been reduced to $\overline{OO'''} = t - \overline{BB'}\sin\theta_3$ (referring to Fig. 2.25). The distance between parallel faces is then $g = \overline{OO'''}\sin\alpha = (t - \overline{BB'}\sin\theta_3)\sin\alpha$.

As expected, the total path through glass is independent of the starting position defined by a. If the two prisms are brought together as in Fig. B.1, they act as a slab of glass with parallel faces, of thickness $g = L_g\cos\theta_1$. There are three contributions to the optical path change from Fig. B.1: one due to the change in index, a second due to the change in angle, and a third because the path length L_g is frequency dependent. Taking the derivative of $\Omega n L_g/c$ with L_g defined by Eq. (B.2):

$$\begin{aligned}\frac{d(kL_g)}{d\Omega} &= \frac{d}{d\Omega}\left(\frac{n\Omega L_g}{c}\right)\\ &= \frac{L_g}{c}\left(n+\Omega\frac{dn}{d\Omega}\right)+\left(\frac{n\Omega L_g}{c}\tan\theta_1\right)\frac{d\theta_1}{d\Omega}\\ &\quad -\left(\frac{n\Omega s}{c\cos^2\theta_3}\right)\frac{\sin\alpha}{\cos\theta_1}\frac{d\theta_3}{d\Omega}\end{aligned} \tag{B.3}$$

The first term can be attributed solely to material dispersion. The next term is the change in length in glass due to the angular dispersion $d\theta_1/d\Omega$, and the last expresses the reduction in path length in the second prism due to the propagation of the angularly dispersed beam in air. The expression above only partly accounts for

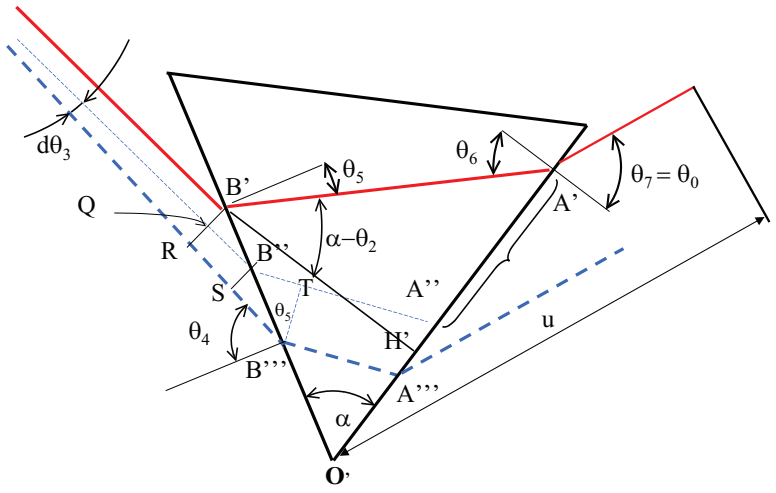

Figure B.2: Details of the beam passage through the second prism.

the energy tilt associated with the angular dispersion $d\theta_3/d\Omega$. Another contribution arises from the path through air to a reference plane.

Path through air between and after the prisms We have here to account for the contributions of the pathlengths $\overline{BB'}$ and $\overline{A'D}$ to the group delay:

$$\frac{d}{d\Omega}\left(\frac{\Omega}{c}\overline{BB'}\right) = \frac{\Omega}{c}\frac{d\overline{BB'}}{d\Omega} + \frac{\overline{BB'}}{c}. \tag{B.4}$$

For the path $\overline{BB'} = s/\cos\theta_3$, there is only a change in length equal to $\overline{S\,B'''}$, which can be obtained by either differentiating $s/\cos\theta_3$, or simply from geometrical considerations using Fig. 2.25 ($\overline{S\,B'''} = \overline{S\,B''}\tan\theta_3 = \overline{BB'}\tan\theta_3 d\theta_3$):

$$\frac{d\overline{BB'}}{d\Omega} = \frac{s}{\cos\theta_3}\tan\theta_3\frac{d\theta_3}{d\Omega}. \tag{B.5}$$

The path in air after the second prism can be expressed as:

$$\overline{A'D} = u - \overline{O'A'}\sin\theta_0. \tag{B.6}$$

Because u is not a function of Ω, the contribution to the group delay is:

$$\frac{1}{c}\frac{d\left(\Omega\overline{A'D}\right)}{d\Omega} = -\frac{\sin\theta_0}{c}\frac{d}{d\Omega}(\Omega\overline{O'A'}). \tag{B.7}$$

For $\overline{O'A'}$ we find:

$$\begin{aligned}\overline{O'A'} &= \overline{O'H'} + \overline{H'A'} = \overline{O'B'}\,[\cos\alpha + \sin\alpha\tan(\alpha-\theta_2)] \\ &= [t - s\tan\theta_3 - a(\cos\alpha + \sin\alpha\tan\theta_2)]\,[\cos\alpha + \sin\alpha\tan(\alpha-\theta_2)] \\ &= \left[t - s\tan\theta_3 - a\frac{\cos\theta_1}{\cos\theta_2}\right][\cos\alpha + \sin\alpha\tan(\alpha-\theta_2)] \\ &= [t - s\tan\theta_3]\,[\cos\alpha + \sin\alpha\tan\theta_1] - a, \end{aligned} \tag{B.8}$$

where we have used $\cos\alpha + \sin\alpha\tan\theta_2 = \cos(\alpha-\theta_2)\cos\theta_2$. The contribution of $\overline{A'D}$ to the group delay is:

$$\begin{aligned}-\frac{\sin\theta_0}{c}\frac{d(\Omega\overline{O'A'})}{d\Omega} &= \frac{\overline{O'A'}\sin\theta_0}{c} - \frac{\Omega s\sin\theta_0}{c\cos^2\theta_3}\,[\cos\alpha + \sin\alpha\tan\theta_1]\,\frac{d\theta_3}{d\Omega} \\ &\quad + \frac{\Omega\sin\theta_0}{c}\,[t - s\tan\theta_3]\,\frac{\sin\alpha}{\cos^2\theta_1}\,\frac{d\theta_1}{d\Omega} \\ &= -\frac{\overline{A'D}}{c} - \frac{n\Omega s}{c\cos^2\theta_3}\left[\cos\alpha\sin\theta_1 + \sin\alpha\frac{\sin^2\theta_1}{\cos\theta_1}\right]\frac{d\theta_3}{d\Omega} \\ &\quad + \frac{n\Omega}{c}\,[t - s\tan\theta_3]\,\frac{\sin\alpha\sin\theta_1}{\cos^2\theta_1}\,\frac{d\theta_1}{d\Omega}. \end{aligned} \tag{B.9}$$

In the last equation we used the fact that u is an arbitrary constant, for example zero, so that $\overline{A'D} = -\overline{O'A'}\sin\theta_0$.

Total path in glass and air After adding all contributions to the total phase

$$\Psi = \frac{\Omega}{c}\left(nL_g + \overline{BB'} + \overline{A'D}\right),$$

we obtain for the group delay using Eqs. (B.3),(B.4) and (B.5), and (B.7) and (B.9):

$$\begin{aligned}
\frac{d\Psi}{d\Omega} &= \frac{d}{d\Omega}\left(\frac{\Omega n L_g}{c}\right) + \frac{d}{d\Omega}\left(\frac{\Omega\overline{BB'}}{c}\right) + \frac{d}{d\Omega}\left(\frac{\Omega\overline{A'D}}{c}\right) \\
&= \frac{nL_g}{c} + \frac{(\overline{BB'}+\overline{A'D})}{c} + \frac{L_g\Omega}{c}\frac{dn}{d\Omega} + \frac{n\Omega L_g}{c}\tan\theta_1\frac{d\theta_1}{d\Omega} \\
&\quad + \left\{-\frac{n\Omega s}{c\cos^2\theta_3}\frac{\sin\alpha}{\cos\theta_1} + \frac{\Omega s}{c\cos\theta_3}\tan\theta_3 + \frac{n\Omega s}{c\cos^2\theta_3}\left[\cos\alpha\sin\theta_1\right.\right. \\
&\quad \left.\left. + \frac{\sin\alpha\sin^2\theta_1}{\cos\theta_1}\right]\right\}\frac{d\theta_3}{d\Omega} - \frac{n\Omega}{c}\left[t - s\tan\theta_3\right]\frac{\sin\alpha\sin\theta_1}{\cos^2\theta_1}\frac{d\theta_1}{d\Omega} \\
&= \frac{OPL(ABB'A'D)}{c} + \frac{L_g\Omega}{c}\frac{dn}{d\Omega} \\
&\quad + \left(\frac{\Omega s}{c\cos^2\theta_3}\right)\left(-n\sin\alpha\cos\theta_1 + \cos\theta_3\tan\theta_3 + n\cos\alpha\sin\theta_1\right)\frac{d\theta_3}{d\Omega},
\end{aligned} \tag{B.10}$$

where we have defined the optical path length $OPL(ABB'A'D) = nL_g + (\overline{BB'} + \overline{A'D})$. The factor preceding $d\theta_3/d\Omega$ cancels, since:

$$\begin{aligned}
\cos\alpha\sin\theta_1 - \sin\alpha\cos\theta_1 + \frac{\sin\theta_3}{n} & \\
&= \cos(\theta_1+\theta_2)\sin\theta_1 - \sin(\theta_1+\theta_2)\cos\theta_1 + \sin\theta_2 \\
&= 0.
\end{aligned}$$

The complete expression for the group delay through the pair of prism reduces to:

$$\boxed{\frac{d\Psi}{d\Omega} = \frac{OPL(ABB'A'D)}{c} + \frac{L_g\Omega}{c}\frac{dn}{d\Omega}} \tag{B.11}$$

The first terms in the last equation represents the travel delay at the phase velocity:

$$\frac{OPL(ABB'A'D)}{c} = \frac{L_g n}{c} + \frac{s}{c\cos\theta_3} + \frac{\overline{A'D}}{c} \tag{B.12}$$

The second part of Eq. (B.11) is the carrier to envelope delay caused by the pair of prisms[1]:

$$\tau_{CE}(\Omega) = \frac{\Omega}{c}\frac{d}{d\Omega}OPL(ABB'A'D) = \frac{L_g\Omega}{c}\frac{dn}{d\Omega}. \tag{B.13}$$

[1] We are assuming that the prisms are in vacuum, i.e. the contribution to the dispersion from air is neglected.

The second derivative of the phase, obtained by taking the derivative of Eq. (B.11), is:

$$\begin{aligned}\left.\frac{d^2\Psi}{d\Omega^2}\right|_{\omega_\ell} &= L_g\left[2\left.\frac{dn}{d\Omega}\right|_{\omega_\ell}+\omega_\ell\left.\frac{d^2n}{d\Omega^2}\right|_{\omega_\ell}\right]\\ &\quad-\frac{\omega_\ell}{c\cos\theta_1}\left.\frac{dn}{d\Omega}\right|_{\omega_\ell}\frac{s\sin\alpha}{\cos^2\theta_3}\left.\frac{d\theta_3}{d\Omega}\right|_{\omega_\ell}\\ &\quad+\frac{\omega_\ell}{c}\left.\frac{dn}{d\Omega}\right|_{\omega_\ell}\left(L_g\tan\theta_1\left.\frac{d\theta_1}{d\Omega}\right|_{\omega_\ell}\right).\end{aligned} \tag{B.14}$$

The derivatives with respect to Ω are related. By differentiating Snell's law for the first interface:

$$d\theta_1 = -\frac{\tan\theta_1}{n}dn = -d\theta_2. \tag{B.15}$$

For the second interface, taking the previous relation into account, we find:

$$\begin{aligned}\cos\theta_3 d\theta_3 &= n\cos\theta_2 d\theta_2+\sin\theta_2 dn = n\cos\theta_2\left(\frac{\tan\theta_1}{n}+\sin\theta_2\right)dn\\ &= (\cos\theta_2\tan\theta_1+\sin\theta_2)\,dn = \frac{\sin\alpha}{\cos\theta_1}dn,\end{aligned} \tag{B.16}$$

or:

$$d\theta_3 = \frac{\sin\alpha}{\cos\theta_1\cos\theta_3}dn. \tag{B.17}$$

Therefore, the second order dispersion Eq. (B.14) reduces to an easily interpretable form:

$$\boxed{\begin{aligned}\left.\frac{d^2\Psi}{d\Omega^2}\right|_{\omega_\ell} &= \frac{L_g}{c}\left[2\left.\frac{dn}{d\Omega}\right|_{\omega_\ell}+\omega_\ell\left.\frac{d^2n}{d\Omega^2}\right|_{\omega_\ell}\right]\\ &\quad-\frac{\omega_\ell}{c}\left(\frac{s}{\cos\theta_3}\right)\left(\left.\frac{d\theta_3}{d\Omega}\right|_{\omega_\ell}\right)^2-\frac{n\omega_\ell}{c}L_g\left(\left.\frac{d\theta_1}{d\Omega}\right|_{\omega_\ell}\right)^2\end{aligned}} \tag{B.18}$$

Index